

**Cell-free Synthetic Biology for Behavior Modules in Microrobots**

by

**Ting-Yen Wei**

Bachelor of Science, National Tsing Hua University, 2017

Submitted to the Graduate Faculty of the  
Swanson School of Engineering in partial fulfillment  
of the requirements for the degree of  
Doctor of Philosophy

University of Pittsburgh

2022

UNIVERSITY OF PITTSBURGH

SWANSON SCHOOL OF ENGINEERING

This dissertation was presented

by

**Ting-Yen Wei**

It was defended on

May 26, 2022

and approved by

Mo R. Ebrahimkhani, PhD, Associate Professor, Department of Pathology, School of Medicine

Natasa Miskov- Zivanov, PhD, Assistant Professor, Department of Electrical and Computer  
Engineering

W. Seth Childers, PhD, Assistant Professor, Department of Chemistry

Dissertation Director: Warren C. Ruder, PhD, Associate Professor and William Kepler  
Whiteford Faculty Fellow, Department of Bioengineering

Copyright © by Ting-Yen Wei

2022

# **Cell-free Synthetic Biology for Behavior Modules in Microrobots**

Ting-Yen Wei, PhD

University of Pittsburgh, 2022

Autonomous biohybrid microrobots with unique features and functions are an emerging technology in biomedical applications. The miniaturized size enables them to access previously unreachable parts throughout the human body, offering localized diagnosis and treatment with greater precision and efficiency. However, autonomous capabilities such as perception-action and communication remain a challenge for robots at a small scale.

By repurposing and reprogramming molecular modules, synthetic biology has constructed autonomous capabilities in living organisms. Cell-free synthetic biology has emerged as a programmable and rapid tool for implementing and characterizing synthetic genetic circuits. Here, we present a cell-free synthetic biology platform to build onboard behavior modules on microrobots. Leveraging the capability of synthetic biology and the cell-free platform for creating complex behaviors, microrobots could acquire the ability to sense, analyze, and respond to complex environments based on designed genetic circuits.

First, we developed a user-friendly microfluidic device to characterize microrobot behaviors demonstrated by fluorescent output, a widely adopted parameter for evaluating genetic circuit performance. Cell-free reactions are frequently quantitatively characterized by plate readers that cannot provide visualization. Microfluidic technology has facilitated cell-free synthetic biology development but has focused mainly on experiment automation instead of rapid characterization. Such microfluidic systems involve exquisite manipulation and operation, hindering widespread adoption. Hence, we present the design of a robust yet straightforward

microfluidic device for rapid cell-free synthetic biology characterization that can be used to characterize the reported biohybrid microrobots.

Next, biohybrid microrobots equipped with basic Boolean logic gates demonstrated the implementation of perception-action modules with the reported cell-free platform. Furthermore, the reported platform enables microrobots to communicate and perform collective behaviors. Biochemical information carriers were exchanged among microrobots and coordinated collective behaviors to analyze multiple inputs and generate responses according to designed logic circuits. This work opens up an opportunity to build autonomous miniaturized clinical tools with potential use in the human body for precise and efficient diagnosis and treatment.

## Table of Contents

Preface.....	xiii
<b>1.0 Introduction.....</b>	<b>1</b>
<b>1.1 Dissertation Contributions .....</b>	<b>4</b>
<b>2.0 Background .....</b>	<b>6</b>
<b>2.1 Overview of Robots at A Small Scale .....</b>	<b>6</b>
<b>2.1.1 Robots at Microscale and Nanoscale .....</b>	<b>6</b>
<b>2.1.2 Molecular Robots .....</b>	<b>8</b>
<b>2.1.3 Robot Swarm .....</b>	<b>11</b>
<b>2.2 Overview of Synthetic Biology and Robotics .....</b>	<b>13</b>
<b>2.2.1 Synthetic Biology and Robots .....</b>	<b>13</b>
<b>2.2.2 Cell-Free Synthetic Biology and Robots .....</b>	<b>16</b>
<b>3.0 Microfluidic Devices for Characterization of Cell-Free Synthetic Biology</b>	
<b>Reactions .....</b>	<b>20</b>
<b>3.1 Introduction .....</b>	<b>21</b>
<b>3.2 Methods .....</b>	<b>24</b>
<b>3.2.1 Design and Construction of Microfluidic Devices.....</b>	<b>25</b>
<b>3.2.2 Device Characterization .....</b>	<b>25</b>
<b>3.2.3 Cell-Free Reaction.....</b>	<b>26</b>
<b>3.2.4 Image Acquisition and Analysis.....</b>	<b>27</b>
<b>3.3 Results.....</b>	<b>28</b>
<b>3.3.1 The Robustness of the Reported Microfluidic Device .....</b>	<b>28</b>

3.3.2 The Dynamic Range of the Reported Microfluidic Device.....	31
3.3.3 Characterization of Cell-Free Reactions with Designed Microfluidic Devices .....	33
3.4 Discussion .....	36
<b>4.0 Cell-Free Synthetic Biology Enabled Perception-Action Behavior Modules on Biohybrid Microrobots .....</b>	<b>39</b>
4.1 Introduction .....	40
4.2 Materials and Methods .....	42
4.2.1 Materials .....	42
4.2.2 Molecular Algorithm Construction.....	43
4.2.3 Microrobot Assembly.....	44
4.2.4 Cell-Free Reaction.....	44
4.2.5 Observation Chamber Preparation.....	45
4.2.6 Material Behavior Observation .....	46
4.2.7 Image and Statistical Analysis .....	46
4.3 Result .....	47
4.3.1 Design of Cell-Free Platform to Build Biohybrid Microrobots .....	47
4.3.2 Perception-Action Enabled via Surface Chemistry. ....	51
4.3.3 Boolean Logic Gate Module Enabled via Synthetic Biology.....	54
4.4 Discussion & Conclusions .....	58
<b>5.0 Cell-Free Synthetic Biology Enabled Communication Modules and Collective Behaviors on Biohybrid Microrobots.....</b>	<b>60</b>
5.1 Introduction .....	60

<b>5.2 Materials and Methods .....</b>	<b>62</b>
<b>5.2.1 Materials .....</b>	<b>63</b>
<b>5.2.2 Molecular Algorithm Construction.....</b>	<b>63</b>
<b>5.2.3 Microrobot Assembly.....</b>	<b>64</b>
<b>5.2.4 Cell-Free Reaction.....</b>	<b>64</b>
<b>5.2.5 Observation Chamber Preparation.....</b>	<b>65</b>
<b>5.2.6 Material Behavior Observation .....</b>	<b>66</b>
<b>5.2.7 Image and Statistical Analysis .....</b>	<b>66</b>
<b>5.3 Result .....</b>	<b>67</b>
<b>5.3.1 Communication via Exchanging Biochemical Information Carriers. ....</b>	<b>67</b>
<b>5.3.2 Collective Behavior Among Cell-Free Microrobots. ....</b>	<b>70</b>
<b>5.4 Discussion &amp; Conclusions .....</b>	<b>73</b>
<b>6.0 Conclusion and Outlook.....</b>	<b>75</b>
<b>6.1 Freeze-Dried Cell-Free Platform for Microrobot Portability .....</b>	<b>75</b>
<b>6.2 Integration with Molecular Robots.....</b>	<b>77</b>
<b>Appendix A Supplementary Materials for Microfluidic Devices for Cell-Free Reaction Characterization.....</b>	<b>80</b>
<b>Appendix A.1 Step-by-Step Protocol .....</b>	<b>80</b>
<b>Appendix A.1.1 Fabrication and Characterization of Microfluidic Devices .....</b>	<b>80</b>
<b>Appendix A.1.2 Cell-Free Reaction .....</b>	<b>80</b>
<b>Appendix A.1.3 Image Acquisition and Analysis .....</b>	<b>80</b>
<b>Appendix A.2 No Fluorescent Interference was Observed Between Channels in     Designed Microfluidic Devices. ....</b>	<b>81</b>

Appendix A.3 P70a-deGFP Positive Control Linear Fragment.....	81
<b>Appendix B Supplementary Materials for Perception-Action Behavior Modules on</b>	
<b>Biohybrid Microrobots .....</b>	<b>83</b>
<b>Appendix B.1 pTXTL-PLtetO1-deGFP .....</b>	<b>83</b>
Appendix B.1.1 Primers for pTXTL-PLtetO1-deGFP .....	83
Appendix B.1.2 pTXTL-PLtetO1-deGFP Plasmid Sequence .....	84
Appendix B.1.3 Linear pTXTL-PLtetO1-deGFP Fragment Sequence.....	87
<b>Appendix B.2 pZS4Int-tetR.....</b>	<b>88</b>
Appendix B.2.1 Primers for pZS4Int-tetR.....	88
Appendix B.2.2 pZS4Int-tetR Plasmid Map and Sequence .....	89
Appendix B.2.3 Linear pZS4Int-tetR Fragment .....	93
<b>Bibliography .....</b>	<b>95</b>

## List of Tables

<b>Appendix Table 1. Primer list for PLtetO1-deGFP.....</b>	<b>83</b>
<b>Appendix Table 2. Primer for pZS4Int-tetR.....</b>	<b>88</b>

## List of Figures

<b>Figure 3-1. Microfluidic devices for cell-free reaction characterization. ....</b>	<b>23</b>
<b>Figure 3-2. Characterization of the reported microfluidic device robustness with CF<sup>®</sup>488A. .....</b>	<b>30</b>
<b>Figure 3-3. The dynamic range of the designed microfluidic device.....</b>	<b>32</b>
<b>Figure 3-4. Characterization of cell-free reactions with various genetic circuit template concentrations within the designed microfluidic device.....</b>	<b>35</b>
<b>Figure 4-1. Biohybrid microrobot with cell-free synthetic biology enabled behavior modules. .....</b>	<b>42</b>
<b>Figure 4-2. Design of cell-free platform to build stimuli-responsive microrobots.....</b>	<b>48</b>
<b>Figure 4-3. Quantification of the fluorescent output signal generated by various particles anchored with or without DNA. ....</b>	<b>49</b>
<b>Figure 4-4. Quantification of the fluorescent output signal generated by microparticles anchored with various DNA template concentrations.....</b>	<b>50</b>
<b>Figure 4-5. Cell-Free microrobots with Boolean logic gates enabled via surface chemistry. .....</b>	<b>52</b>
<b>Figure 4-6. Quantification of the fluorescent response of the reported microrobots with Biotin NOT gate in various biotin concentrations. ....</b>	<b>54</b>
<b>Figure 4-7. Microrobots with tetR NOT Gate enabled via synthetic biology. ....</b>	<b>55</b>
<b>Figure 4-8. Quantification of the fluorescent response of microrobots with tetR NOT gate in various tetR concentrations. ....</b>	<b>56</b>
<b>Figure 4-9. Microrobots with aTc Buffer enabled via synthetic biology. ....</b>	<b>57</b>

<b>Figure 4-10. Quantification of the fluorescent response of microrobot with aTc Buffer in various aTc concentrations. ....</b>	<b>58</b>
<b>Figure 5-1. Communication via exchanging biochemical information carriers. ....</b>	<b>68</b>
<b>Figure 5-2. Quantification of the fluorescent output signal generated by microrobots labeled with Atto590-Biotin.....</b>	<b>69</b>
<b>Figure 5-3. A Collective behavior among microrobots.....</b>	<b>71</b>
<b>Figure 5-4. aTc potentially hinders cell-free reaction efficiency. ....</b>	<b>73</b>
<b>Appendix Figure 1. No fluorescent interference was observed between channels in designed microfluidic devices. ....</b>	<b>81</b>
<b>Appendix Figure 2. P70a-deGFP linear fragment map. ....</b>	<b>81</b>
<b>Appendix Figure 3. pTXTL-PLtetO1-deGFP plasmid map. ....</b>	<b>84</b>
<b>Appendix Figure 4. Linear PLtetO1-deGFP fragment. ....</b>	<b>87</b>
<b>Appendix Figure 5. pZS4Int-tetR plasmid map.....</b>	<b>89</b>
<b>Appendix Figure 6. Linear pZS4Int-tetR fragment. ....</b>	<b>93</b>

## Preface

I would like to gratefully acknowledge the support and guidance I have received from my mentor, Professor Warren C. Ruder. Only through his guidance and support was I able to begin and complete these exciting projects. Likewise, I would like to acknowledge the guidance I have received from Professor Mo R. Ebrahimkhani, Professor Natasa Miskov- Zivanov, and Professor W. Seth Childers, for their help and guidance in completing my research.

I would like to thank my colleagues and also my friends in lab who have inspired me, collaborated with me, laughed with me, traveled with me, and accompanied me over the last five years, including Keith Heyde, Michael Behrens, Ming-Cheng Chen, Haley Fuller, and all the others who have helped me along the way. Special thanks to my dear doggie friends, Logan and Beaux, who always cheer me up with their love and affection.

I am fortunate to have my family and friends around me for everything leading up to this moment. I would like to thank my grandma, Mom and Dad, my two sisters, Auntie Ann, my Pittsburgh family, C, C, and A, my pillow and bed, and everyone else. I cannot do this without their love and support.

This work was funded by federal agencies of the USA, including the National Institutes of Health through the Director's New Innovator Award No. DP2-GM132934, the National Science Foundation, Grant No. DMR 1709238, and the Air Force Office of Scientific Research, Grant No. FA9550-18-1-0262.

## 1.0 Introduction

Microrobots with unique features and functions are a promising technology in medical robots, especially for applications in drug delivery, precision surgery, detoxification, and diagnosis [1, 2]. Their miniaturized size allows operations within the whole human body, leading to therapies down to the cellular level and offering localized diagnosis and treatment with greater precision and efficiency [1]. The potential of biohybrid microrobots for medical application is demonstrated by magnetic microparticle-based robots for tackling biomedical problems, such as active drug delivery [3, 4] and image-guided therapy [5]. However, their miniaturized size confines their ability to multitask. A robot swarm can resolve this limitation by having individual robots working collectively, which can emulate high adaptability and enhance tasking capabilities and flexibility [6, 7].

Nowadays, microrobot swarm behaviors rely heavily on human feedback [3, 7]. Autonomous robot swarms capable of self-directed targeting, tracking, and delivery remain a challenge at the microscale [3, 7]. Perception-action modules, the ability to analyze complex surroundings and respond accordingly, make up the foundation for autonomous robotic behavior that allows these microrobots to function in unstructured environments [3]. The next step of building an autonomous microrobot swarm is communication behavior. Communication enables these perception-action modules to be executed collectively, resulting in individual robots acting together and accomplishing more significant tasks through collective robotic behaviors [7, 8, 11]. While robot autonomy at the macroscale is built on electronics, a platform to build the same level of autonomy is left to be identified in microrobots. Integrating onboard behavior modules into

microrobot that enables perception-action and communication behaviors is therefore desirable and essential.

Synthetic biology has engineered cells with complex perception-action behaviors via rewiring and repurposing biological components [8]. Inspired by electrical engineering, synthetic biology has developed a variety of genetic circuits reminiscent of electronic circuits in biological systems. Since logic gates are fundamental building blocks of digital electronics, essential Boolean logic gates and memory units were some of the first synthetic circuits created in living cells [9, 10]. The first engineered genetic circuit, the toggle switch, demonstrates a digital circuit-like behavior and can serve as memory units in bacteria by switching the host between on- and off-states [11]. Next, digital circuits such as counters were constructed in cells [12], paving the way to realize computational devices in biological systems. Recently, a protein-based central processing unit (CPUs) was demonstrated to run multiple molecular algorithms, including binary arithmetic, which provides the potential to do large-scale biocomputing inside cells [13].

Furthermore, communication behaviors have been implemented via synthetic biology to build artificial multicellular consortia capable of collective behaviors, such as artificial quorum sensing [14] and biocomputing [15, 16]. These communication modules utilize transcriptional and translational regulation systems as information carriers [14, 15]. Engineered cells equipped with simple perception-action modules can work collectively and perform complex computations via communication between each other [15].

Researchers have embraced synthetic biology as robot behavior modules. Kumar and colleagues utilized genetic toggle switches as sensors, signal processors, and memory units in microrobots [17]. Apart from using genetic toggle switches in microrobots, macroscale robots can leverage synthetic biology tools as their perception-action modules. Previous work in our lab has

demonstrated an *in silico* model of using engineered bacteria equipped with genetic toggle switches to maneuver a biomimetic, macroscale robot [18]. Inspired by microbiome-host interactions, we created an *in silico* model of a microbiome consisting of engineered cells carrying synthetic genetic circuits, together with a robotic host housing an onboard microfluidic chemostat and microscope. Apart from the abovementioned examples, genetically engineered cardiomyocytes [19], skeletal muscle [20, 21], and bacteria [22, 23] have been used as perception-action modules for robots.

The use of whole cells as the chassis for autonomous behavior modules requires laborious genetic engineering and suffers from unpredictable interplays between designed and natural systems due to the complex environment within living organisms [24]. Cell-free synthetic biology provides a platform to implement these circuits without the aforementioned limitations. Consisting of molecular machinery extracted from cells, cell-free systems were initially designed for *in vitro* protein synthesis by containing essential enzymes for transcription and translation, allowing the synthetic genetic circuit to be transcribed and translated without cells [24]. Furthermore, the flexibility of cell-free platforms enables customization and optimization of reactions [25]. Moreover, synthetic genetic material can be directly added to cell-free reactions at desired concentrations, providing precise control over gene expression by eliminating endogenous variables introduced while putting genetic constructs into cells [26]. Hence, cell-free platforms offer an ideal testbed for developing genetic circuits and potentially for controlling microrobots.

In this dissertation, we report a cell-free platform to build onboard behavior modules on microrobots. Leveraging the capability of synthetic biology and the cell-free platform for creating complex behaviors, microrobots could acquire the ability to sense, analyze, and respond to complex environments. Also, the microrobots we propose can communicate with each other and

form a robot swarm with collective behaviors, addressing the limitation posed by their miniaturized size. This work advances the development of autonomous miniaturized clinical tools with potential use in the human body for precise and efficient diagnosis and treatment.

## **1.1 Dissertation Contributions**

Chapter 2 presents a brief overview of biohybrid robots at small scales and highlights how cell-free synthetic biology can advance the development of robot autonomy at micro-, nano- and molecular levels.

Chapter 3 presents a straightforward yet robust microfluidic device for cell-free reaction characterization that provides the ability to quantify and visualize synthetic genetic circuit behaviors. The device was employed to characterize the reported cell-free microrobot behaviors and can be generalized to characterize cell-free reactions with fluorescent outputs.

Chapter 4 reports the cell-free platform for building behaviors modules on biohybrid microrobots. Three cell-free platform-based perception-action modules have been developed and implemented on microrobots as a proof of concept. The perception-action systems will detect small molecules such as biotin and tetracycline (aTc) by leveraging surface chemistry and genetic circuits. Microrobots with perception-action modules can perceive disease-related markers and respond with therapeutic delivery.

Chapter 5 reports using the cell-free platform to build a communication interface between microrobots with cell-free synthetic circuits to perform sophisticated collective behaviors. The communication behaviors allow for the information exchange via biochemical molecules as

carriers between microrobots. Communication behavior is the first step for microrobots to perform sophisticated collective behavior exemplified by logic circuits capable of analyzing multiple inputs.

Chapter 6 discusses the conclusion and outlook of the cell-free platform for building microrobot autonomy presented in this dissertation. By integrating synthetic circuit-based behavior modules with cell-free reactions and biohybrid microrobots, we anticipate that this dissertation will positively impact this by enabling autonomous miniaturized clinical tools with potential use in the human body for precise and efficient use diagnosis and treatment.

## **2.0 Background**

### **2.1 Overview of Robots at A Small Scale**

#### **2.1.1 Robots at Microscale and Nanoscale**

Microrobots and nanorobots are booming technology for various biomedical applications, ranging from targeted drug delivery to minimally invasive surgery [1, 2, 27, 28]. These tiny robots can cruise through the whole human body, performing medical tasks down to cellular level and offering localized diagnosis and treatment with greater precision and efficiency [29]. For example, small devices capable of locomotion within physiological relevant liquid environments showcase the mobility and accessibility of miniaturized machines [30, 31]. For another example, magnetic, microparticle-based robots have demonstrated their ability in stimuli-responsive drug delivery [3, 32] and image-guided therapy [33]. Even though the microrobots are currently not yet running around in patient bodies as depicted in movies, the recent advance in microrobot and nanorobot actuation has brought the sci-fi scenario closer to reality [34, 35]. However, robot autonomy, the ability to sense and respond to complex environments such as human bodies, remains a missing piece in these miniaturized robots.

Autonomous robots require three essential components: an actuator, a sensor, and a processor [28, 36]. Actuators power robot actions and mobility. Sensors detect the environmental information while processors analyze the gathered information and respond according to predetermined algorithms. The ability to sense, analyze, and react to complex environments through a process in robotics known as a perception-action loop is essential for building

autonomous robotic systems [28]. However, while robot autonomy relies on electronics at macro scales, a platform for building robot autonomy at small scales remains to be identified.

Using the inherently available onboard actuation and sensing mechanisms of biological components, biohybrid robots become an attractive candidate for autonomous microrobot and nanorobot systems for biomedical applications [28, 35]. Biohybrid microrobots and nanorobots compose of biological components, such as microorganisms or DNA, and artificial components, such as magnetic microparticles. The biological and artificial components are usually joined together by noncovalent interactions, such as biotin-streptavidin interaction [29, 35]. For example, Maier and coworkers developed magnetic microswimmers with the DNA-based flagellar bundles, similar to self-propelling peritrichous bacteria [37]. The DNA flagella were attached to magnetic iron oxide microparticles through hybridizing complementary DNA strands and biotin-streptavidin interaction. They actuated the biohybrid microrobots by the homogeneous magnetic field rotating perpendicular to the swimming direction [37]. For another example, Alapan *et al.* utilized the biotin-streptavidin interaction to anchor bacteria with red blood cells carrying drug-loaded superparamagnetic iron oxide nanoparticles [38]. As a result, the bacteria provide autonomous and onboard propulsion while the magnetic nanoparticles serve as external guidance [38].

Biohybrid microrobot and nanorobot have validated their diagnostic and therapeutic potentials through *in vivo* studies. The first *in vivo* study was carried out by Akin and coworkers using biohybrid microrobots delivering DNA-based drug molecules inside mice [39]. The biohybrid microrobot consists of nanoparticles conjugated with plasmid encoding fluorescent proteins and the bacteria as the actuator. The microrobots were internalized when incubated with cells, and the plasmid was released and expressed in cells. Then, they injected the biohybrid

microrobot carrying GFP-encoding plasmids into mice. As a result, they showed the biohybrid microrobots effectively delivered the DNA cargoes and eventually transfected the cells demonstrated by GFP fluorescent images expressed three days after the treatment of the mice [39]. Their research pioneered using biohybrid microrobots to deliver nucleic acid cargoes for applications such as targeted gene therapy.

For another example, *E. coli* probiotic strain-based microrobots, such as microrobots consisting of *E. coli* Nissle 1917, were used to deliver anticancer drug molecules and molecular imaging in tumor environments [40, 41]. Xie and colleagues built the biohybrid microrobots by conjugating doxorubicin, an anticancer drug, onto bacterial cell membranes through conjugation methods enabling an acid-responsive release of the drug molecules in the tumor environment [40]. Then, they injected the reported biohybrid microrobots into mice with 4T1 tumor models and investigated their accumulation inside the tumor environment. The results demonstrated effective tumor growth inhibition, tumor cell apoptosis, and prolonged survival in mice. Furthermore, the biohybrid microrobots were removed with an antimicrobial treatment, addressing the safety concern of using biohybrid microrobots inside animal bodies [40].

### **2.1.2 Molecular Robots**

Biohybrid microrobots and nanorobots have shown their potential for *in vivo* applications, such as targeted drug delivery, because of their ability to provide great precision down to the cellular level. Apart from microrobots and nanorobots, molecular robots will be an exciting option for achieving cellular-level diagnosis and therapy.

Molecular robots can be categorized into two major categories based on their composition, non-biological and biological. Catenanes and rotaxanes, two primary non-biological molecular

robots, have dominated the field of non-biological machinery since the 1990s [42]. Catenanes consist of two interlocking rings, with one ring gliding around the other ring. Rotaxanes consist of a cyclic molecule threaded onto an axle molecule. The structure of catenanes and rotaxanes enables motions of one component relative to the other component. The molecular dynamic properties of catenanes and rotaxanes have been exploited to build miniaturized versions of macro machines, such as nanomotors [43] and pumps [44].

Biological molecular machines exploit characteristics of biological molecules as actuators and sensors. For example, Famulok and colleagues employed transcription machines to build a DNA nanoengine [45]. Similar to catenane-based motors, the nanoengine consisted of two interlocked DNA rings. An engineered DNA polymerase can attach to the DNA rings and produce RNA transcripts that are used to guide machine movement along predefined DNA tracks [45]. Another example is using protein-protein interactions to build molecular machines with actuators and sensors. By exploiting the interaction between ligands and cell-surface receptors, Tour and colleagues built a ligand-attached molecular machine that can drill through target cell membrane at specific regions [46].

Because of its unique sequence-dictated structural and functional features, DNA has been widely adopted to construct molecular machines and robots. Their selective and sensitive responses to small molecules, proteins, and nucleic acids allow DNA structures to respond to various input molecules [47]. Church and colleagues developed an autonomous molecular robot based on DNA aptamer-encoded logic gates, enabling it to respond to a wide array of inputs [48]. When the autonomous robot perceived environmental cues, the robot processed inputs according to implemented logic gates and decided whether or not to dropoff payloads [48].

Furthermore, DNA is highly stable and programmable, allowing precise and predictable nanostructure designs via base-pairing rules. By designing a sequence of DNA building blocks, these DNA fragments can self-assemble into almost any arbitrary structure on the nanoscale level. This process is called DNA origami. Through dynamic interactions between building blocks, these DNA structures can change shapes in response to input stimuli via sequence-specific binding [49]. For example, via DNA origami, DNA-assembled multicomponent systems imitating macroscopic gear trains, such as rack-and-pinion gearing and epicyclic gearing, can be produced at nanoscale [50].

In addition to forming arbitrary structures, the base-pairing rule can be used to implement perception-action behaviors in autonomous molecular robots. Qian and colleagues developed an autonomous DNA robot capable of performing cargo-sorting tasks [51]. Sorting cargo is a complicated task, including steps like picking up the cargo, recognizing it, and discarding it in the correct storage place. Composed of one arm, one hand, and a single-stranded DNA walker, the DNA robot can stroll around a DNA origami surface via a reversible strand-displacement reaction. While exploring the DNA origami surface, the robot picked up different encountered cargo and delivered them to designated areas via an irreversible strand-displacement reaction between robot and surface. After dropping off cargo, the DNA robot kept walking around randomly and repeated the process until all cargo was sorted out. In this way, the robot perceived environment cues, analyzed inputs and made actions all based on algorithms implemented via base-pairing property. To test the robot, they put it on DNA origami surfaces with six disorganized cargoes. The robot sorted six molecular cargoes into two categories and put the cargoes at the correct locations within 24 hours. The researchers suggested that multiple DNA robots working simultaneously can reduce

the task-completion time. The cargo-sorting DNA robots have potential applications in manufacturing molecular devices, such as molecular robots.

Even though sequence-specific actuation can be precisely designed, DNA hybridization is a slow process. To increase translational speed, recently, Salaita and colleagues developed a DNA motor that can run at up to 100 nanometers per minute, which is ten times faster than previous motors [52]. Simmel and colleagues built a DNA origami robot arm that can be directly controlled by external applied electric fields to bypass the slow DNA hybridization process [53]. The 25 nm-long robot arm was made out of DNA double helices bundled together. The robot arm was placed on a 55 nm-by-55 nm DNA origami plate. The arm was connected to the plate via a flexible single-stranded DNA, allowing the arm to rotate freely relative to the platform. Since DNA is a charged molecule, DNA moves in response to applied electric fields. The researchers utilized this property to control the DNA robot arm with an externally applied electric field. Protruding single-stranded DNA monomers were placed on the platform to latch down the molecular robot arm temporarily, achieving precise control of the DNA arm. As a result, a computer-controlled electric field switched the molecular robot arm between predefined positions within milliseconds. Next, the team used the developed molecular robot arm to transport molecules and nanoparticles over tens of nanometers, which can be useful for controlling photonic and plasmonic processes. The team proposed that adopting nanostructure electrodes may enable control over individual robot arms, which have the potential to become molecular mechanical memory.

### **2.1.3 Robot Swarm**

Small-scale biohybrid robots feature mainly with their miniaturized size, their mobility, and some degree of autonomy provided by biological components. However, while their

microscopic size and mobility could enable them to navigate and locally deliver therapeutics in previously inaccessible areas, their miniaturized size also limits their ability to multitask and confines them to predetermined tasks. A robot swarm can resolve this limitation by having individual robots working collectively, which can emulate high adaptability and enhance tasking capabilities and flexibility [6, 7].

Robot swarms allow straightforward modular robotic units to be reconfigured into a team depending on the task [28, 54]. The paradigm has existed in nature, such as a school of fish and insects working together to achieve tasks unattainable to individuals. Similarly, individual robot units can collaborate and coordinate to complete a complex task and adapt to changing environments, achieving collective intelligence [54]. Apart from perception-action behaviors, communication ability is essential to a robot swarm and should be embedded in the feedback loop of individual robots. Thus, perception-action-communication loops are crucial to designing multifunctional, adaptive robot swarms. Unfortunately, there are no systematic approaches for designing such multidimensional feedback loops across large groups.

Currently, robot swarm collective behaviors focus mainly on actuation, such as self-assembly, shape-forming, and group motions [54-56]. For example, Xie and colleagues developed magnetic microparticle swarm robots exhibiting various intriguing collective behaviors, ranging from dynamic self-organization to coherent motions [55]. The hematite colloidal particle-based microrobots can quickly and reversibly transform between liquid, chain, vortex, and ribbon-like shapes. The chain mode can pass through a narrow channel, while the vortex mode can handle heavy cargo. This magnetic particle microrobot swarm can address environmental variations or multitasking requirements by switching between different collective modes. The microrobot

swarm has the potential to serve as a functional microrobot system for unstructured environments like the human body [55].

At the molecular level, Keya and colleagues used the base-pairing property of DNA in controlling local interactions between molecular robots to create robot swarms [57]. Using DNA as an input signal, molecular robots glide on a kinesin-coated substrate and form a large swarm. All individuals moved in the same direction determined by the polarity of microtubules. The DNA inputs were used not only for swarm formation but also for dissociating the swarms into single molecular robots. The DNA signal prompted the groups of molecular robots to separate into single robots through strand displacement reaction of the complementary DNA of neighbor robots. Furthermore, Keya and colleagues showed various swarm behaviors such as forming translational and circular motions by tuning the microtubule stiffness [57].

Although robot swarms' motion and global control have been demonstrated, the perception-action-communication loops and collective behavior rely heavily on human feedback. In addition, the autonomous interactions between neighboring individual robots and swarm coordination have not been investigated or engineered.

## **2.2 Overview of Synthetic Biology and Robotics**

### **2.2.1 Synthetic Biology and Robots**

Nature provides abundant examples of such autonomous systems, from macrophages chasing pathogens to animals preying on their next meal. Engineers often turn to nature for inspiration. For example, supplying power to bioelectronics in soft robots is often a limiting factor

[58]. Inspired by the electric organ of electric eels, Mayer and colleagues developed a power source from stacked hydrogels. Using ion gradients between polyacrylamide hydrogel compartments and a repeating sequence of cation- and anion-selective hydrogel membranes, their system can generate 110 volts in open circuits [58]. This soft power source can be used to power bioelectronics in soft robots without sacrificing stretchability.

Nature provides not only inspiration but also building blocks for robots. For example, in a bio-inspired swimming robot ray developed by Parker and colleagues, cardiomyocytes powered the actuation and served as a perception-action module [19]. The way batoid fish swim is highly energy-efficient, which is a desirable trait in robotic systems. To mimic how batoid fish swim, they simulated their musculoskeletal structure by sandwiching a gold skeleton between two elastomer layers. On the interstitial elastomer layer, fibronectin was printed to guide rat cardiomyocytes growing in a specific pattern similar to living ray muscles. With a single layer of heart muscle cells capable of downward contraction, the robot ray used the gold skeleton to actuate its fins, enabling chordwise front-to-rear undulatory motions. To mimic the neural system controlling the sequential activation of fin muscles in real rays, the researchers genetically engineered cardiomyocytes to create heart muscle cells that only contracted in response to blue light. Using genetically engineered cardiomyocytes, the robot ray swam at various speeds and maneuvered around obstacles by modulating light frequency and independently actuating right and left fins. In the example of the ray, the cardiomyocytes provided the perception-action module, sensing light inputs (perception) and responding by waving the ray fins (action).

Inspired by electrical engineering, synthetic biology has developed a variety of genetic circuits reminiscent of electronic circuits in biological systems, such as the toggle switch [11]. Since logic gates are fundamental building blocks of digital electronics, essential Boolean logic

gates and memory units were some of the first synthetic circuits created in living cells [9, 10]. Next, digital circuits such as counters [12] were constructed in cells, paving the ways to realizing computational devices in biological systems. Recently, a protein-based central processing unit (CPUs) was demonstrated to run multiple molecular algorithms, including binary arithmetic, which provides the potential to do large-scale biocomputing inside cells [13].

Synthetic biology has been adopted to provide perception-action behaviors in robots at the macroscale and microscale. Apart from the cardiomyocytes in the robotic ray discussed [19], genetically engineered skeletal muscle [20, 21] and bacteria [22, 23] have been used as perception-action modules for robots. For example, Kumar and colleagues utilized genetic toggle switches as sensors, signal processors, and memory units, in their biohybrid microrobots [17]. In this genetic toggle switch, green fluorescent protein (GFP) was synthetically engineered in parallel with *lacI* transcription and used as an optical reporter molecule. The researchers incorporated engineered bacteria carrying this genetic toggle switch on microrobots and deployed them to detect UV light in a workspace. When microrobots returned to base, the engineered bacteria onboard reported whether the visited area was exposed to UV light by the green fluorescence readout [17].

Apart from using genetic toggle switches in microrobots, macroscale robots can adopt synthetic biology tools as their perception-action loop modules. Heyde and Ruder proposed using engineered bacteria equipped with genetic toggle switches to maneuver a biomimetic, macroscale robot [18]. Inspired by microbiome-host interactions, they created an *in silico* model of a microbiome consisting of engineered cells carrying synthetic genetic circuits, together with a robotic host housing an onboard microfluidic chemostat and microscope. The onboard microfluidic chemostat was used to mimic a microbiome environment within an organism. Heyde and Ruder used this system to simulate how various genetically engineered bacteria could affect

robot behavior. With the increased complexity of genetic circuits, a variety of behaviors emerged, such as stalk-pause-strike predation. Their model provides a tool to investigate host-microbiome interactions and offers a novel paradigm to create perception-action loops in autonomous robots.

### **2.2.2 Cell-Free Synthetic Biology and Robots**

While robots at the macroscale and microscale have embraced synthetic biology as their perception-action modules, most of the examples mentioned above utilized whole cells to implement these synthetic biology-based sensors and processors. The use of whole cells as chassis requires laborious genetic engineering and suffers from an unpredictable interplay between designed and natural systems due to the complex environment within living organisms [24]. Cell-free synthetic biology provides a platform to execute these circuits without the limitations mentioned above. Consisting of molecular machinery extracted from cells, cell-free systems were initially designed for *in vitro* protein synthesis. Cell-free systems contain essential enzymes for transcription and translation, allowing the synthetic genetic circuit to be transcribed and translated without cells.

Furthermore, the flexibility of cell-free platforms enables customization and optimization of reactions, such as adding proteins or small molecules to improve synthetic genetic circuit performance [25]. A holistic approach has been developed and performed to optimize cell-free platforms and yields higher protein expression level than classical cell-free systems [59]. Hence, cell-free platforms offer an ideal test-bed for developing genetic circuits and potentially for controlling robots at small scales.

Logic-operating synthetic genetic circuits are also available in cell-free platforms. Even though some synthetic genetic circuits may be limited to specific cell types, recent developments

in synthetic genetic circuits improve transferability. For example, Baker and colleagues developed a set of logic gates, including gates with multiple inputs that function in cell-free systems, yeast, and human cells [60]. These protein-based logic gates enable faster responses than synthetic circuits based on transcription systems. Additionally, the tunable nature of cell-free platforms enables modification to mirror a specific cell environment, rendering the possibility to execute genetic circuits that are not designed for cell-free platforms [25]. Moreover, genetic circuits can be directly added to cell-free reactions at desired concentrations, providing precise control over gene expression by eliminating endogenous variables introduced while putting genetic constructs into cells [26].

Cell-free platforms provide a new paradigm for building autonomous robots with actuator and perception-action behaviors. For example, Simmel and colleagues utilized a cell-free oscillator to operate a DNA-based nanomechanical device termed the DNA tweezer [61]. Comprised of two double-helical domains connected by a hinge, this DNA tweezer has two single-stranded areas capable of binding to their individual target and, therefore, closes the tweezer. While oscillators generate clock signals in electronics, oscillators in cells control the timing of cellular processes. To create a molecular clock for timing downstream events, the team turned to synthetic circuits and cell-free platforms. The synthetic circuits in this work consisted of gene templates called genelets which were used to transcribe RNA molecules. A simple oscillator circuit consisted of genelets SW21 and SW12 with an inhibiting RNA, rI2, and an activating RNA, rA1. When switch SW 21 was ON, the cell-free platform transcribed an inhibiting RNA, rI2. The rI2 inhibited transcription of switch SW12 by removing part of its promoter region. rI2 turned switch SW12 off, resulting in no transcription of activating RNA, rA1. The activating RNA, rA1, activated transcription from SW21 by releasing the promotor region in SW21.

To minimize downstream load effect on the oscillator circuit, the researchers added an insulator to the genetic circuit, reminiscent of an amplifier stage in electric circuits. The insulator genelets, Ins, operated in parallel with an oscillator switch SW12, which allowed for Ins activation by A2 and inhibition by rI2. The insulator produced a new RNA species, InsOut, which opened the tweezers previously closed by the DNA strand, TwCIs. Next, the TwCIs·InsOut complex was degraded, creating free TwCIs. The insulator stage enabled the oscillator to drive the opening and closing of more tweezers while isolating tweezer operation from oscillators. Recently, Franco and colleagues used a similar cell-free oscillator module to control DNA molecular machine self-assembly [62]. As building blocks, DNA double-crossover tiles can self-assemble into a DNA nanotube. On each building block, there was a single strand area that can bind to an invader strand. The tile-invader complex resulted in the disassembly of DNA nanotubes. In this oscillator, the insulator produced the invader strand that caused the disassembly of DNA nanorobots. These projects demonstrate using cell-free synthetic tools to drive molecular robot behaviors with high-level complexity.

Instead of using cell-free circuits to drive perception-action behaviors, Luo and colleagues developed an onboard metabolism system on DNA robots with a cell-free platform [63]. Through the cell-free based artificial metabolism, a DNA material can autonomously self-assemble and disassemble, like a living organism growing and decaying. Even though cell-free platforms were not directly used in this work, Rondelez and colleagues proposed to build memory, perception-action, and communication via putting synthetic DNA circuits on microparticles in an enzymatic solution similar to the cell-free platform [64]. In this way, Rondelez and colleagues were able to produce collective behaviors among microparticles, such as retrieving information over long distances.

From macroscale to molecular robotics, robots at various scales have taken advantage of synthetic biology tools to achieve complex perception-action and communication behaviors. Synthetic biology-based perception-action-communication loops are of particular interest to robots at a small scale since they can be readily integrated at the molecular size. We have highlighted a myriad of synthetic genetic circuits reminiscent of electronic digital circuits available. The complexity of robot behaviors can improve with advances in biocomputing synthetic genetic circuits. Synthetic biology offers behavior modules, which we believe, can advance robot autonomy from the microscale to the molecular level. Presently, synthetic biologists have gene-based versions of CPU. In the future, synthetic circuits can confer intelligence and become the control system for autonomous robots.

Cell-free systems power synthetic genetic circuits without reliance on living cells, extending synthetic biology into the real world. If molecular robots adopt synthetic biology-based tools as their perception-action modules, their movements and functions will no longer be confined to specific reaction criteria. Cell-free systems have freed synthetic biology from lab settings. Likewise, cell-free platforms can help molecular robots step outside the laboratory in the future.

Ultimately, we envision next-generation small-scale robots with greater autonomy will be biohybrid robots containing synthetic biology-based perception-action-communication modules encoded on DNA molecules. Cell-free platforms will power and perform onboard behavior modules. The cell-free biohybrid microrobots reported in this dissertation will be the first step toward building next-generation biohybrid robots at small scales.

### 3.0 Microfluidic Devices for Characterization of Cell-Free Synthetic Biology Reactions

We have discussed how synthetic biology provides potential behavior modules for building autonomous microrobots. Cell-free synthetic biology has emerged as a programmable and rapid tool for implementing and characterizing synthetic genetic circuits. Fluorescent output, a widely adopted parameter for evaluating cell-free genetic circuit performance, was employed to evaluate cell-free synthetic biology enabled microrobot behaviors. In cell-free reactions, the fluorescent output frequently is quantitatively characterized by plate readers that cannot provide visualization of microrobot behaviors. Microfluidic technology has facilitated cell-free synthetic biology development but has focused mainly on experiment automation instead of rapid characterization. Such microfluidic systems involve exquisite manipulation and operation, hindering widespread adoption.

Here, we present a user-friendly and robust microfluidic device to bridge the gap between quantification-only systems and complex microfluidic platforms for cell-free reaction characterization, specifically for rapid cell-free microrobot behavior observation. The identical channels in the reported device allow the characterization of multiple cell-free reactions simultaneously, while the microfabricated markers ensure reproducibility from device to device. Measurement of channels with fluorescent dye suggests excellent performance in characterizing fluorescent output. This microfluidic device enjoys simplicity and flexibility and can be easily integrated with existing microfluidic modules for cell-free reaction characterization and advances cell-free synthetic biology development.

### 3.1 Introduction

Synthetic biology has been widely adopted for multiple applications in the past two decades, especially for biomedical purposes, material production, and exploring fundamental biological principles [18, 65-68]. Synthetic biology rewires and repurposes biological components inside whole cells to perform novel functions in a programmable manner [68]. However, using whole cells as the chassis for synthetic biology suffers from the unpredictable interplay between designed and natural systems due to the complex environment within living organisms [24]. Cell-free synthetic biology offers an alternative to circumvent limitations posted by using cellular hosts and eliminates biosafety concerns and laborious genetic encoding processes [24, 69].

Consisting of molecular machinery extracted from cells, cell-free systems were initially designed for *in vitro* protein synthesis by containing essential enzymes for transcription and translation, allowing the synthetic genetic circuit to be transcribed and translated without cells [24]. (Figure 3-1A) The flexibility of cell-free platforms enables customization and optimization of reactions [25, 70]. Moreover, synthetic genetic material can be directly added to cell-free reactions at desired concentrations, providing precise control over gene expression by eliminating endogenous variables introduced while putting genetic constructs into cells [26]. Hence, cell-free platforms offer an ideal testbed for developing synthetic genetic circuits.

Fluorescent proteins are standard output signals for evaluating cell-free genetic circuit performance because of their abundant options and well-characteristic properties [71]. (Figure 3-1 B) Plate readers are the primary tool for characterizing fluorescent output signals generated by cell-free synthetic genetic circuits [72]. For example, cell-free genetic biosensors that can generate fluorescent proteins in the presence of viruses of interest, such as SARS-CoV-2 [73] and Zika [74], were first screened with plate readers to optimize the sensor design. For another example, genetic

circuits emulating electronic circuit behaviors, such as integral controllers [75] and Boolean logic gates [26], were characterized by fluorescent proteins as outputs with plate readers. However, the characterization is limited to quantifying fluorescent output signals generated by cell-free synthetic biology and cannot provide visualization of cell-free reactions.

Microfluidic platforms have facilitated cell-free synthetic biology development via increased throughputs and improved spatial controls of cell-free reactions [76]. Moreover, microfluidics renders output visualization and the observation of spatial behaviors of cell-free reactions under microscopes [77]. For example, the Bar-Ziv group has utilized microfluidic platforms to demonstrate geometry-controlled cell-free genetic circuits and their biochemical dynamics [78, 79]. Alternatively, microfluidic devices and cell-free reactions were designed to emulate living systems for behaviors, such as communication, self-organization, and development, which advance understanding of underlying biological principles [80]. Also, the ability to manipulate cell-free reactions at a small scale with microfluidics reduces the cost of prototyping synthetic genetic circuits [81]. However, most microfluidic devices proposed for cell-free synthetic biology focused on performing cell-free reactions. Such microfluidic systems involve exquisite manipulation and operation, hindering widespread adoption and can be time-consuming in setting up.

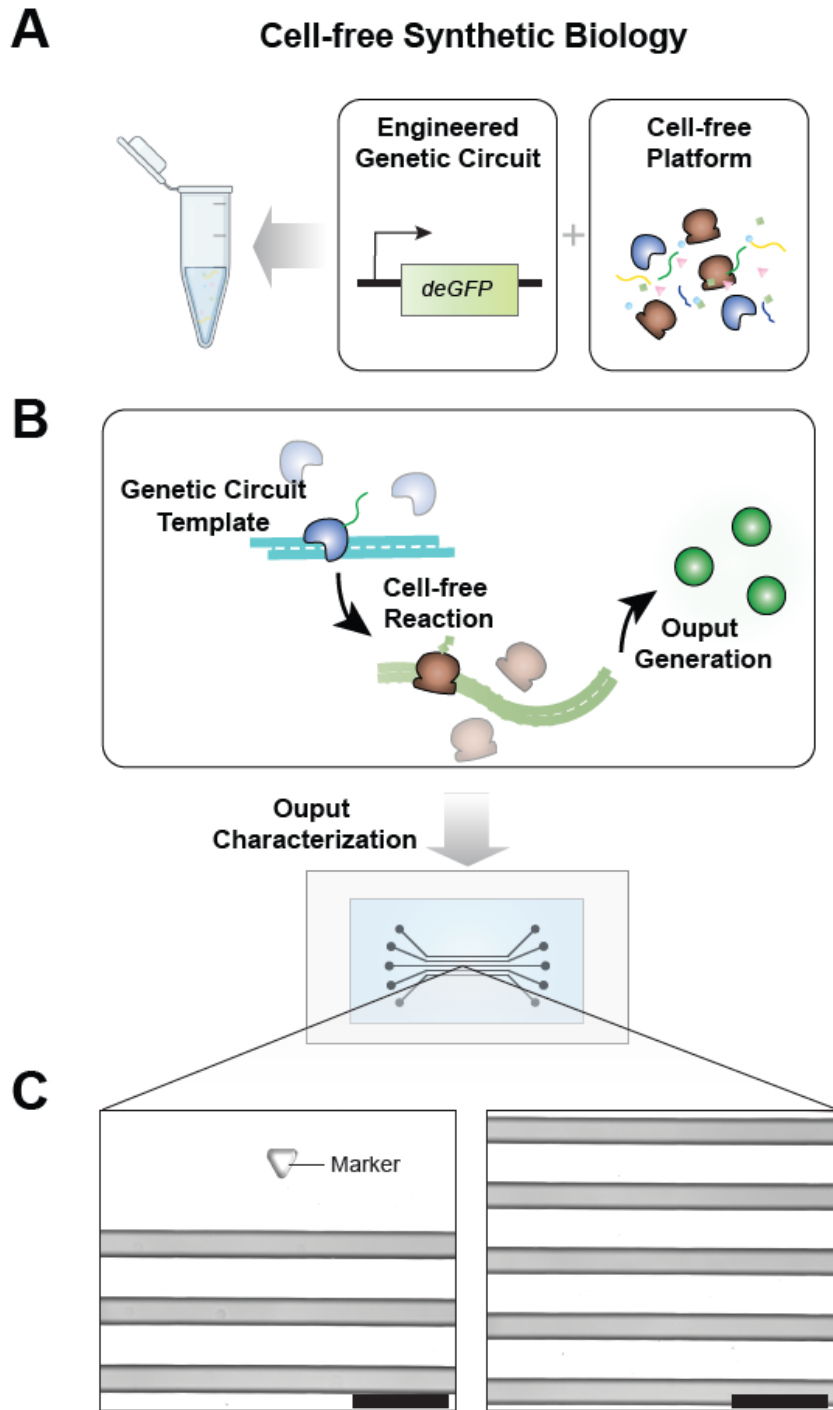


**Figure 3-1. Microfluidic devices for cell-free reaction characterization. (A) Cell-free synthetic biology utilizes cell-free gene expression platforms, which provide rapid and robust tools for prototyping engineered genetic circuits. (B) Cell-free gene expression harvests transcription and translation machinery from cells and generates output. As a robust alternative, microfluidic devices can be used to characterize cell-free reactions.**

**(C) DIC images of the microfluidic devices. The microfabricated marker ensures reproducible results from device to device. Five parallel and identical channels allow simultaneous observation of multiple reactions in a single device. (Scale bar: 200  $\mu\text{m}$ )**

Here, we present a robust yet straightforward microfluidic device for rapid cell-free synthetic biology characterization, which offers quantification and visualization of designed synthetic genetic circuit behaviors. (Figure 3-1C) The uniform channels in the designed device allow the observation of multiple cell-free reactions, enabling a direct comparison between reactions. Microfabricated markers, the triangle structures, are placed next to denote the channel position to ensure robustness and reproducibility. Since fluorescent proteins are widely-adopted outputs in cell-free reactions [71], the channel width and the width between channels were designed to reduce the potential fluorescence interference tailored by the fluorescent level generated with cell-free reactions. (Appendix Figure 1) The simplicity of our design allows the device mold to be easily manufactured with nanofabrication techniques and, potentially, 3D printing technology. Furthermore, the reported microfluidic devices are user-friendly and do not require complex fluid manipulation, allowing users to rapidly characterize cell-free synthetic biology reactions with steps as simple as pipetting.

### **3.2 Methods**

Detailed protocols for the approach described in this article are provided as the Step-by-Step Protocol in Appendix A.1.1 Page 80.

### 3.2.1 Design and Construction of Microfluidic Devices

Master molds for microfluidic devices were prepared via soft lithography. SU-8 photoresist was spin-coated onto a 100 mm silicon wafer (University Wafer, Cat No. 452) to the height of 87  $\mu\text{m}$ . The channel geometry was first specified in Autodesk AutoCAD and then was transferred to a maskless aligner using an acceptable format via Klayout software. The design was lithographically patterned via the maskless aligner (Heidelberg MLA100 Direct Write Lithographer) onto an SU-8 coated wafer. The master mold's surface was characterized using a Bruker DektakXT Surface Profiler. Then, the master mold was silanized with Alfa Aesar™ 1H,1H,2H,2H-Perfluorooctyltrichlorosilane, 97% (Fisher Scientific, Cat No. 78560-45-9).

To make microfluidic devices, polydimethylsiloxane (PDMS) (Sylgard™ 184, Dow Corning) was mixed at a 10:1 base to curing agent ratio and poured over the wafer. The PDMS was degassed in a vacuum chamber and cured in an oven at 65 °C for 1 h. Then, the PDMS was carefully recovered from the wafer and sliced into individual microfluidic devices. Inlet and outlet holes were punched with a 1 mm biopsy punch (Miltex® Biopsy Punch with Plunger). Next, the devices were bonded to glass coverslips (22 × 40 mm) via a plasma cleaner (PDC-32G, Harrick Plasma) for 20 s. The devices were then incubated at 65 °C for 1 h to ensure a tight bond between the glass and the PDMS.

### 3.2.2 Device Characterization

CF<sup>®</sup>488A (Sigma Aldrich) was used to characterize the capability of the designed microfluidic devices to support fluorescent microscopy, due to the similarity of its excitation and emission profiles to green fluorescent protein (GFP). The master stock of CF<sup>®</sup>488A in DI water at

the concentration of 33.75 ng/  $\mu\text{L}$  was stored at  $-20\text{ }^{\circ}\text{C}$ . The CF<sup>®</sup>488A stock (33.75 ng/  $\mu\text{L}$ ) was thawed entirely at room temperature and diluted with DI water to the desired concentration if serial dilutions were performed. Then, 2  $\mu\text{L}$  of CF<sup>®</sup>488A were pipetted into the designed microfluidic devices for fluorescent signal measurement.

### 3.2.3 Cell-Free Reaction

The cell-free protein expression platform used in this work was the myTXTL<sup>®</sup> linear DNA expression kit from Arbor Biosciences. While we used a premade kit, the detailed protocol for making and using the cell-free protein expression system was described in previous publications [26, 82-84]. Briefly, the cell-free reaction has three components – cell extract, buffer, and the DNA template encoding designed genetic circuits. To make cell extract, cells are typically grown to OD<sub>600</sub> 1.5–2.0. Then, cells are lysed via bead-beating in S30A buffer. Beads are removed by running the extract through micro-chromatography columns. Next, essential transcription and translation components, such as core RNA polymerases and transcription factors, are extracted through dialysis using 10k MWCO dialysis cassettes. The cell extract is flash-frozen and stored at  $-80\text{ }^{\circ}\text{C}$ . Finally, a buffer containing amino acids and energy solutions was assembled and calibrated to optimize protein production in cell-free reactions and stored at  $-80\text{ }^{\circ}\text{C}$  [83].

The myTXTL<sup>®</sup> linear DNA Expression kit contains cell-free solutions (Sigma 70 master mix), a premix of cell extract and buffer. We set up cell-free reactions by thawing the Sigma 70 master mix, containing cell extract and buffer. Next, the cell-free solution was gently mixed with DNA template or with DI water as a negative control. The DNA template used in this work was the P70a-deGFP linear DNA fragment (20 nM). The sequence is available at **Error! Reference source not found.** The DNA stock was diluted to desired concentrations with DI water. The

concentration of DNA was adjusted as needed by calculating the molar concentration of the stock and varying the ratio of DI water to DNA during reaction construction. The cell-free reactions were assembled to volumes of 12  $\mu\text{L}$  with 9  $\mu\text{L}$  cell-free solutions and 3  $\mu\text{L}$  DNA templates in 1.5 mL microcentrifuge tubes and incubated at 29 °C for 12 h. Air bubbles should be avoided. The cell-free reactions were put on ice to stop reactions. 2  $\mu\text{L}$  of incubated reactions were pipetted into the designed microfluidic devices for fluorescent signal measurement.

### **3.2.4 Image Acquisition and Analysis**

The microfluidic device was placed onto the stage of a Nikon Eclipse Ti2 microscope and viewed through a 20X objective lens. Images were captured and analyzed with an Andor Zyla 5.5 sCMOS camera and NIS-Elements software (Nikon). Different fluorescence intensities from regions of interest (ROI) with fixed size and position were recorded. The acquired data was normalized to the reference signal intensity. In the robustness experiment, the reference signal intensity was defined as the average fluorescent intensity of all five channels. In dynamic range experiments, the highest CF<sup>®</sup>488A concentration was defined as the reference. In quantifying cell-free reactions,  $3.375 \times 10^{-2}$  ng/ $\mu\text{L}$  CF<sup>®</sup>488A was defined as the reference. All experiments were performed in triplicate and reported as mean +/- standard deviation. One-way ANOVA was performed and a significance level of 0.05 was determined.

### 3.3 Results

#### 3.3.1 The Robustness of the Reported Microfluidic Device

The microfluidic devices reported in this work serve as a straightforward way to characterize cell-free synthetic biology reactions by quantifying fluorescent output and visualizing reactions. Therefore, robustness, defined as giving the same readouts for the fluorescent signal at the same level, is essential and critical for designed microfluidic devices. CF<sup>®</sup>488A was used as a fluorescent signal to test the robustness of the designed devices because of its similarity to GFP in fluorescent spectral profile. While various fluorescent proteins can be used for evaluating cell-free genetic circuits, GFP is the most common candidate and is often used as a standard for quantifying performance of cell-free protein expression platforms [69]. Using CF<sup>®</sup>488A to characterize the reported microfluidic devices provides a validation of their robustness for quantifying and evaluating fluorescent signals such as those produced by cell-free reactions.

The microfluidic devices reported in this work were fabricated by polydimethylsiloxane (PDMS) soft photolithography. The master mold was made with a SU-8 patterned silicon wafer which yields eight microfluidic devices. 2  $\mu$ L of CF<sup>®</sup>488A at the same concentration (33.75 ng/ $\mu$ L) were injected into all five channels in one single device. Figure 3-2A highlighted three channels out of the five channels filled with CF<sup>®</sup>488A at the same concentration in designed microfluidic devices in the fluorescent field. The fluorescent image demonstrates the same fluorescent signal intensity for dye at the same concentration across different channels. Furthermore, the image gives the first glimpse of how these channels can serve as a characterization tool for visualizing fluorescent signals.

The quantification of fluorescent intensity in all 5 channels was carried out by normalizing the readouts to the average readouts across channels. Figure 3-2B shows the normalized fluorescent intensity from channel 1 to channel 5. There is no statistical significance between channels ( $p = 0.26 > \alpha = 0.05$ ), indicating that the designed microfluidic devices give the same readout to the same fluorescent intensity.

Furthermore, Figure 3-2C shows the normalized fluorescent intensity for device 1 to device 3. The average normalized readout of each device was plotted, with the variance being the channel variance in the specific device. In Figure 3-2C, there is no statistical significance between devices ( $p = 1 > \alpha = 0.05$ ), indicating that the designed microfluidic devices give the same readouts to fluorescent signals at the same level. Overall, Figure 3-2 demonstrates the robustness of designed microfluidic devices for characterizing fluorescent signals across channels and devices, respectively. The results illustrate the potential of using reported devices for cell-free reaction output characterization.

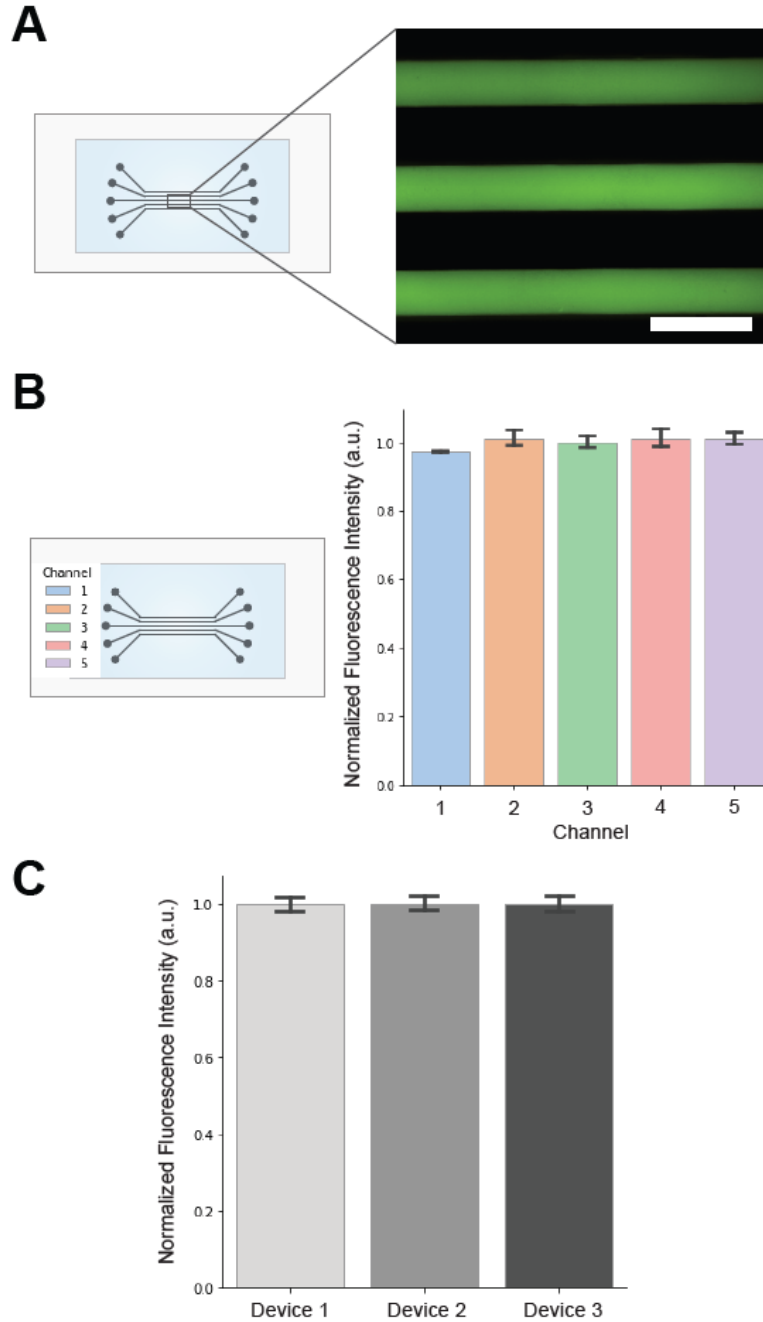


**Figure 3-2. Characterization of the reported microfluidic device robustness with CF<sup>®</sup>488A. (A) Green fluorescent images of microfluidic devices filled with 2  $\mu$ L 33.75 ng/  $\mu$ L CF<sup>®</sup>488A. (Scale bar: 200  $\mu$ m) Normalized fluorescent values of all five channels (B) and normalized fluorescent values of three devices (C) were plotted. There is no statistical significance with a significance level of  $p=0.05$ .**

### 3.3.2 The Dynamic Range of the Reported Microfluidic Device

We have shown that the reported microfluidic devices are robust in quantifying fluorescent signals at the same intensity level. The next step is to test the ability of the device to quantify different fluorescent intensities. Ideally, the reported devices should cover the fluorescent dynamic range that matches cell-free reaction fluorescent outputs.

To determine the dynamic range of designed microfluidic devices, the green fluorescent dye CF<sup>®</sup>488A was diluted five times at two-fold serial dilution starting at 33.75 ng/  $\mu$ L. Then, the dye concentration was normalized to the starting concentration (33.75 ng/  $\mu$ L). Hence, 0.5x concentration represents 16.88 ng/  $\mu$ L, and 0.25x concentration represents 8.44 ng/  $\mu$ L and so on. Then, 2  $\mu$ L of CF<sup>®</sup>488A at each concentration was injected into the channels.

Figure 3-3A shows the fluorescent microscope image of CF<sup>®</sup>488A at a normalized concentration of 0.25x, 0.5x, and 1x in designed microfluidic devices. As shown in Figure 3-3A, the higher the fluorescent dye concentration, the higher the fluorescent intensity that was observed with designed microfluidic devices. The results demonstrate the ability of designed microfluidic devices to capture the fluorescent dynamic range, and the difference between fluorescent intensities is evident with designed microfluidic devices.

The measured fluorescent intensity level of CF<sup>®</sup>488A at two-fold serial dilution was normalized and plotted in Figure 3-3B. Linear regression was extrapolated to indicate the relationship between measured fluorescent intensity and the normalized fluorescent dye concentration. The extrapolated equation is  $y = 1.0034x + 0.0277$  with a R-squared value of 0.989. The slope value is expected since the fluorescent intensity and the fluorescent dye concentration were normalized. The R-squared value of 0.989 indicates that the designed microfluidic devices yield a linear relationship between fluorescent signals and the dye concentrations with great

confidence. Therefore, we can use the linear relationship to quantify fluorescent signals with the reported device.

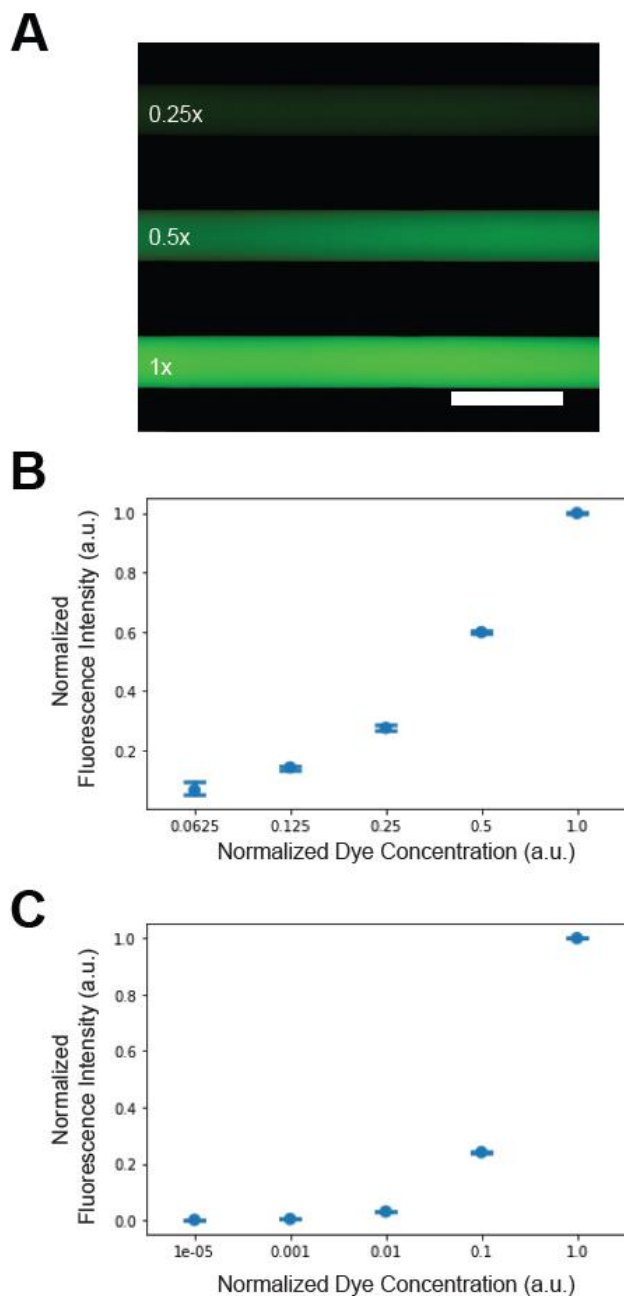


**Figure 3-3. The dynamic range of the designed microfluidic device. (A) Fluorescent images of microfluidic devices filled with 2  $\mu$ L CF@488A at the two-fold dilution. (Scale bar: 200  $\mu$ m) Quantification of fluorescent values of microfluidic devices filled with 2  $\mu$ L CF@488A at (B) the two-fold dilution and (C) the ten-fold dilution. Both dilutions started at 33.75 ng/  $\mu$ L.**

To investigate the limit of the designed microfluidic devices for fluorescent signal characterization, CF<sup>®</sup>488A was diluted five times at ten-fold serial dilution starting at 33.75 ng/ $\mu$ L. The results give a larger fluorescent signal range than the two-fold serial dilutions, and we can test the limits of designed devices with a wider fluorescent dynamic range. The measured fluorescent intensity level of dye at ten-fold serial dilution was normalized and plotted in Figure 3-3C. The extrapolated linear regression equation is  $y = 0.9704x + 0.0398$  with a R-squared value of 0.980. The R-squared value of 0.980 is lower than the two-fold serial dilution results. However, the result suggests that the designed microfluidic devices cover a dynamic range of five decades with an R-squared value of 0.980.

A closer look at Figure 3-3B and Figure 3-3C data suggests that the significant variance comes from the high concentration. Excluding the highest concentration improves the performance demonstrated by an increased R-squared value from 0.98 to 0.99. If the highest concentration is excluded, the linear regression for two-fold serial dilutions is  $y = 1.015x - 0.0237$  with an R-squared value of 0.998. Furthermore, if the highest concentration is excluded, the linear regression for ten-fold serial dilutions is  $y = 0.9888x + 0.0126$  with an R-squared value of 0.999. The results suggest that the designed microfluidic devices have a fluorescent dynamic range of four decades, which covers the ranges of cell-free synthetic biology fluorescent outputs.

### **3.3.3 Characterization of Cell-Free Reactions with Designed Microfluidic Devices**

After establishing the robustness and determining the dynamic range of the designed devices, we tested the microfluidic devices' ability to characterize cell-free synthetic biology reactions with a standard genetic circuit template producing fluorescent proteins. The *E. coli* based

cell-free protein expression platform [83] was employed in this work since it is well-characterized and highly efficient and can be made in-house at a low cost.

The genetic circuit template used for characterization consists of a constitutively expressed promoter,  $P_{70a}$ , driving a green fluorescent protein, deGFP [26]. (Figure 3-4A) deGFP, a truncated version of eGFP that shares similar excitation/emission profiles, is more translatable in the cell-free platform and is used as the standard fluorescent reporter [26, 85]. The promoter  $P_{70a}$  is the strongest promoter reported in this cell-free protein expression platform [26, 82]. Hence, the genetic circuit template, a  $P_{70a}$  driving deGFP, gives a robust fluorescent signal expression after incubation, yielding about 10  $\mu\text{M}$  deGFP with a 5 nM linear genetic template in 12 h [26]. Moreover, the deGFP amount in cell-free reactions depends on the supplied genetic circuit template concentration and the incubation time [26, 83]. Hence, we can vary the genetic template concentration to get a range of fluorescent signal levels in cell-free reactions.

Cell-free synthetic biology reactions were carried out with 0, 1.25, 2.5, and 5 nM linear genetic circuit templates. 2  $\mu\text{L}$  of each incubated reaction with varied linear genetic circuit templates concentrations were injected into the channels. 2  $\mu\text{L}$  of CF<sup>®</sup>488A (0.3375 ng/  $\mu\text{L}$ ) were injected into the channels to serve as a reference point. Figure 3-4B shows the differential interference contrast (DIC) and fluorescent images of cell-free synthetic biology reactions with 1.25, 2.5, and 5 nM DNA templates in designed microfluidic devices. With an increased genetic circuit template concentration, a higher fluorescent intensity was observed with designed microfluidic devices, aligning with previously reported results [26, 82]. The images demonstrate the ability of designed microfluidic devices to capture the fluorescent dynamic ranges of cell-free reactions. Furthermore, the images provide visual feedback on multiple cell-free synthetic biology reactions in both brightfield and the fluorescent field. It offers the platform to examine output

signals beyond fluorescent proteins, such as synthesized nanotubes [86, 87], and characterize genetic circuit spatial behaviors [14, 79].

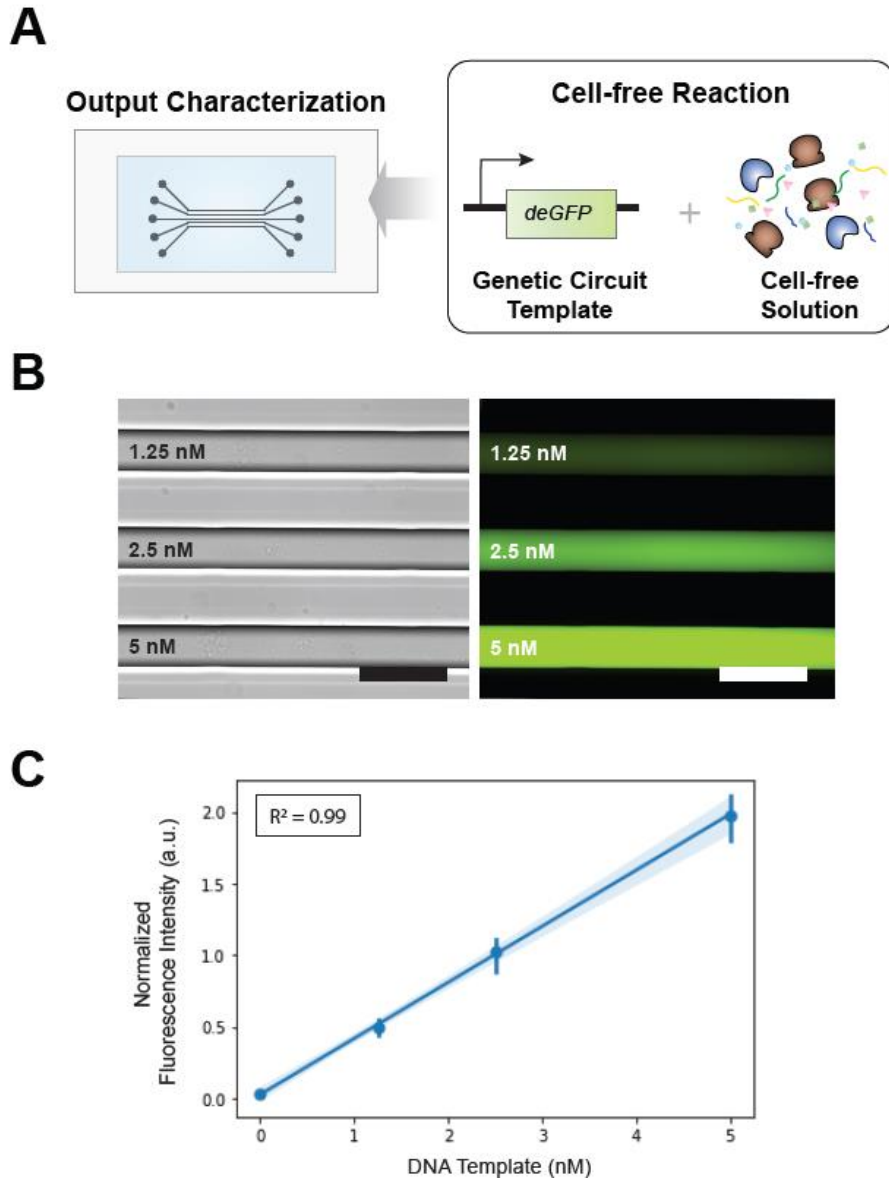


**Figure 3-4. Characterization of cell-free reactions with various genetic circuit template concentrations within the designed microfluidic device.** (A) Cell-free gene expression of genetic circuits were quantified and characterized within designed microfluidic device. The linear genetic circuit template contains promoter P70a driving deGFP, a green fluorescent protein. (B) DIC and fluorescent images of cell-free protein expression with 1.25, 2.5, and 5 nM DNA templates in designed microfluidic devices. (Scale bar: 200  $\mu\text{m}$ ) (C) Quantification of

**cell-free protein expression with 1.25, 2.5, and 5 nM DNA templates. Linear regression was plotted, and a 95% confidence interval for that regression was shown in the blue shaded region.**

The quantification of cell-free synthetic biology reactions with 0, 1.25, 2.5, and 5 nM DNA templates was plotted in Figure 3-4C. Linear regression was extrapolated to indicate the relationship between measured fluorescent intensity and the linear genetic circuit template concentration. The R-squared value of the linear regression is 0.99, which demonstrates that the designed microfluidic devices can be used to quantify cell-free synthetic biology reactions. The R-squared value is higher than the one calculated in Figure 3-3 because the designed microfluidic devices have a higher variance at a high fluorescent dye concentration in Figure 3-3. Since the output saturates when linear genetic circuit template concentration is above 10 nM [82], the microfluidic devices have sufficient dynamic ranges to quantify cell-free synthetic biology reactions. Apart from offering cell-free reactions images, Figure 3-4 proves that the reported microfluidic devices can characterize multiple fluorescent signals generated by cell-free reactions.

### **3.4 Discussion**

We have presented a specific microfluidic device for cell-free synthetic biology reaction characterization that balances the simplicity of the quantification-only system and the advantages of microfluidics. The reported device provides equal robustness and comparative dynamic range to characterize cell-free synthetic biology reactions as the conventional plate reader method. While the fluorescent dynamic range of cell-free synthetic biology reactions ranges from one decade to four decades with an average of around two decades [73, 74, 88], the reported device has a dynamic

range of up to five decades with an R-squared value of 0.98. For example, the CRISPR-based cell-free biosensors for SARS-CoV-2 detection give two to four decades of fluorescent output signals in the presence of SARS-CoV-2 viruses when characterized with a plate reader [89]. Alternatively, the reported device can capture the same fluorescent dynamics of the CRISPR-based cell-free biosensors for SARS-CoV-2 detection as a plate reader does.

Furthermore, the reported device enjoys the advantages of using microfluidics for characterization, such as visualizing cell-free reaction products and observing spatial regulations of genetic circuits, while simplifying the process from exquisite fluid manipulation to steps as simple as pipetting. Visualizing cell-free synthetic biology reactions can confirm product production and observe the dynamics of genetic circuits. One of the significant applications of cell-free synthetic biology is to mimic and study the underlying principles of biology [90, 91]. For example, Garenne *et al.* developed cell-free synthetic cells that change shapes to recapitulate the cytoskeleton dynamics inside cells [92]. Therefore, visualizing the cell-free synthetic cells is essential for evaluating the designed genetic circuits. Moreover, visualization allows researchers to study how spatial parameters affect the designed cell-free synthetic circuits [93, 94].

Moreover, the simplicity of the designed microfluidic device makes it easy to integrate with existing microfluidic modules [77] and easy to manufacture the master mold, whether via traditional nanofabrication techniques or potentially via 3D printing technology [95-97]. For example, in 2014, Comina *et al.* used a stereolithography 3D printer to create molds for PDMS microfluidic devices. They created channels that are 50  $\mu\text{m}$  wide with various heights ranging from 50  $\mu\text{m}$  to several mm [97]. Over the past few years, the field has improved the print resolution and reduced the roughness of 3D structures [98, 99]. The microfluidic devices reported in this work fit easily into the specification described with the 3D-printed molds. The 3D-printed mold will

eliminate cleanroom work and make the reported microfluidic devices more accessible and cheaper for rapid cell-free synthetic biology reaction characterization.

Lastly, we have demonstrated the microfluidic device's feasibility as a straightforward tool for cell-free synthetic biology reaction characterization by deploying our device to measure the fluorescent proteins produced by varied DNA template concentrations in the cell-free reactions. Our results revealed that our microfluidic device could be used with standard fluorescent imaging settings, such as inverted epifluorescence microscopes, to visualize cell-free reactions. Also, they demonstrated that our device was able to quantify different fluorescent intensity levels precisely. Although many microfluidic devices have been proposed for cell-free synthetic biology [77], the uniqueness of our design can be executed at a considerably lower operational technique requirement. Therefore, we believe our device will allow rapid, user-friendly, and robust characterization of cell-free synthetic biology reactions that advance the development of synthetic biology and improves the progress of cell-free microrobots.

## **4.0 Cell-Free Synthetic Biology Enabled Perception-Action Behavior Modules on Biohybrid Microrobots**

Autonomous biohybrid microrobots with unique features and functions are an emerging technology in biomedical applications. The miniaturized size enables them to access previously unreachable parts throughout the human body, offering localized diagnosis and treatment with greater precision and efficiency. However, autonomous capabilities such as perception-action and communication remain a challenge for robots at a small scale. Here, we report a cell-free synthetic biology platform to build onboard behavior modules on microrobots. Leveraging the capability of synthetic biology and the cell-free platform for creating complex behaviors, microrobots could acquire the ability to sense, analyze, and respond to complex environments based on designed molecular algorithms. This work aims to develop a cell-free platform for implementing perception-action modules on microrobots by exploiting the surface chemistry of microparticle-based microrobots and designed cell-free genetic circuits. Biohybrid microrobots equipped with basic Boolean logic gates demonstrated the implementation of perception-action modules with the reported cell-free platform. This work opens up an opportunity to build autonomous miniaturized clinical tools for precise and efficient diagnosis and treatment with potential use in the human body.

## 4.1 Introduction

Microrobots with unique features and functions are a promising technology in biomedical robots, especially for targeted drug delivery and onsite diagnosis [100-102]. Biologically responsive microrobots that are sensitive to biological signals and can be activated by stimuli are essential for applications such as diagnostics and controlled drug delivery [29, 103]. Because of its unique sequence-encoded structural and functional features, DNA has been widely adopted to construct actuation and stimuli-responsive behaviors on systems ranging from the molecular level to the microscale [52, 104, 105]. In addition, their selective and sensitive responses to small molecules, proteins, and nucleic acids allow DNA structures to respond to a wide range of stimuli [106, 107]. Therefore, DNA nanostructures have been used as molecular computational units to analyze multiple inputs in complex environments, exemplified by applications in cancer diagnosis and intelligent drug delivery [108, 109].

However, these DNA computational units rely heavily on the conformational change of DNA to perform preprogrammed responses [110-112]. Few of these systems utilize encoded genetic information to create and perform perception-action behaviors [113]. Furthermore, while the field focuses on investigating the design principles of DNA structural changes on system surfaces [114-116], using the interaction between surfaces and DNA polymers to create perception-action behaviors remains underexplored.

By repurposing and reprogramming molecular modules, synthetic biologists have utilized genetic information stored in DNA to construct perception-action behaviors in living organisms, generating designed output in response to specific inputs. Programmable synthetic genetic circuits equip cells with the ability to detect a broad range of stimuli, perform biocomputation, and respond with biosynthesized outputs [65, 117-120]. These synthetic perception-action behaviors and

biocomputation power can be readily integrated to create novel materials that can be used as biohybrid robotic systems [113, 121-124]. Previously, we have used engineered cells to control and manipulate programmable material surfaces, creating an interface between living organisms and inorganic materials [66, 67, 125]. However, using living cells as chassis requires laborious genetic engineering and suffers from unpredictable interplay between designed and natural systems [24, 72, 126]. Consisting of transcription and translation machinery extracted from cells, cell-free platforms provide a tool to execute genetic circuits without the limitations of living cells [26, 70, 126].

Here, we report a cell-free platform to build biohybrid microrobots with synthetic biology enabled perception-action behaviors. (Figure 4-1) We anchored the synthetic genetic circuits on microrobot surfaces via non-covalent interactions, which allows the microrobot to selectively bind to programmed stimuli-responsive behaviors. The cell-free platforms provide essential transcription and translation machinery assembling on the microrobot surface, generating desirable biological output responses according to the anchored genetic circuits. Incorporating surface chemistry, synthetic biology, and the cell-free platform, the reported biohybrid microrobot could acquire the ability to sense, analyze, and respond to environmental stimuli, which is demonstrated by implementing fundamental Boolean logic gates. Moreover, microrobots with different stimuli-responsive behaviors can perform distributed computation via exchanging biochemical information carriers among individual onboard Boolean logic gates, expanding the complexity level of molecular computation, which will be discussed in detail in Chapter 5.

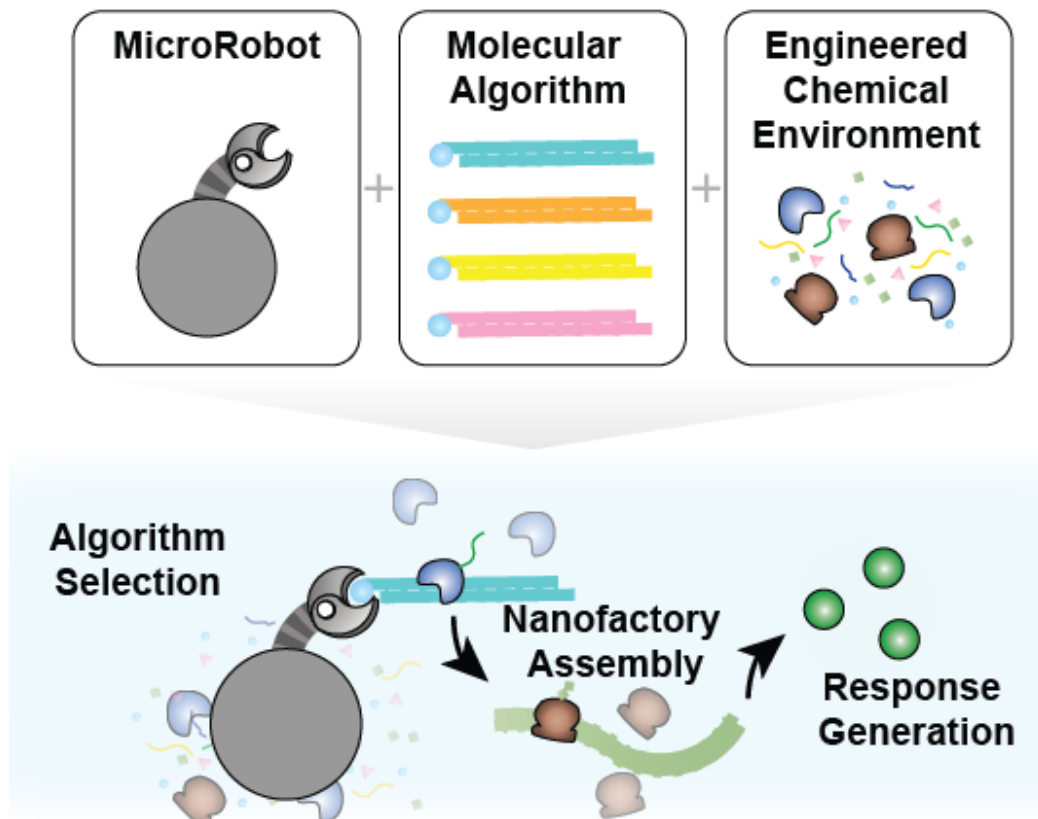


Figure 4-1. Biohybrid microrobot with cell-free synthetic biology enabled behavior modules. The reported biohybrid microbots can selectively bind to molecular algorithms, synthetic genetic circuits carrying designed behaviors. The engineered chemical environment, the cell-free reactions, powers robot behaviors and generates responses through nanofactory assembly to perform transcription and translation.

## 4.2 Materials and Methods

### 4.2.1 Materials

PCR was performed with Q5® High-Fidelity PCR Kit (New England Biolabs) and a thermal cycler (Bio-Rad, C1000 Touch Thermal Cycler). The oligonucleotides were synthesized

by IDT Corporation. Primer sequences are available in Appendix B. Page 83. Tetracycline was obtained from Sigma Aldrich (Cat No. 31741).

#### **4.2.2 Molecular Algorithm Construction**

The molecular algorithm reported in this work were embedded in biotinylated linear DNA templates. The linear DNA template was designed and optimized according to the previously reported protocol [84, 123]. Briefly, the linear DNA template should contain 250 bp upstream from the promoter and 100 bp downstream from the terminator. We performed PCR with biotinylated primers on the plasmid carrying designed synthetic genetic circuits to make the biotinylated linear DNA templates. For the fluorescent reporter, a PCR with biotinylated forward primer and non-biotinylated reverse primer isolating gene fragment of promoter  $P_{L,tetO-1}$  driving deGFP from plasmid pTXTL-PLtetO1-deGFP (Arbor Biosciences, Cat No. 502098) [26]. The biotinylated forward primer and non-biotinylated reverse primer ensure the same direction of anchoring DNA linear template to material surfaces. For the tetR and aTc related experiments, a PCR with biotinylated forward primer and non-biotinylated reverse primer was performed to extract gene encoding tetR from plasmid pZS4Int-tetR from our group [127]. Plasmid maps and sequences are available in Appendix B. Page 83. After PCR, we checked the product size by running electrophoresis at 110 mV for 60 minutes with a gel made of TAE with 1% agarose. Then, we extracted the biotinylated linear DNA template using a Monarch® DNA Gel Extraction Kit (New England Biolabs) and DI water as elution buffer. The concentration of linear DNA template was determined by a Bio-tek Synergy™ HT plate reader with Take3 Micro-Volume Plate.

### **4.2.3 Microrobot Assembly**

The genetic circuits were anchored to microparticle-based microrobots via the SA-biotin interaction. First, 10 nM biotinylated linear DNA templates were mixed with 10  $\mu$ l SA coated, 1  $\mu$ m diameter, superparamagnetic microparticles (Thermo Fisher, Dynabeads™ MyOne™ Streptavidin T1). The binding procedure was carried out according to the Dynabeads™ MyOne™ Streptavidin T1 protocol. Briefly, the particles were washed with 1X PBS buffer three times before introducing biotinylated linear DNA templates. For Biotin NOT gate experiments, biotin was added to the biotinylated DNA mixture before the addition of the microparticles. After 15 minutes of incubation, the microparticle anchored with linear DNA template was separated with magnetic racks and then washed the unbound biotin and biotinylated DNA template was washed away with PBS. Lastly, the microparticle-DNA template complex was resuspended in DI water for the following experiments.

### **4.2.4 Cell-Free Reaction**

The cell-free platform used in this work was the myTXTL® linear DNA Expression kit from Arbor Biosciences. The detailed protocol for making and using the cell-free protein expression system was described in previous publications [26, 83]. Briefly, the cell-free reaction has three components – cell extract, buffer, and the DNA template encoding designed genetic circuits. To make cell extract containing transcription and translation machinery, cells are grown to OD<sub>600</sub> 1.5–2.0 and lysed via bead-beating in S30A buffer. Then, run the extract through microchromatography columns to remove beads and through dialysis using 10k MWCO dialysis cassettes to retain essential transcription and translation components, such as core RNA

polymerases and transcription factors. The cell extract is flash-frozen and stored at  $-80\text{ }^{\circ}\text{C}$  to ensure cell-free activity. Finally, a buffer containing amino acids and energy solutions was assembled and calibrated to optimize protein production in cell-free reactions and stored at  $-80\text{ }^{\circ}\text{C}$

The cell-free solution (Sigma 70 master mix) in the myTXTL<sup>®</sup> linear DNA Expression kit is a premix of cell extract and buffer. To set up cell-free reactions, the cell-free solution (sigma 70 master mix) was thawed completely from  $-80\text{ }^{\circ}\text{C}$  frozen stock and was gently mixed with the microparticle-DNA template complex prepared in the previous section. Alternatively, the cell-free solution was mixed with microparticle and DI water for negative control. The cell-free reactions were assembled to volumes of  $10.5\text{ }\mu\text{L}$  with  $7.88\text{ }\mu\text{L}$  cell-free solutions and  $2.64\text{ }\mu\text{L}$  materials mixture solution prepared in the previous section in  $1.5\text{ mL}$  microcentrifuge tubes and incubated at  $29\text{ }^{\circ}\text{C}$  for 12 hours. The cell-free reactions were put on ice to stop reactions.  $2\text{ }\mu\text{L}$  of incubated reactions were pipetted into a microfluidic imaging chamber for material fluorescent response observation. Then, the incubated reactions were put on the magnetic rack to separate the magnetic microparticle-based materials.  $2\text{ }\mu\text{L}$  of supernatant were extracted and pipetted into the observation chamber for fluorescent signal quantification to avoid the non-fluorescent material interfering fluorescent readouts.

#### **4.2.5 Observation Chamber Preparation**

Polydimethylsiloxane (PDMS) observation chamber was used to host the materials and observe their behaviors. The master mold of microfluidic devices was prepared via soft lithography at the University of Pittsburgh Nanoscale Fabrication Characterization Facility Cleanroom and was detailed in Chapter 3. To make microfluidic devices, PDMS (Sylgard<sup>™</sup> 184, Dow Corning) was mixed at a 10:1 base to curing agent ratio and poured over the wafer. The PDMS mixture was

degassed in a vacuum chamber and cured in an oven at 65 °C for 1 h. Then, the PDMS was then carefully recovered from the wafer and sliced into individual microfluidic devices. Inlet and outlet holes were punched with a 1 mm biopsy punch (Miltex® Biopsy Punch with Plunger). Next, the devices were bonded to glass coverslips (22 × 40 mm) via a plasma cleaner (PDC-32G, Harrick Plasma) for 20 s. The devices were then incubated at 65 °C for 1 hour to ensure a tight bond between the glass and the PDMS.

#### **4.2.6 Material Behavior Observation**

Fluorescent was used as an indicator for evaluating microrobot behaviors. The microfluidic device hosting the cell-free materials was placed onto the stage of a Nikon Eclipse Ti2 microscope and viewed through a 20X objective lens. Images were captured and analyzed with a mounted Andor Zyla 5.5 sCMOS camera and the NIS-Elements software (Nikon).

#### **4.2.7 Image and Statistical Analysis**

We characterized the microrobot behaviors by quantifying the biosynthesized fluorescent output signal. A region of interest area with fixed size and position was marked to obtain the fluorescent intensity. The acquired data was normalized to the average signal intensity of the reference. The reference signal is defined as the corresponding control reaction or the highest fluorescent signal output among the experiment set. For example, in the Figure 1 experiment, the reference signal intensity was defined as the average fluorescent intensity of all cell-free microrobots anchored with DNA templates. In Biotin NOT gate experiments, the average fluorescent intensity of all cell-free microrobots responses with no Biotin in the environment was

defined as the reference. All experiments were performed in triplicate and reported as mean +/- standard deviation. One-way ANOVA was performed and a significance level of 0.05 was determined.

## **4.3 Result**

### **4.3.1 Design of Cell-Free Platform to Build Biohybrid Microrobots**

We validated and optimized the reported platform design by first constructing the biohybrid microrobot with a standard genetic circuit generating fluorescent reporter in cell-free reactions. The reported microrobot consisted of surface-functionalized magnetic microparticles that can anchor genetic circuits on the surface via specific non-covalent interactions. Magnetic particles are a popular microrobot in biomedical applications because of their unique feature allowing remote manipulation for targeted drug delivery [55, 128-130]. Furthermore, since biotin's binding to streptavidin (SA) is one of the most robust non-covalent interactions found in nature, it is widely used in chemical construction [131]. Hence, we used the SA-biotin interaction to anchor genetic circuits onto magnetic microparticles to create the reported microrobots. (Figure 4-2A)

Next, the genetic circuit producing fluorescent reporter was embedded in biotinylated linear DNA templates. It contains a constitutively expressed deGFP (GFP). deGFP, a truncated version of eGFP that shares similar excitation/emission profiles, is more translatable in the cell-free platform and is used as the standard fluorescent reporter in cell-free reactions [26, 82]. Leveraging the SA-biotin interaction, we anchored the microrobot surface with the DNA templates carrying the fluorescent reporter GFP. The biotinylated DNA template is called GFP DNA.

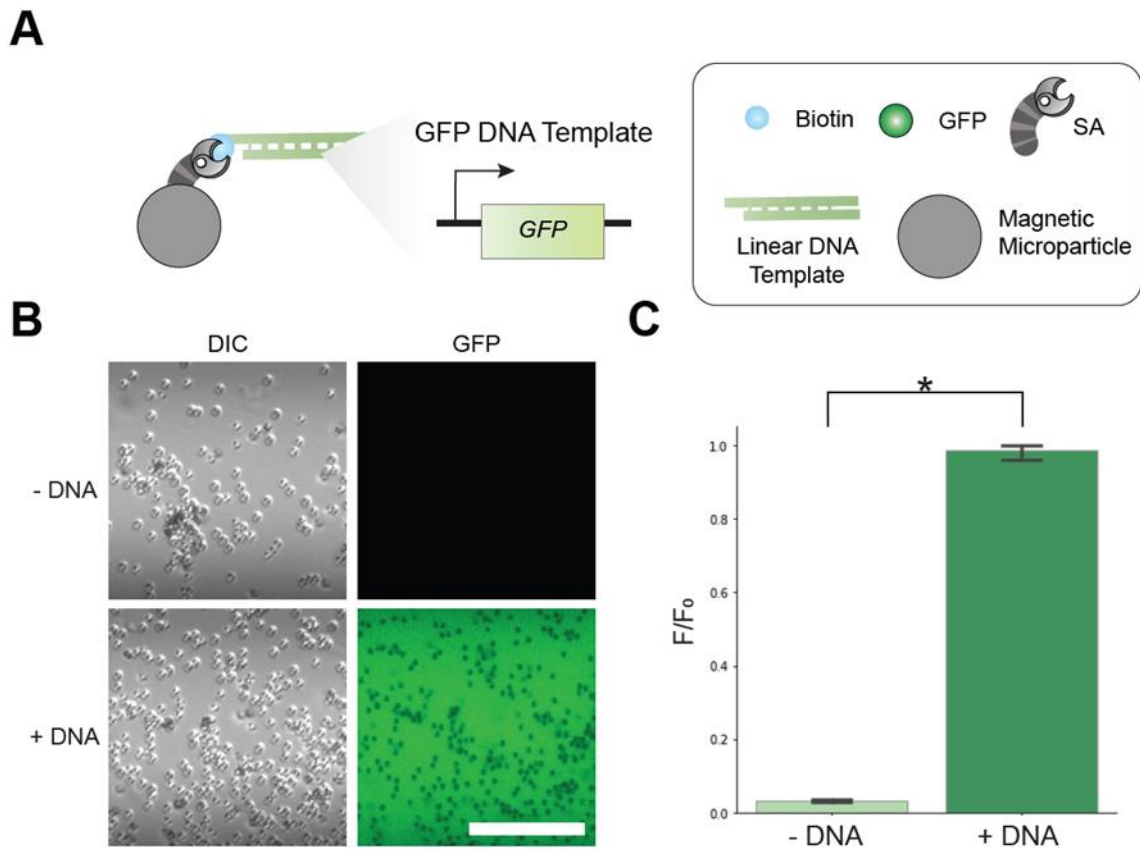


**Figure 4-2. Design of cell-free platform to build stimuli-responsive microrobots. (A)** A standard genetic circuit producing GFP, the GFP DNA, was used to characterize and optimize the platform design. Microparticle was coated with streptavidin (SA). The genetic circuit containing constitutively expressed GFP was embedded in a biotinylated linear DNA template. Via SA-biotin interaction, the biotinylated GFP DNA template was anchored on the microparticle surface to create the reported microrobot. **(B)** Differential interference contrast (DIC) and green fluorescent images of microparticles anchored with or without DNA template. (Scale bar: 25  $\mu\text{m}$ ) **(C)** Quantification of fluorescence intensity generated by the reported microrobot with or without anchored GFP DNA template. (\* $p < 0.05$ )

A cell-free reaction consists of the cell-free solution and the genetic circuit. Cell-free solutions provide the transcription and translation machinery and execute the genetic circuits [83]. Here, the particles anchored with the GFP DNA were put into the cell-free solution as the genetic

circuit template. The cell-free solution provided resources and produced GFP according to the genetic circuits embedded in the GFP DNA template. Figure 4-2B shows the microrobot anchored with or without the GFP DNA template. The microrobot expressed GFP and produced green fluorescent with the GFP DNA template. Without GFP DNA, the microrobot itself did not yield any green fluorescent. Quantification of the output signal GFP shows that the microrobot with the GFP DNA template generates a higher GFP signal than the microrobot without the template. (Figure 4-2C) After validating the cell-free platform, we optimized the reported microrobot design by screening particles to select the one that gives the most robust output signal. (Figure 4-3)

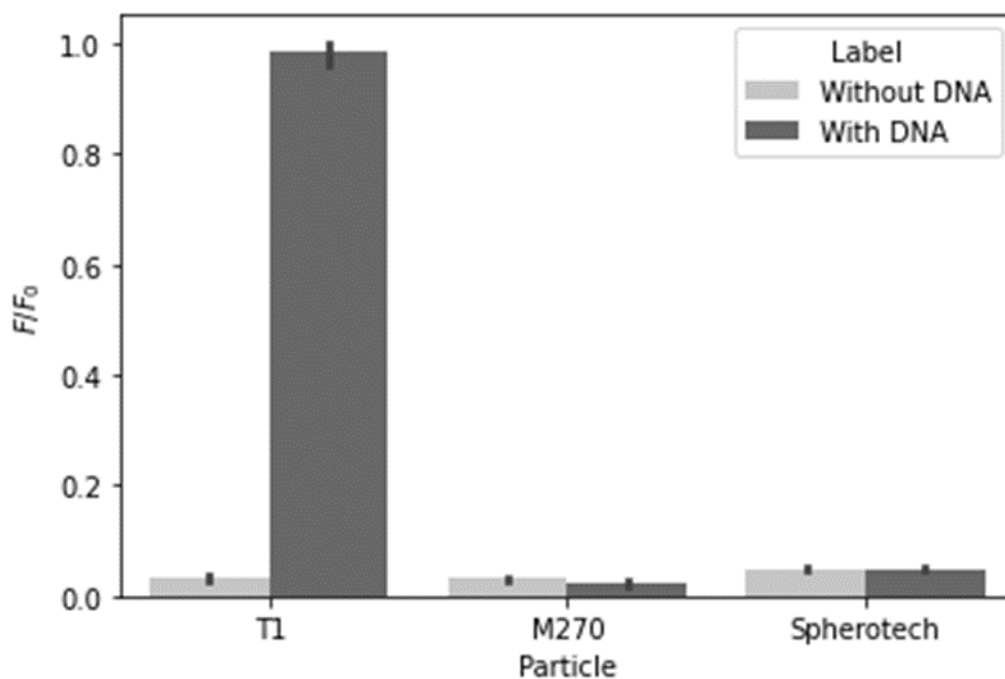


**Figure 4-3. Quantification of the fluorescent output signal generated by various particles anchored with or without DNA. The combination producing the highest fluorescent intensity difference was selected to build the reported platform.**

Furthermore, we can tune the microrobot output signal intensity by varying the amount of DNA template anchored on the surfaces. (Figure 4-4) The fluorescent intensity depends on the GFP concentration, while the GFP concentration depends on the DNA template concentration in cell-free reactions [26]. The results demonstrate the feasibility of the reported platform to construct microrobots with cell-free synthetic biology enabled behaviors. The microrobot can generate biosynthesized output response according to programmed genetic circuits. The reported platform enables the customization of stimuli-responsive microrobot behaviors and their output signal intensity by altering the genetic circuit and its amount on the microrobot surface.

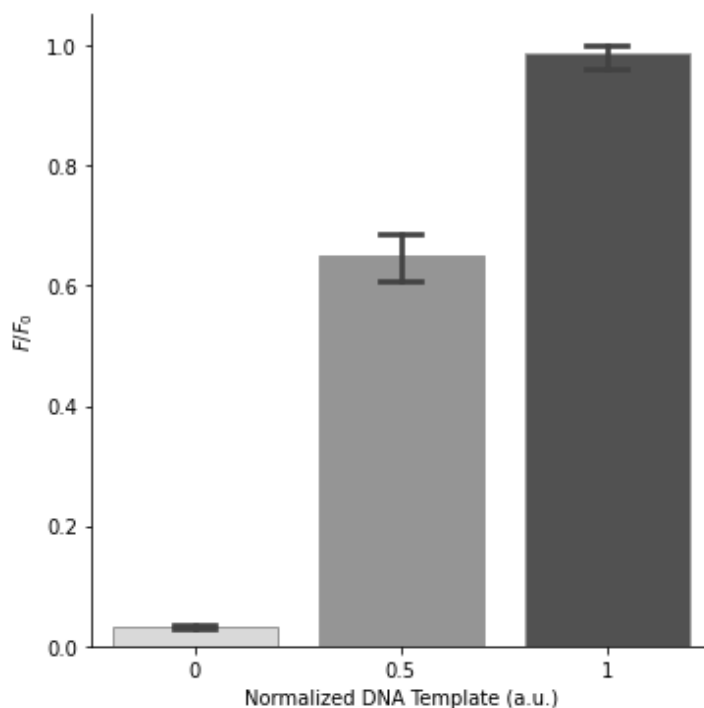


**Figure 4-4. Quantification of the fluorescent output signal generated by microparticles anchored with various DNA template concentrations. The fluorescent intensity produced depends on the amount of DNA templates anchored on particle surfaces.**

### 4.3.2 Perception-Action Enabled via Surface Chemistry.

After establishing the platform design with the standard fluorescent reporter, we created perception-action behaviors utilizing surface chemistry. We used the surface-functionalized SA as a sensing module to build a Biotin NOT gate, demonstrating the construction of perception-action behaviors via surface chemistry. The Boolean logic gates are the fundamental elements of electronic circuit computation and represent straightforward perception-action behaviors. Therefore, recreating the Boolean logic behaviors is essential and the first step to building perception-action and computation units in microrobots with the reported cell-free platform.

The designed perception-action module functions as a NOT gate in Boolean logic, with biotin as input and GFP as output. (Figure 4-5A) A biotinylated GFP DNA encoding the constitutively expressed GFP competes with free biotin in the environment for SA binding sites on the microrobot surface. (Figure 4-5B) Without biotin in the environment, the biotinylated GFP DNA can bind to the microrobot surface and access transcription and translation machinery in cell-free reactions, generating GFP as output. With biotin in the environment, biotin competitively binds with the biotinylated GFP DNA for the SA binding sites on the microrobot surface, blocking biotinylated GFP DNA from accessing cell-free reactions. A lower output fluorescent signal intensity is expected as fewer biotinylated GFP DNA are attached to the microrobot surface and, therefore, fewer DNA templates for cell-free reactions.

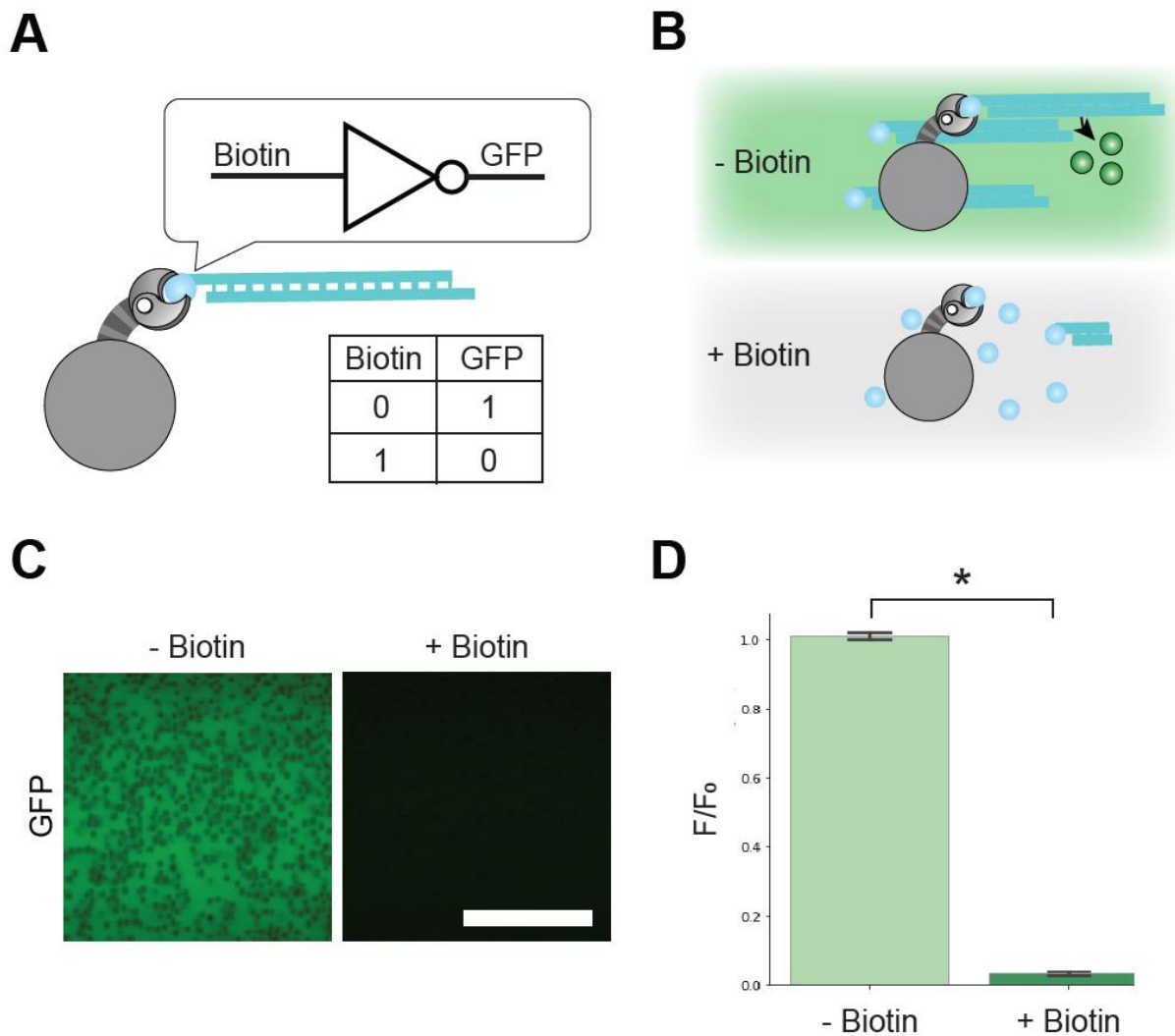


**Figure 4-5. Cell-Free microrobots with Boolean logic gates enabled via surface chemistry.** (A) The schematic of a Biotin NOT gate is an example of using surface chemistry to build microrobots with the reported cell-free platform. (B) The mechanism of the Biotin NOT gate. The microrobot perceives the presence of biotin input (blue circle) via competitive binding sites, SA, on its surface. Without biotin, the biotinylated GFP DNA bind to the microparticle surface and has access to cell-free reaction generating GFP. With biotin, less biotinylated GFP DNA binds to the surface and produces fewer GFP. (C) Green fluorescent images of microrobot with Biotin NOT gate with or without free biotin (input) in the environment. (Scale bar: 25  $\mu$ m) (D) Quantification of the fluorescent responses of microrobot with Biotin NOT gate with or without biotin. (\* $p < 0.05$ ).

We mixed the biotinylated GFP DNA with or without biotin before introducing the SA-coated magnetic microparticles to ensure competitive binding. After the competitive binding, the unbound biotin or biotinylated GFP DNA was washed away. Then, the biotin-DNA-microparticle complex was added to a cell-free reaction as a DNA template. As a result, Figure 4-5C shows the fluorescent response of the microrobot anchored with Biotin NOT gate with or without free biotin in the environment. When biotin was absent in the environment, the microrobot with Biotin NOT gate generated GFP since the biotinylated GFP DNA bound to the microrobot and served as DNA templates in cell-free reactions. However, when biotin was present, the microrobot had a less bound biotinylated GFP DNA due to the competitive binding. As a result, the cell-free microrobot produced less GFP than in the environment with no biotin since there was less GFP DNA as DNA template in the cell-free reaction. Figure 4-5D and Figure 4-6 demonstrate the quantification of the stimuli-responsive behaviors of the microrobot carrying a Biotin NOT gate. The results show the employment of using the interaction between microrobot surfaces and DNA polymers to create stimuli-responsive behaviors in the reported cell-free platform. Also, the results demonstrate the possibility of building Boolean logic on the reported microrobot that can be expanded into complex computations.

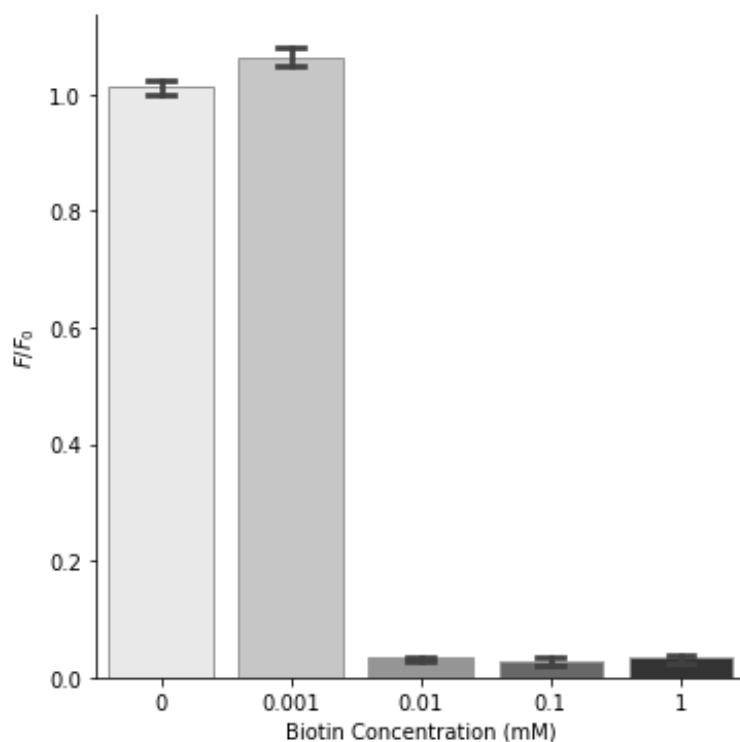


**Figure 4-6. Quantification of the fluorescent response of the reported microrobots with Biotin NOT gate in various biotin concentrations. The fluorescent intensity decreased as the concentration of free biotin in the environment increased due to the competitive binding between free biotin and the biotinylated DNA template generating fluorescent reporter.**

### **4.3.3 Boolean Logic Gate Module Enabled via Synthetic Biology.**

Apart from using surface chemistry, we employed synthetic biology to create perception-action behaviors by engineering the genetic circuits encoded on linear DNA templates. The tet repressor (tetR) regulation system is a well-characterized and broadly applied tool in synthetic biology [132]. The tet regulation system contains a promoter,  $P_{L,tetO-1}$ , that is inhibited by tetR. And, tetR is regulated by tetracycline (aTc) [132]. Leveraging the tet regulation system from synthetic biology, we built Boolean logic based perception-action behaviors on the reported cell-free microrobots.

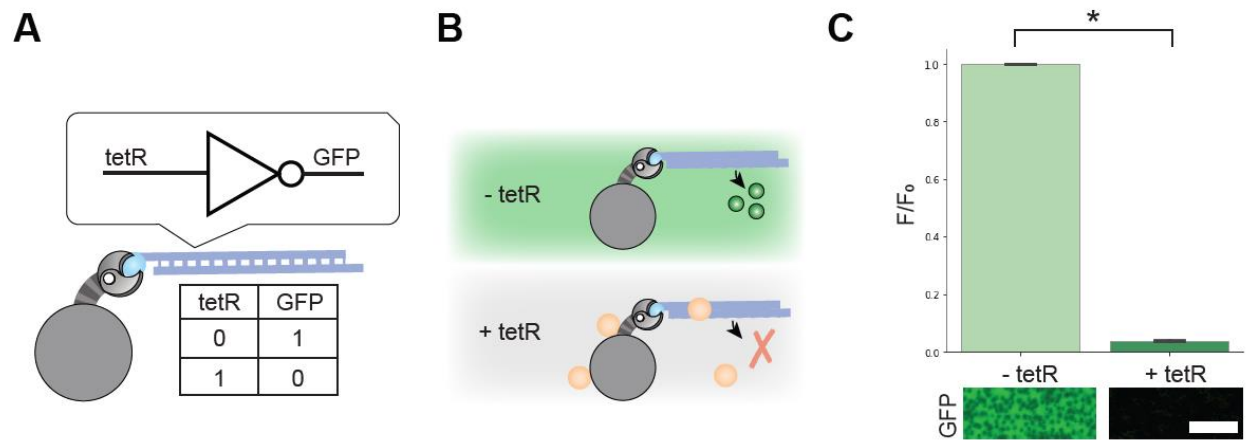


**Figure 4-7. Microrobots with tetR NOT Gate enabled via synthetic biology. (A) The microrobot with a tetR NOT gate with tetR as input and GFP as output. (B) When tetR (orange circle) is present, the microrobot with tetR NOT gate perceives tetR via tet repressor system programmed on the genetic circuit and inhibits GFP production. (C) Images and quantification of the fluorescent responses of microrobot with a tetR NOT gate with or without tetR. (Scale bar: 12.5  $\mu\text{m}$ , \* $p < 0.05$ )**

First, we employed tet repressor regulation to create a tetR Boolean NOT gate with tetR as input and GFP as output. (Figure 4-7A) Since tetR represses the promoter  $P_{L,tetO-1}$  on the biotinylated DNA template, the GFP production is repressed under the presence of tetR [11]. The fluorescent response of the cell-free microrobot with the tetR Boolean NOT gate with or without tetR was reported in Figure 4-7B and Figure 4-7C. When tetR was absent in the environment, the promoter on the biotinylated DNA template was not inhibited and the microrobot generated GFP. With tetR present in the environment, the microrobot perceived tetR via the tet repressor system implemented on the DNA template, and GFP production was inhibited. A higher tetR concentration results in a more significant GFP inhibition. (Figure 4-8)

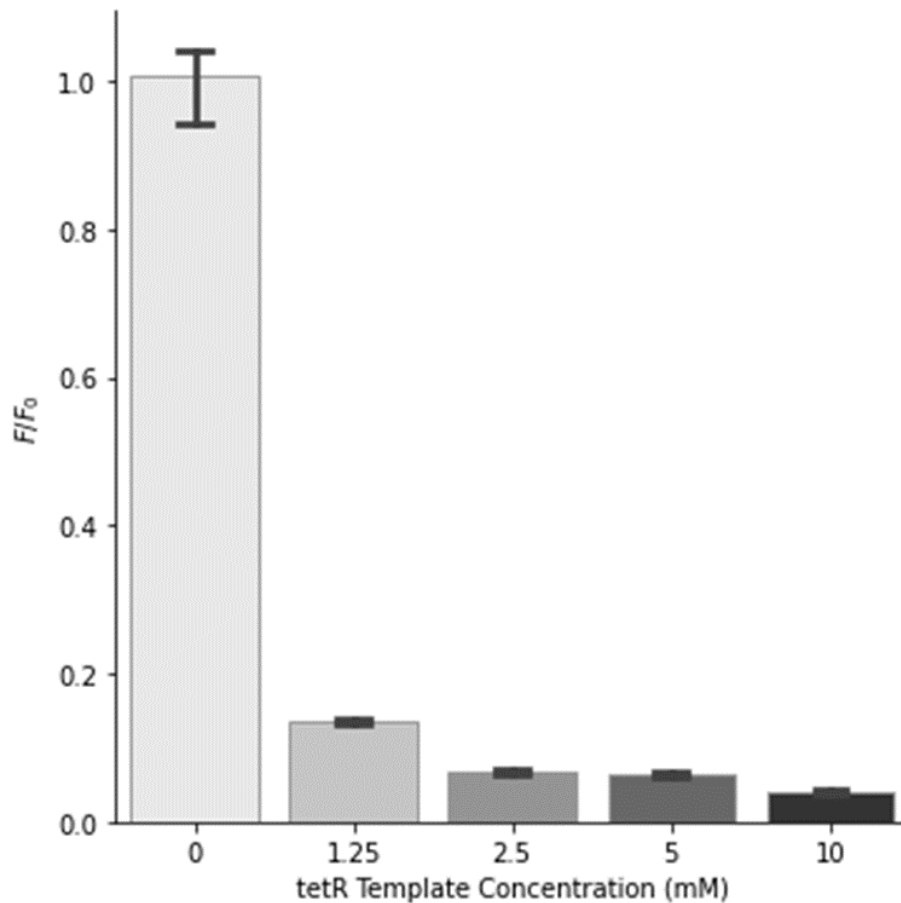


**Figure 4-8. Quantification of the fluorescent response of microrobots with tetR NOT gate in various tetR concentrations. The fluorescent intensity decreased as the tetR concentration increased since tetR repressed the promoter activity on the anchored DNA template generating fluorescent reporter.**

Moreover, the tet regulation system can function as a stimuli-responsive module for aTc. The designed stimuli-responsive module functions like an aTc buffer in Boolean logic with aTc as input and GFP as output (Figure 4-9A). Since tetR represses promoter  $P_{L,tetO-1}$  on the biotinylated linear DNA template on the microrobot surface, the GFP production is repressed under the presence of tetR. When aTc is present, it represses tetR. Hence, the promoter function is restored and the GFP expression is rescued [11]. (Figure 4-9B) The fluorescent response of microrobot with the aTc Boolean buffer with or without aTc was reported in Figure 3F. When aTc was absent

in the environment, tetR repressed GFP production. When aTc was present, the microrobot perceived the presence of aTc via a tet repressor system on its surfaces and, therefore, rescued GFP production. Therefore, when aTc was present, the fluorescence signal increased since aTc inhibited tetR's inhibition on GFP production (Figure 4-9C & Figure 4-10).

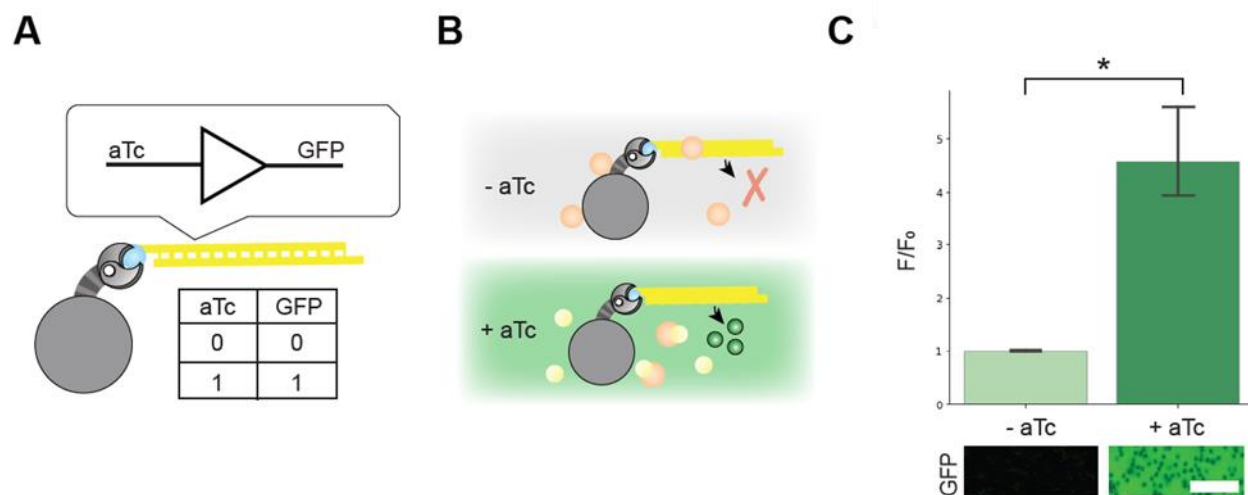


**Figure 4-9. Microrobots with aTc Buffer enabled via synthetic biology. (A) The microrobot with an aTc buffer with aTc as input and GFP as output. (B) When aTc (yellow circle) is absent, tetR inhibits GFP production. When aTc is present, the microrobot perceives aTc via a tet repressor system and rescues GFP production. (C) Images and quantification of the fluorescent responses of the microrobot with an aTc buffer with or without aTc. (Scale bar: 12.5  $\mu\text{m}$ , \* $p < 0.05$ )**

The results validate the construction of perception-action behavior modules on the reported biohybrid microrobots by programming the genetic circuits anchored on their surface. Also, the results demonstrate the feasibility of using synthetic biology's previously developed perception-action behavior modules to build smart microrobots.

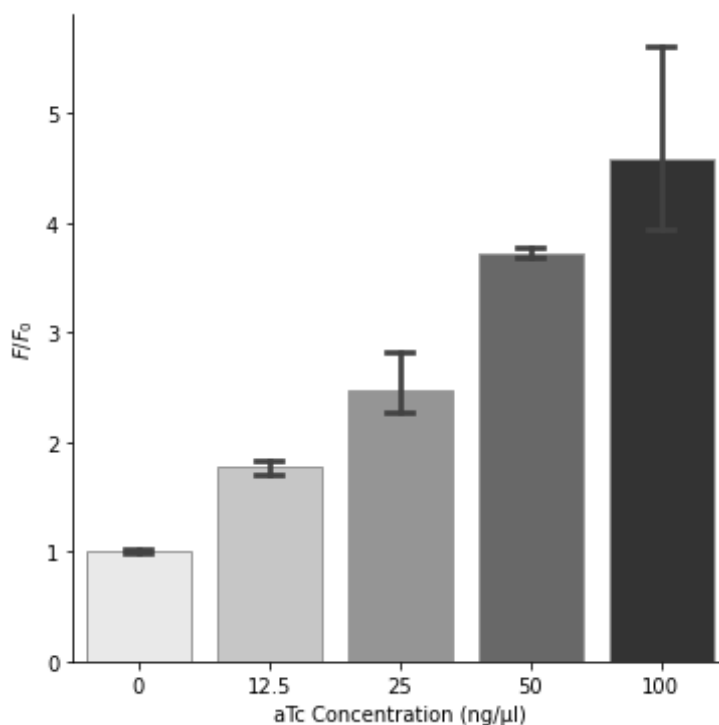


**Figure 4-10. Quantification of the fluorescent response of microrobot with aTc Buffer in various aTc concentrations. tetR was added to all reactions. The fluorescent intensity increased as the aTc concentration increased since aTc rescued the promoter activity by inhibiting tetR.**

#### **4.4 Discussion & Conclusions**

This work presents a cell-free synthetic biology platform to build perception-action behaviors and Boolean logic computation units as novel intelligent biohybrid microrobots. The platform consists of three major components- the microparticle-based microrobots, programmable genetic circuits, and an engineered cell-free system. The platform allows perception-action behavior customization by straightforward swapping to desired genetic circuits on microrobot surfaces. Experimental results showed that the reported platform implemented perception-action behavior modules via surface chemistry or synthetic biology genetic circuits. Moreover,

perception-action behaviors based on Boolean logic gates provide a foundation for expanding the reported microrobot behavior complexity level reminiscent of electrical circuit development.

Furthermore, this work demonstrates the advantage of integrating cell-free synthetic biology into the biohybrid microrobot world by utilizing genetic information embedded in the DNA template to program microrobot behaviors. Even though the work focuses on utilizing genetic information, the reported platform can be integrated with biohybrid microrobots based on DNA conformational change as an actuator to diversify microrobot behaviors [121]. For example, DNA functionalized colloidal particle systems use conformational change to alter physicochemical properties to mediate self-assembly and cellular interaction [133-135]. Our platform can be readily applied to these materials by anchoring the biotinylated synthetic biology perception-action modules to the particles to create onboard computation units on these colloidal particle systems. These materials can be used to create microrobots with diverse behaviors.

In summary, we reported a cell-free platform to leverage synthetic biology to create perception-action behavior and Boolean logic operation on biohybrid microrobots. This work can be readily applicable to a wide range of microrobot surfaces and advance the autonomy and computational power of biohybrid microrobots. Furthermore, this work opens up an opportunity to build autonomous clinical tools for precise and efficient diagnosis and treatment.

## **5.0 Cell-Free Synthetic Biology Enabled Communication Modules and Collective Behaviors on Biohybrid Microrobots**

This chapter aims to establish communication behaviors between microrobots, which would enable swarm forming and collective behaviors. Autonomous biohybrid microrobots with unique features and functions are an emerging technology in biomedical applications. However, the miniaturized size confines their autonomous capabilities. Microrobot swarm, collective microrobots that can communicate and work closely and cooperatively, will significantly enhance the robot autonomy. We used the reported cell-free synthetic biology platform to build onboard communication modules on microrobots to achieve collective behaviors. Leveraging the capability of synthetic biology and the cell-free platform for creating complex behaviors, the reported biohybrid microrobots could acquire the ability to communicate by exchanging biosynthesized chemical information carriers. Via communication, microrobots with different perception-action behaviors can coordinate collective behaviors to analyze multiple inputs and generate responses according to designed logic circuits. This work opens up an opportunity to build microrobot swarms with embedded perception-action-communication loops and complex collective behaviors for precise and efficient diagnosis and treatment.

### **5.1 Introduction**

Biohybrid microrobots leveraging unique features and functions of biological modules are a promising technology in biotechnology and biomedical application [100-102]. Their

miniaturized size allows operations within the whole human body, leading to therapies down to the cellular level and offering localized diagnosis and treatment with greater precision and efficiency [100]. For example, magnetic microparticle-based robots demonstrate their ability in targeted drug delivery [3, 32] and image-guided therapy [33]. However, their miniaturized size confines their ability to multitask. A robot swarm can resolve this limitation by having individual robots working collectively, which can emulate high adaptability and enhance tasking capabilities and flexibility [28, 55].

Nowadays, microrobot swarm behaviors rely heavily on human feedback [28, 55, 130]. Autonomous robot swarms capable of perception-action and communication remain a challenge at the microscale [28]. Perception-action is the foundation for autonomous robotic behavior that we established in Chapter 4. These series of perception-action modules executed collectively enable individual robots to communicate, act together, and accomplish more complicated tasks through collective robotic behaviors [7, 55, 102]. While the autonomy of macroscale robots is built on electronics, a platform to build the same autonomy level is left to be identified in micro-, nano-, and even molecular scales [124].

Inspired by electrical engineering, synthetic biology has developed a variety of genetic circuits reminiscent of electronic circuits in biological systems. Synthetic biology has engineered cells with complex perception-action behaviors via rewiring and repurposing biological components [8, 65]. Furthermore, synthetic biology implemented communication behaviors to build artificial multicellular consortia capable of collective behaviors, such as artificial quorum sensing [14] and biocomputing [15, 16]. Researchers have embraced synthetic biology as robot behavior modules but are confined to laboratory settings due to using cells [18, 19, 124]. Cell-free synthetic biology provides a platform to implement these synthetic biology-based behavior

modules without the limitations of using whole cells [70, 126]. Consisting of molecular nanofactories extracted from cells, cell-free systems are engineered chemical environments which allow the synthetic genetic circuit to be transcribed and translated without cells [26, 126].

We utilized the reported cell-free platform in Chapter 4 to build onboard communication modules and collective behaviors on biohybrid microrobots. The platform consists of microparticle-based microrobots, genetic circuit molecular algorithms, and the engineered chemical environment. The engineered chemical environments, the cell-free system, power and carry out microrobot actions by transcription and translation of the onboard genetic circuits. Leveraging the capability of synthetic biology and the cell-free platform for creating complex behaviors, the biohybrid microrobots equipped with different perception-action behaviors can communicate and perform collective behaviors, addressing the limitation posed by their miniaturized size. Via exchanging biochemical information carriers among individual microrobots, the microrobots with different perception-action behaviors work collectively to analyze multiple inputs according to the programmed Boolean logic circuits, expanding the complexity level of molecular computation power of biohybrid microrobots.

## **5.2 Materials and Methods**

The materials and methods were based on the approaches described in Chapter 4. This chapter will briefly discuss the developed methods and added details specific to this chapter.

### 5.2.1 Materials

Q5® High-Fidelity PCR Kit (New England Biolabs) and a thermal cycler (Bio-Rad, C1000 Touch Thermal Cycler) were used to perform PCR for making linear DNA templates. The oligonucleotides were synthesized by IDT Corporation, and sequences are documented in Appendix B. Tetracycline was obtained from Sigma Aldrich (Cat No. 31741).

### 5.2.2 Molecular Algorithm Construction

The molecular algorithm reported in this work were embedded in biotinylated linear DNA templates. We performed PCR with biotinylated primers on the plasmid carrying designed synthetic genetic circuits to make the biotinylated linear DNA templates. For the fluorescent reporter, a PCR with biotinylated forward primer and non-biotinylated reverse primer isolating gene fragment of promoter  $P_{L,tetO-1}$  driving deGFP from plasmid pTXTL-PLtetO1-deGFP (Arbor Biosciences, Cat No. 502098) [26]. The biotinylated forward primer and non-biotinylated reverse primer ensure the same direction of anchoring DNA linear template to material surfaces. For the tetR and aTc related experiments, a PCR with biotinylated forward primer and non-biotinylated reverse primer was performed to extract gene encoding tetR from plasmid pZS4Int-tetR from our group [127]. After PCR, we checked the product size by running electrophoresis at 110 mV for 60 minutes with a gel made of TAE with 1% agarose. Then, we extracted the biotinylated linear DNA template using a Monarch® DNA Gel Extraction Kit (New England Biolabs) and DI water as elution buffer. The concentration of linear DNA template was determined by a Bio-tek Synergy™ HT plate reader with Take3 Micro-Volume Plate.

### 5.2.3 Microrobot Assembly

The genetic circuits were anchored to microparticle-based microrobots via the SA-biotin interaction. First, 10 nM biotinylated linear DNA templates were mixed with 10  $\mu$ l SA coated, 1  $\mu$ m diameter, superparamagnetic microparticles (Thermo Fisher, Dynabeads™ MyOne™ Streptavidin T1). The binding procedure was carried out according to the Dynabeads™ MyOne™ Streptavidin T1 protocol. Briefly, the particles were washed with 1X PBS buffer three times before introducing biotinylated linear DNA templates. For Biotin NOT gate experiments, biotin was added to the biotinylated DNA mixture before the addition of the microparticles. For labeling and differentiating materials, 10 nM Atto 590-Biotin was added to the microparticle that was already mixed with biotinylated linear DNA templates. After 15 minutes of incubation, the microparticle anchored with linear DNA template was separated with magnetic racks and then washed the unbound biotin and biotinylated DNA template was washed away with PBS. Lastly, the microparticle-DNA template complex was resuspended in DI water for the following experiments.

### 5.2.4 Cell-Free Reaction

The cell-free platform used in this work was the myTXTL® linear DNA Expression kit from Arbor Biosciences. The detailed protocol for making and using the cell-free protein expression system was described in previous publications [26, 83]. Briefly, the cell-free reaction has three components – cell extract, buffer, and the DNA template encoding designed genetic circuits. To make cell extract containing transcription and translation machinery, cells are grown to OD<sub>600</sub> 1.5–2.0 and lysed via bead-beating in S30A buffer. Then, run the extract through microchromatography columns to remove beads and through dialysis using 10k MWCO dialysis

cassettes to retain essential transcription and translation components, such as core RNA polymerases and transcription factors. The cell extract is flash-frozen and stored at  $-80\text{ }^{\circ}\text{C}$  to ensure cell-free activity. Finally, a buffer containing amino acids and energy solutions was assembled and calibrated to optimize protein production in cell-free reactions and stored at  $-80\text{ }^{\circ}\text{C}$

The cell-free solution (Sigma 70 master mix) in the myTXTL<sup>®</sup> linear DNA Expression kit is a premix of cell extract and buffer. To set up cell-free reactions, the cell-free solution (sigma 70 master mix) was thawed completely from  $-80\text{ }^{\circ}\text{C}$  frozen stock and was gently mixed with the microparticle-DNA template complex prepared in the previous section. Alternatively, the cell-free solution was mixed with microparticle and DI water for negative control. The cell-free reactions were assembled to volumes of  $10.5\text{ }\mu\text{L}$  with  $7.88\text{ }\mu\text{L}$  cell-free solutions and  $2.64\text{ }\mu\text{L}$  materials mixture solution prepared in the previous section in  $1.5\text{ mL}$  microcentrifuge tubes and incubated at  $29\text{ }^{\circ}\text{C}$  for 12 hours. The cell-free reactions were put on ice to stop reactions.  $2\text{ }\mu\text{L}$  of incubated reactions were pipetted into a microfluidic imaging chamber for material fluorescent response observation. Then, the incubated reactions were put on the magnetic rack to separate the magnetic microparticle-based materials.  $2\text{ }\mu\text{L}$  of supernatant were extracted and pipetted into the observation chamber for fluorescent signal quantification to avoid the non-fluorescent material interfering fluorescent readouts.

### **5.2.5 Observation Chamber Preparation**

Polydimethylsiloxane (PDMS) observation chamber was used to host the materials and observe their behaviors. The master mold of microfluidic devices was prepared via soft lithography at the University of Pittsburgh Nanoscale Fabrication Characterization Facility Cleanroom and was detailed in Chapter 3. To make microfluidic devices, PDMS (Sylgard<sup>™</sup> 184, Dow Corning)

was mixed at a 10:1 base to curing agent ratio and poured over the wafer. The PDMS mixture was degassed in a vacuum chamber and cured in an oven at 65 °C for 1 h. Then, the PDMS was then carefully recovered from the wafer and sliced into individual microfluidic devices. Inlet and outlet holes were punched with a 1 mm biopsy punch (Miltex® Biopsy Punch with Plunger). Next, the devices were bonded to glass coverslips (22 × 40 mm) via a plasma cleaner (PDC-32G, Harrick Plasma) for 20 s. The devices were then incubated at 65 °C for 1 hour to ensure a tight bond between the glass and the PDMS.

### **5.2.6 Material Behavior Observation**

Fluorescent was used as an indicator for evaluating microrobot behaviors. The microfluidic device hosting the cell-free materials was placed onto the stage of a Nikon Eclipse Ti2 microscope and viewed through a 20X objective lens. Images were captured and analyzed with a mounted Andor Zyla 5.5 sCMOS camera and the NIS-Elements software (Nikon).

### **5.2.7 Image and Statistical Analysis**

We characterized the microrobot behaviors by quantifying the biosynthesized fluorescent output signal. A region of interest area with fixed size and position was marked to obtain the fluorescent intensity. The acquired data was normalized to the average signal intensity of the reference. The reference signal is defined as the corresponding control reaction or the highest fluorescent signal output among the experiment set. For example, in the multiple-input experiments, the average fluorescent intensity of all cell-free microrobots responses with no Biotin, no tetR and no aTc in the environment was defined as the reference. All experiments were

performed in triplicate and reported as mean +/- standard deviation. One-way ANOVA was performed and a significance level of 0.05 was determined.

## 5.3 Result

### 5.3.1 Communication via Exchanging Biochemical Information Carriers.

Chapter 4 established the reported cell-free platform utilizing synthetic biology to build perception-action behaviors and perform Boolean logic circuits on microrobots. In this chapter, we harvested the natural communication behavior modules from the living systems to build information exchange on the reported microrobot. Communication is the foundation of collective behaviors and the first step to building multilayer Boolean logic computations on the reported microrobot.

Cell-free synthetic biology has demonstrated its ability to recapitulate the communication between living systems via exchanging biochemical information carriers [14, 136]. Again, we utilized the tetR regulation system to demonstrate the communication behaviors between two designed microrobots – Receiver and Sender. Receiver carried a  $P_{L,tetO-1}$  driving GFP, which constantly produced GFP unless the tetR was present in the environment. Sender produced tetR as the information carrier to communicate with Receiver. Through the tetR regulation system, Sender can control the Receiver's behaviors via the biochemical information carrier, tetR, establishing the information flow between Sender and Receiver. (Figure 5-1A)

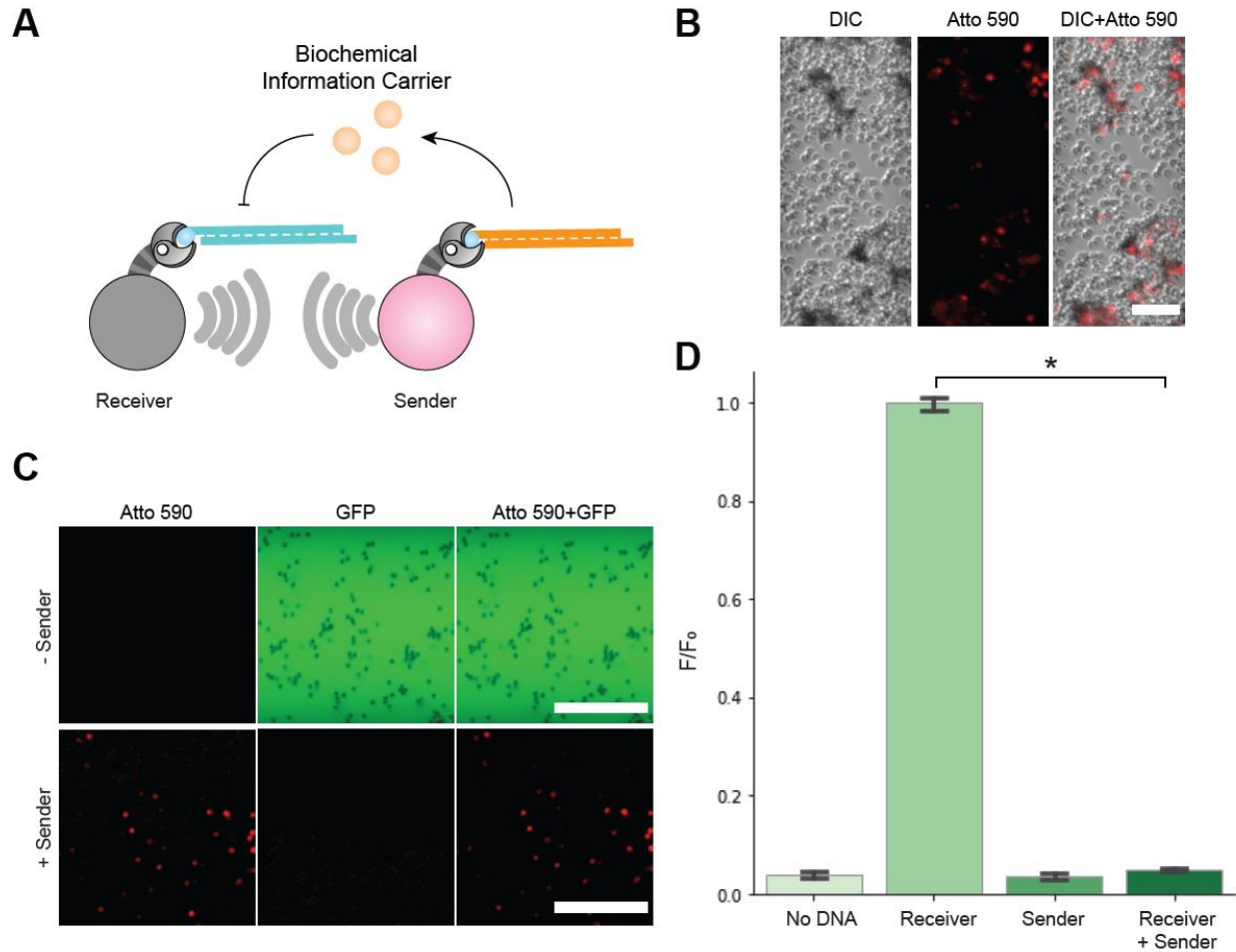


**Figure 5-1. Communication via exchanging biochemical information carriers. (A) Microrobots anchored with different perception-action behaviors can communicate by exchanging biochemical information carriers. (B) DIC and red fluorescent images show the mixture of two microrobots. Sender was tagged with Atto 590, showing red fluorescent. (Scale bar: 12.5  $\mu$ m) (C) The green and red fluorescent images of Receiver with or without Sender. Sender inhibits Receiver from expressing GFP via the biochemical information carrier, tetR. (Scale bar: 25  $\mu$ m) (D) The quantification of fluorescent responses of Receiver and Sender. (\* $p < 0.05$ )**

We demonstrated the interaction between Sender and Receiver by incubating Receiver with or without Sender. Sender was labeled with Atto590-biotin, which showed red fluorescent to differentiate two microrobot types. (Figure 5-2) Figure 5-1B demonstrates a mixture of Sender (red fluorescent) and Receiver (no red fluorescent). Without Sender, Receiver produced GFP since

the Sender-generated tetR did not inhibit the promoter on the Receiver. With the Sender in the environment, the Receiver did not produce GFP since the promoter on its surface was inhibited by Sender-generated tetR. (Figure 5-1C)

Figure 5-1D shows the fluorescent response of Receiver and Sender. Receiver produced GFP when there was no sender. No GFP production was observed with only Sender in the system since Sender does not carry any GFP generating genetic circuit. However, when Sender was present, GFP production by Receiver was inhibited to the same level as there was no DNA template anchored on the microrobot. The results demonstrate the communication between these two microrobots via exchanging biochemical information carriers. Relaying information is the first step for collective behaviors, such as performing multilayer Boolean computation. Hence, the results display the possibility of the reported cell-free stimuli-responsive microrobots that can communicate and execute collective behaviors by harvesting the existing communication modules in synthetic biology.

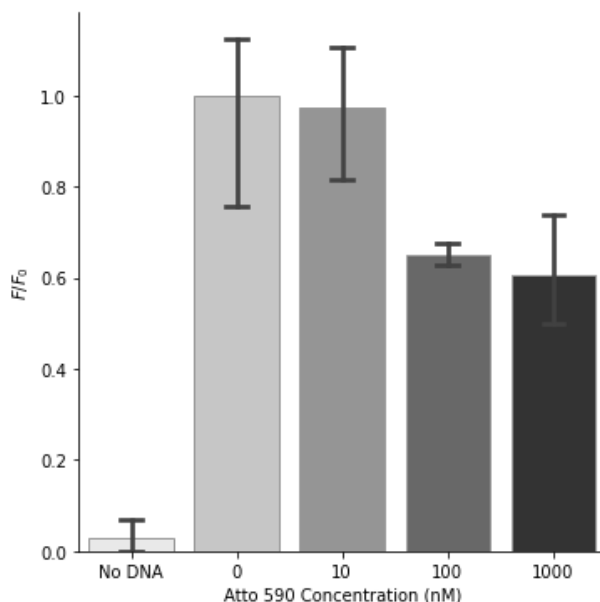


**Figure 5-2. Quantification of the fluorescent output signal generated by microrobots labeled with Atto590-Biotin. The fluorescent intensity generated was not affected by introducing 10 nM Atto590-Biotin.**

### 5.3.2 Collective Behavior Among Cell-Free Microrobots.

Leveraging the perception-action units and communication modules we built, we created a collective behavior between two types of microrobots that take three inputs and generate output according to the designed multilayer Boolean logic circuits. Two types of microrobots anchored with different perception-action units communicate via communication modules and work collaboratively to accomplish environment input analysis and Boolean computation. One microrobot perceives biotin via the surface chemistry enabled Biotin NOT gate. The other microrobot communicates with the Biotin perception-action microrobot via the biochemical information carrier, tetR. The tetR-generating microrobot can perceive aTc via the tetR repressor module. Together, the designed microrobots can analyze the presence of biotin, tetR, and aTc, via surface-functionalized SA and the  $P_{L,tetO-1}$  promoter component on their surfaces, respectively. (Figure 5-3A)

Figure 5-3B denotes the logic table of the designed collective behavior – a multilayer Boolean logic circuit. Biotin, tetR, and aTc as inputs and GFP as output. When there is no biotin or tetR in the system, the GFP production is not inhibited by either the competitive binding or the tetR repressor. However, when tetR is present, the microrobots will generate GFP only when there is aTc to rescue the tetR inhibition and no biotin to competitively bind with the biotinylated DNA generating GFP.

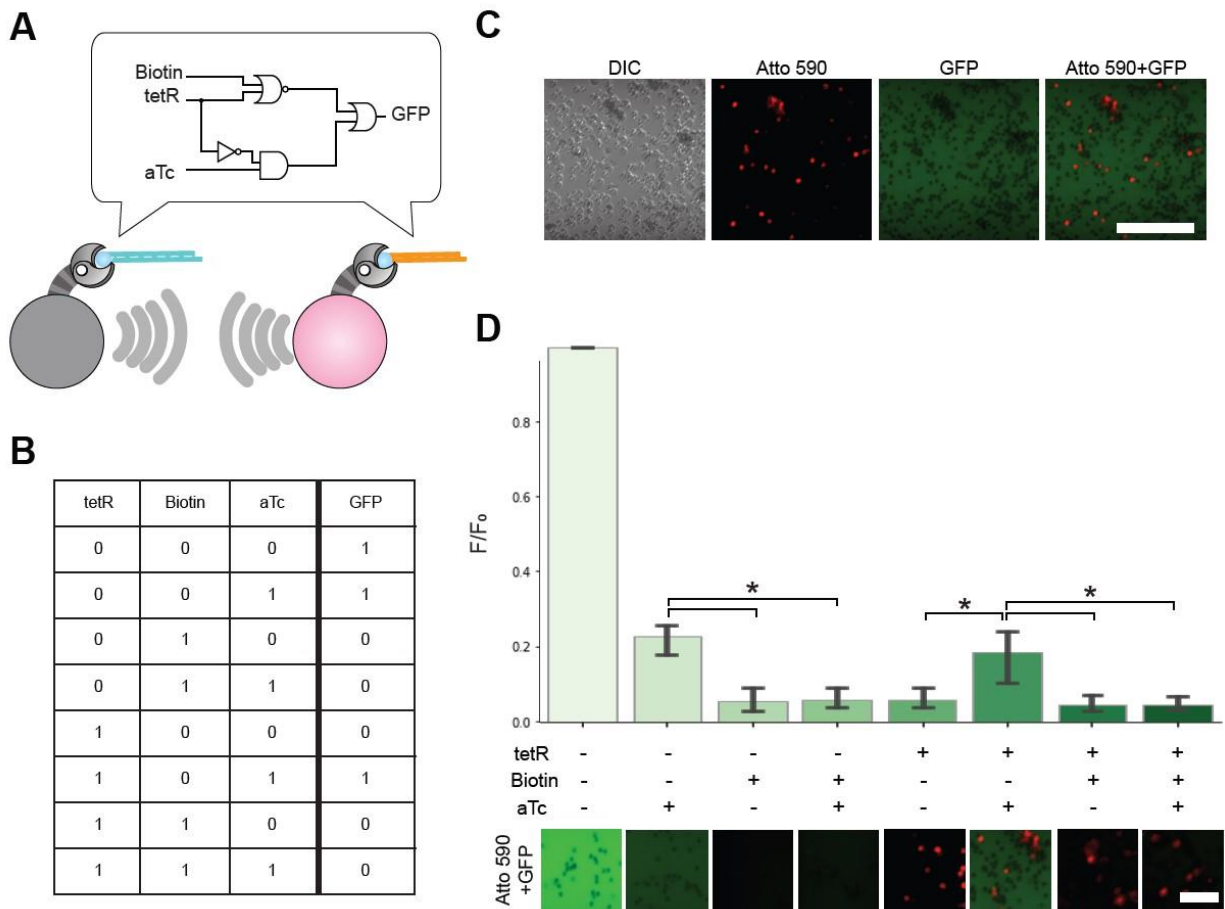


**Figure 5-3. A Collective behavior among microrobots. (A)** The communication among microrobots with different perception-action modules allows them to achieve the denoted Boolean logic circuits. One microrobot carried the biotin perception-action modules while the other carried the aTc perception-action modules. Together, they can perform distributed computation, processing three inputs and generating GFP as output. **(B)** The logic table of the collective behaviors with TetR, biotin, and aTc as inputs and GFP as output. **(C)** DIC, red, and green microscope images of microrobot mixture in the environment without biotin but with tetR and aTc. The Atto 590 differentiated two types of microrobots while the GFP images recorded the output response. (Scale bar: 25  $\mu\text{m}$ ) **(D)** The quantification of fluorescent responses of the material mixture in the environments with or without tetR, biotin, and aTc. (Scale bar: 12.5  $\mu\text{m}$ , \* $p < 0.05$ .)

Figure 5-3C demonstrates the collective behavior between two microrobots under the condition of no biotin but with both tetR and aTc in the system. Since there was no biotin, the

microrobot equipped with the Biotin NOT gate perceived no biotin in the environment and generated GFP as a response. Since both tetR and aTc were present, aTc rescued the tetR inhibition on the fluorescent reporter production. The tetR microrobot equipped with aTc stimuli-responsive module was labeled with Atto590, which showed red fluorescent. The fluorescent reporter GFP indicated the joint action of two microrobots. When overlaying red and green fluorescent together, we could see a mixture of two microrobots and their collective behaviors. Figure 5-3D quantified the collective behavior under all eight possible conditions. As expected, there was observable GFP production in conditions with no biotin and no tetR and the condition with no biotin but with both tetR and aTc. However, conditions with aTc present showed a lower fluorescent intensity level than expected. It was because aTc partially hindered cell-free reaction efficiency. (Figure 5-4)

The results present collective behaviors between microrobots implemented with the reported cell-free platform. Two types of microrobots with different stimuli-responsive modules can communicate via the biochemical information carriers. Together, these two microrobots can analyze three environmental inputs and generate output according to the design Boolean logic circuit. The results demonstrate the potential for using the reported platform in distributed molecular computation systems which can advance the computational power of biological stimuli-responsive microrobots.

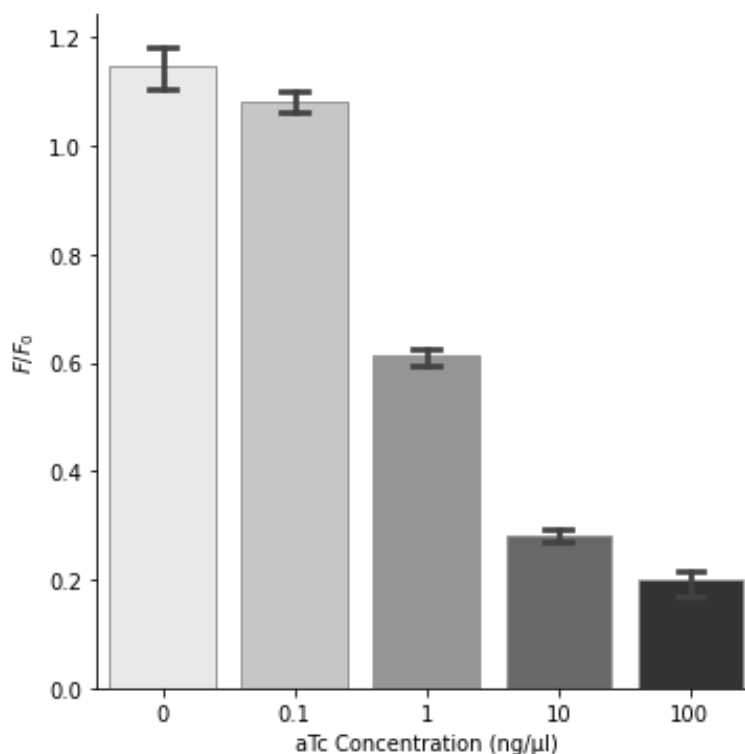


**Figure 5-4. aTc potentially hinders cell-free reaction efficiency.** Cell-free reactions were carried out with 10 nM GFP DNA in various aTc concentrations without tetR. The decreased fluorescent signal intensity suggests that aTc decreases cell-free reaction efficiency.

## 5.4 Discussion & Conclusions

This chapter presents using the reported cell-free synthetic biology platform to build communication modules and collective behaviors for the development of novel intelligent microrobots. The platform allows information exchange among microrobots via the biosynthesized chemical information carriers. The communication between microrobots allows coordination among microrobots and provides the foundation for collective behaviors. Integrating perception-action and communication modules, the reported microrobots carrying different

Boolean computation units worked collectively to implement a logic circuit that processed three inputs and generated fluorescent responses according to the programmed Boolean logic circuits.

The communication and collective behavior demonstrate the feasibility of implementing distributed multilayer Boolean computations, advancing the computation power of the reported smart microrobots. Distributed computation provides a way to increase the complexity of the computation while lessening the burden on individual computation units [137, 138]. The advantage of the distributed computation system has been exemplified by engineered multicellular systems that communicate and perform collective behaviors [10, 139, 140]. Hence, the work established the foundation for implementing distributed computation at the molecular level on the reported microrobots.

In summary, we reported a cell-free platform to leverage synthetic biology as perception-action-communication behaviors modules on biohybrid microrobots. This work reported preliminary results of building collective behaviors for intelligent microrobot swarms. Furthermore, this work opens up an opportunity to build autonomous miniaturized clinical tools with potential use in the human body for precise and efficient diagnosis and treatment.

## 6.0 Conclusion and Outlook

In conclusion, we have reported a cell-free platform to implement behavior modules on microrobots, making the next-generation small-scale robot with complex behaviors possible. First, we built a straightforward yet robust microfluidic tool for cell-free reaction characterization and for observing cell-free microrobot behaviors. Next, we utilized surface chemistry and designed genetic circuits to construct perception-action behavior units on biohybrid microrobots. The reported cell-free platform renders excellent flexibility to implement different synthetic biology-based behavior modules. Furthermore, the platform constructs communication modules for robot swarm collective behavior exemplified by implementing Boolean logic circuits processing multiple inputs. With the ability to create perception-action and communication behaviors, this platform has the potential to become a novel paradigm for enabling autonomy and intelligence in microrobots via the implementation of complex behaviors, as well as creating the possibility for novel therapeutic and diagnostic devices.

### 6.1 Freeze-Dried Cell-Free Platform for Microrobot Portability

Biohybrid microrobot is confined to lab settings despite all the exciting developments due to the need to maintain reactions under specific conditions. Even though this work remains in the laboratory setting, cell-free platforms are known for stability and portability and their immense potential in the field [126]. Pioneered by Collins and colleagues, cell-free platforms can be freeze-dried and stored at room temperature [88]. Simply adding water to the freeze-dried cell-free

solution can activate the transcription and translation of genetic circuits at the time of need. This feature offers solutions to deploying synthetic biology and potentially biohybrid microrobots in the field for applications, including diagnostics and biomanufacturing [74, 141].

As an example, Collins and colleagues have successfully moved synthetic biology outside of the lab by embedding freeze-dried cell-free solution and genetic constructs onto paper [88]. This construct was stable at room temperature and readily stored and distributed to the field. Collins and colleagues applied cell-free platform and DNA elements to small 2 mm filter paper discs and freeze-dried them overnight. After being freeze-dried, these paper discs were rehydrated with water, and the cell-free reactions were successfully carried out on the paper discs. Using this paper-based cell-free platform, Collins and colleagues built strain-specific Ebola and Zika sensors for in vitro diagnostics [74, 88].

Moreover, the team demonstrated a stable and abiotic paper-based platform for synthetic biology that may also apply to materials apart from papers. Later, Collins and colleagues created fabrics embedded with the freeze-dried cell-free solution and nucleic acid biosensors [73]. The fabric is wearable and is made into face masks with lyophilized nucleic acid biosensors generating fluorescent responses or colorimetric changes in the presence of the SARS-CoV-2 virus [73]. The detection limits for the cell-free fabric rival current laboratory methods such as quantitative PCR.

Hence, lyophilized cell-free platforms can extend synthetic biology-based biohybrid microrobots into the real world by eliminating the need to maintain specific reaction criteria. Specifically, with the reported cell-free platform, the magnetic particle based microrobots embedded with genetic circuit behavior modules will be freeze-dried with cell-free solutions. The biohybrid microrobot will be stored and distributed to the field in the lyophilized form and activated by simply adding water. With the lyophilized cell-free platforms, the reported biohybrid

microrobots can be deployed beyond laboratory settings with long-term storage stability and easy distribution conditions, demonstrating their potential use for localized active drug delivery within the human body and their point-of-care ability in the field.

## **6.2 Integration with Molecular Robots**

From macroscale to molecular robotics, robots at various scales have taken advantage of synthetic biology tools to achieve complex behaviors. Synthetic biology based behavior modules are of particular interest to molecular robots since they can be readily integrated at the molecular scale. Embarking from catenanes and rotaxanes, molecular machines have gradually evolved into molecular robots capable of more complex tasks.

Compared to their macroscale counterparts, there is a considerable gap between molecular machines and molecular robots. As the synergy between synthetic biology and microrobots, synthetic biology offers perception-action modules, which we believe, can fill the gap between molecular machines and molecular robots. We have highlighted a myriad of synthetic genetic circuits reminiscent of electronic digital circuits available to engineer molecular robots. The complexity of molecular robot behaviors can improve with advances in biocomputing synthetic genetic circuits. Presently, synthetic biologists have gene-based versions of CPU in human cells and cell-free reactions [13, 118]. In the future, synthetic circuits can confer intelligence and become the control system for autonomous molecular robots.

Biological components have changed the actuation systems of robots at small scales [35]. Exploiting unique characteristics of bacteria and cells, microscale biohybrid robots can autonomously actuate, deliver cargo, and serve as novel therapies [38, 142]. While bacteria and

cells are too large for molecular robots, biological molecules such as DNA and proteins are at the scale for integration for molecular robots.

With the current progress in DNA origami, DNA is an ideal candidate as an actuator in molecular robots. Apart from carrying genetic information, DNA can be used as biological molecular robots capable of self-assembly and actuation [87, 143]. DNA is an ideal material in molecular robots because of its high stability, programmability, and modularity [124, 144]. For example, Qian and co-workers developed an autonomous DNA robot capable of performing cargo-sorting tasks [105]. Furthermore, Praetorius et al. reported a mass-production method of designing and producing DNA origami [145]. This technology will allow the large-scale production of synthetic biology-based biohybrid robots.

Furthermore, DNA based actuators and sensors can be integrated with molecular robots consisting of carbon nanotubes and magnetic nanoparticles. Systems integrating biomolecules and carbon nanotubes have been used as biosensors to build complex nanostructures for nanobioelectronics [146]. The unique electrical and mechanical properties of carbon nanotubes have made them exciting candidates to be used as molecular robot chassis. At the same time, magnetic particles as molecular robot chassis enable contactless control of robots via externally applied magnetic fields [147]. Magnetic control is a most promising method for steering molecular robots for medical applications due to its efficiency, contactless nature, precision, and the established safety of penetrating the human body with magnetic fields (e.g., MRI). Leveraging the capability of synthetic biology and the cell-free platform in creating complex perception-action behaviors, molecular robots can acquire the ability to sense, analyze, and respond to complex environments. Ultimately, we envision next-generation molecular robots with greater autonomy will be biohybrid robots containing synthetic biology-based perception-action modules encoded

on DNA molecules. Cell-free platforms will power on-board perception-action modules and carry out designed behaviors.

In summary, this work demonstrates the advantage of integrating cell-free synthetic biology into the microrobot world, which can be further scaled down to the nanoscale or molecular scale. Our work focused on establishing the fundamental cell-free platform of biohybrid microrobots and designing molecular algorithms that enable autonomous behaviors embedded in the DNA template. We believe that this platform has the potential to become a novel paradigm for enabling autonomy and intelligence in small-scale robots and create the possibility for novel therapeutic and diagnostic devices.

**Appendix A Supplementary Materials for Microfluidic Devices for Cell-Free Reaction  
Characterization**

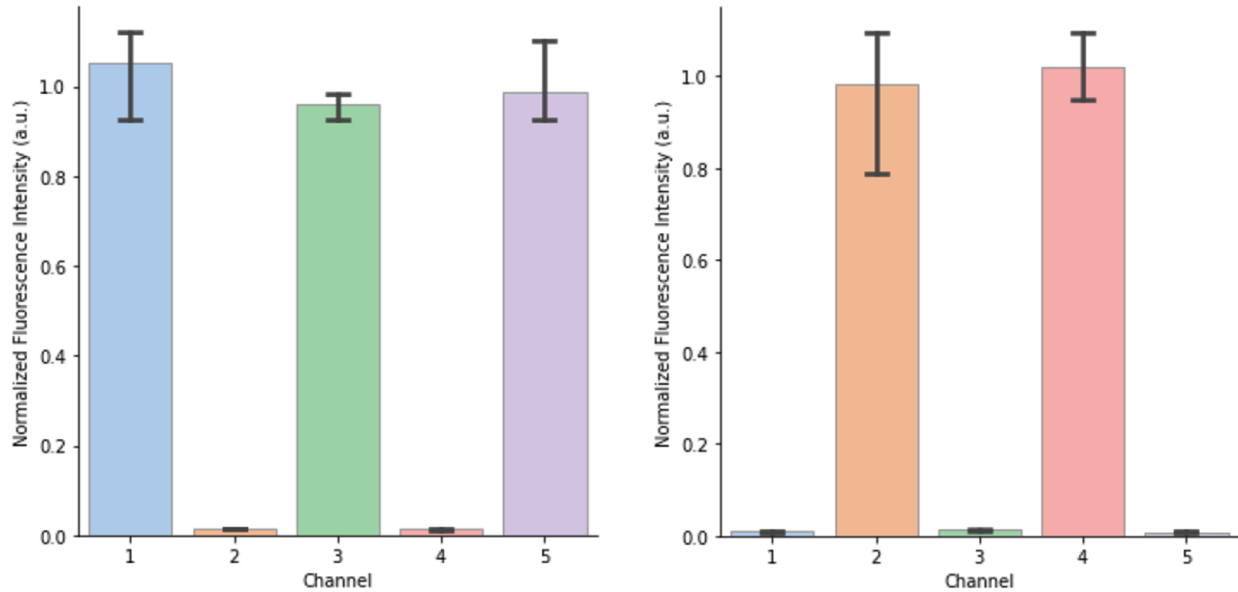
**Appendix A.1 Step-by-Step Protocol**

**Appendix A.1.1 Fabrication and Characterization of Microfluidic Devices**

**Appendix A.1.2 Cell-Free Reaction**

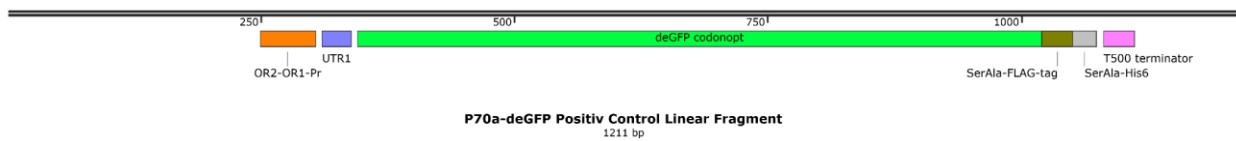
**Appendix A.1.3 Image Acquisition and Analysis**

## Appendix A.2 No Fluorescent Interference was Observed Between Channels in Designed Microfluidic Devices.



Appendix Figure 1. No fluorescent interference was observed between channels in designed microfluidic devices. Microfluidic device channels were filled with 2  $\mu$ L CF<sup>®</sup>488A or 2  $\mu$ L DI water, alternatively. Quantification of devices with (A) three channels of CF<sup>®</sup>488A and (B) two channels of CF<sup>®</sup>488A.

## Appendix A.3 P70a-deGFP Positive Control Linear Fragment



Appendix Figure 2. P70a-deGFP linear fragment map.

GGCTGCAGTTCATGTGGTGGGACAGCACCCGCGGCAAGCCCTAGTGCAATGGCGGT  
ATCCTACCACTCGTACCGTGGTAGAGGCGACGCCACTAGTAGGGATACTGGGAAGG  
CTCACAGGCCTCCGCCTTGTAGGCCGGTGCTTACCCCTACATAACAGGGGCTGCCAG  
TGTTACCCCGCGAGGATCCGAAAAGGCGAGCCGGCTCCGGTCCGACCCGGGAGGTG  
ACGGGCCTCAAAGCCGCGTGGGAGTGAGCTAACACCGTGCGTGTTGACAATTTTACC  
TCTGGCGGTGATAATGGTTGCAGCTACTAATAATTTTGTTTAACTTTAAGAAGGAGA  
TATACCATGGAAGTGTTCACCGGTGTTGTTCCGATTCTGGTTGAACTGGATGGTGAT  
GTTAATGGCCACAAATTCTCAGTTAGCGGTGAAGGCGAAGGTGATGCAACCTATGG  
TAAACTGACCCTGAAGTTTATCTGTACCACCGGCAAAGTCCCGGTTCCGTGGCCGAC  
CCTGGTTACCACCCTGACCTATGGTGTTTCAGTGTTTCAGCCGTTATCCGGATCACATG  
AAACAGCACGACTTCTTTAAGAGCGCAATGCCGGAAGGTTATGTTCAAGAACGTAC  
CATCTTCTTCAAAGATGACGGCAAAGTATAAGACCCGTGCCGAAGTTAAATTTGAAGG  
TGATACCCTGGTGAATCGCATTGAACTGAAAGGCATCGATTTCAAAGAGGATGGTA  
ATATCCTGGGTCACAAACTGGAATATAATTATAATAGCCACAACGTGTATATCATGG  
CAGACAAACAGAAGAATGGCATCAAAGTGAAGTTCAAGATCCGCCACAACATTGAA  
GATGGTAGCGTTCAGCTGGCAGATCATTATCAGCAGAATACGCCGATTGGTGATGGT  
CCGGTTCTGCTGCCGATAATCATTATCTGAGCACCCAGAGCGCACTGAGCAAAGAT  
CCGAATGAGAAACGTGATCACATGGTGCTGCTGGAATTCGTTACCGCAGCAGGTATT  
AGCGCTGATTACAAGGATGATGACGATAAGAGCGCTCACCATCACCATCACCATTA  
AAATGCAAAGCCCGCCGAAAGGCGGGCTTTTCTGTACTTCGCAACGATTTTCGGAGTC  
CGGAGACTCGCTGTTTTCGAAATTTGCGCTCAAGGGCGGGTATTGAACCAGGCTTAC  
GCCAGGAACGTAGCAAGGTG

**Appendix B Supplementary Materials for Perception-Action Behavior Modules on  
Biohybrid Microrobots**

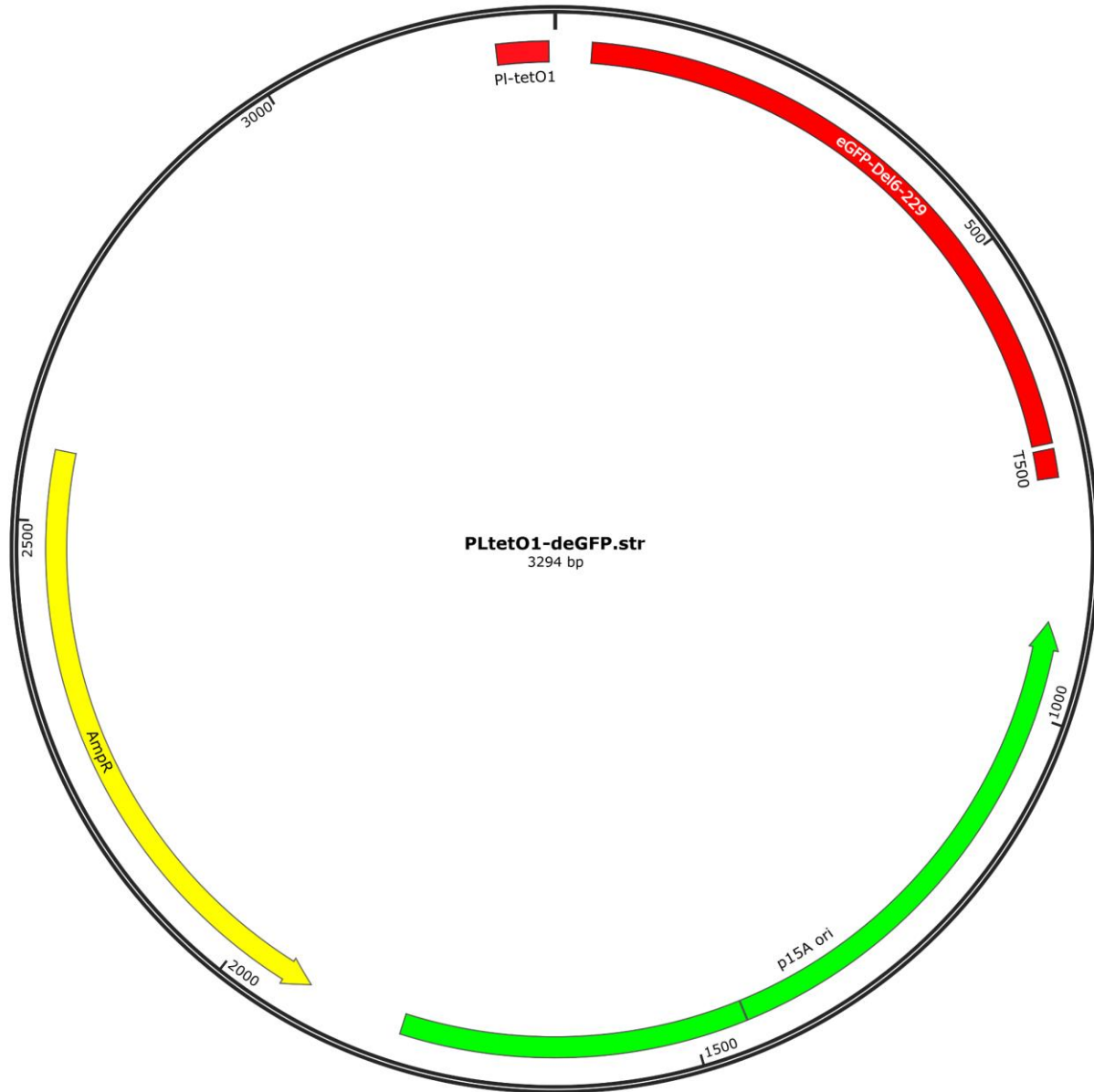
**Appendix B.1 pTXTL-PLtetO1-deGFP**

**Appendix B.1.1 Primers for pTXTL-PLtetO1-deGFP**

**Appendix Table 1. Primer list for PLtetO1-deGFP.**

Primer Name	Sequence (5' 3')
deGFP Forward Primer	CTGGCGAATCCTCTGACCAG
deGFP Reverse Primer	ATGATAAAGAAGACAGTCATAAGTGCGGC

### Appendix B.1.2 pTXTL-PLtetO1-deGFP Plasmid Sequence



Appendix Figure 3. pTXTL-PLtetO1-deGFP plasmid map.

```
AATAATTTTGTTTAACTTTAAGAAGGAGATATACCATGGAGCTTTTCACTGGCGTTG  
TTCCCATCCTGGTCGAGCTGGACGGCGACGTAAACGGCCACAAGTTCAGCGTGTCCG
```

GCGAGGGCGAGGGCGATGCCACCTACGGCAAGCTGACCCTGAAGTTCATCTGCACC  
ACCGGCAAGCTGCCCCTGCCCTGGCCACCTCGTGACCACCTGACCTACGGCGTG  
CAGTGCTTCAGCCGCTACCCCGACCACATGAAGCAGCACGACTTCTTCAAGTCCGCC  
ATGCCCCGAAGGCTACGTCCAGGAGCGCACCATCTTCTTCAAGGACGACGGCAACTA  
CAAGACCCGCGCCGAGGTGAAGTTCGAGGGCGACACCCTGGTGAACCGCATCGAGC  
TGAAGGGCATCGACTTCAAGGAGGACGGCAACATCCTGGGGCACAAGCTGGAGTAC  
AACTACAACAGCCACAACGTCTATATCATGGCCGACAAGCAGAAGAACGGCATCAA  
GGTGAACTTCAAGATCCGCCACAACATCGAGGACGGCAGCGTGCAGCTCGCCGACC  
ACTACCAGCAGAACACCCCATCGGCGACGGCCCCGTGCTGCTGCCGACAACCAC  
TACCTGAGCACCCAGTCCGCCCTGAGCAAAGACCCCAACGAGAAGCGCGATCACAT  
GGTCCTGCTGGAGTTCGTGACCGCCGCCGGGATCTAACTCGAGCAAAGCCCGCCGA  
AAGGCGGGCTTTTCTGTGTCAACCGATGCCCTTGAGAGCCTTCAACCCAGTCAGCTC  
CTTCCGGTGGGCGCGGGGCATGACTATCGTCGCCGCACTTATGACTGTCTTCTTTATC  
ATGCAACTCGTAGGACAGGTGCCGGCATGATAAGCTGTCAAACATGAGAATTGCAA  
CTTATATCGTATGGGGCTGACTTCAGGTGCTACATTTGAAGAGATAAATTGCACTGA  
AATCTAGAAATATTTTATCTGATTAATAAGATGATCTTCTTGAGATCGTTTTGGTCTG  
CGCGTAATCTCTTGCTCTGAAAACGAAAAAACCGCCTTGCAGGGCGGTTTTTCGAAG  
GTTCTCTGAGCTACCAACTCTTTGAACCGAGGTAACCTGGCTTGGAGGAGCGCAGTCA  
CCAAA ACTTGTCTTT CAGTTTAGCCTTAACCGGCGCATGACTTCAAGACTAACTCCT  
CTAAATCAATTACCAGTGGCTGCTGCCAGTGGTGCTTTTGCATGTCTTTCCGGGTTGG  
ACTCAAGACGATAGTTACCGGATAAGGCGCAGCGGTCGGACTGAACGGGGGGTTCCG  
TGCATACAGTCCAGCTTGGAGCGAACTGCCTACCCGGA ACTGAGTGTCAGGCGTGG  
AATGAGACAAACGCGGCCATAACAGCGGAATGACACCGGTAAACCGAAAGGCAGG

AACAGGAGAGCGCACGAGGGAGCCGCCAGGGGGAAACGCCTGGTATCTTTATAGTC  
CTGTCCGGGTTTCGCCACCACTGATTTGAGCGTCAGATTTTCGTGATGCTTGTCAGGGG  
GGCGGAGCCTATGGAAAAACGGCTTTGCCGCGGCCCTCTCACTTCCCTGTTAAGTAT  
CTTCCTGGCATCTTCCAGGAAATCTCCGCCCCGTTTCGTAAGCCATTTCCGCTCGCCGC  
AGTCGAACGACCGAGCGTAGCGAGTCAGTGAGCGAGGAAGCGGAATATATCCTGTA  
TCACATATTCTGCTGACGCACCGGTGCAGCCTTTTTTCTCCTGCCACATGAAGCACTT  
CACTGACACCCTCATCAGTGCCAACATAGTAAGCCAGTATACACTCCGCTAGGGTCA  
TGAGATTATCAAAAAGGATCTTCACCTAGATCCTTTTAAATTA AAAAATGAAGTTTTA  
AATCAATCTAAAGTATATATGAGTAAACTTGGTCTGACAGTTACCAATGCTTAATCA  
GTGAGGCACCTATCTCAGCGATCTGTCTATTTTCGTTTCATCCATAGTTGCCTGACTCCC  
CGTCGTGTAGATAACTACGATACGGGAGGGCTTACCATCTGGCCCCAGTGCTGCAAT  
GATACCGCGAGACCCACGCTCACCGGCTCCAGATTTATCAGCAATAAACCAGCCAG  
CCGGAAGGGCCGAGCGCAGAAGTGGTCCTGCAACTTTATCCGCTCCATCCAGTCTA  
TTAATTGTTGCCGGGAAGCTAGAGTAAGTAGTTCGCCAGTTAATAGTTTTCGCAACG  
TTGTTGCCATTGCTACAGGCATCGTGGTGTACGCTCGTCGTTTGGTATGGCTTCATT  
CAGCTCCGGTTC CAACGATCAAGGCGAGTTACATGATCCCCATGTTGTGCAAAAA  
AGCGGTTAGCTCCTTCGGTCCTCCGATCGTTGTCAGAAGTAAGTTGGCCGCAGTGTT  
ATCACTCATGGTTATGGCAGCACTGCATAATTCTCTTACTGTCATGCCATCCGTAAG  
ATGCTTTTCTGTGACTGGTGAGTACTCAACCAAGTCATTCTGAGAATAGTGTATGCG  
GCGACCGAGTTGCTCTTGCCCGGCGTCAATACGGGATAATACCGCGCCACATAGCA  
GAACTTTAAAAGTGCTCATCATTGGAAAACGTTCTTCGGGGCGAAA ACTCTCAAGGA  
TCTTACCGCTGTTGAGATCCAGTTCGATGTAACCCACTCGTGCACCCA ACTGATCTTC  
AGCATCTTTTACTTTCACCAGCGTTTCTGGGTGAGCAAAAACAGGAAGGCAAAAATGC

CGCAAAAAGGGAATAAGGGCGACACGGAAATGTTGAATACTCATACTCTTCCTTTT  
TCAATATTATTGAAGCATTATCAGGGTTATTGTCTCATGAGCGGATACATATTTGA  
ATGTATTTAGAAAAATAACAAATAGGGGTTCGCGCACATTTCCCCGAAAAGTGC  
CACCTGACGTCTAAGAAACCATTATTATCATGACATTAACCTATAAAAATAGGCGTA  
TCACGAGGCCCTTTCGTCTTCAAGAATTCTGGCGAATCCTCTGACCAGCCAGAAAAC  
GACCTTTCTGTGGTGAAACCGGATGCTGCAATTCAGAGCGCCAGCAAGTGGGGGAC  
AGCAGAAGACCTGACCGCCGCAGAGTGGATGTTTGACATGGTGAAGACTATCGCAC  
CATCAGCCAGAAAACCGAATTTTGCTGGGTGGGCTAACGATATCCGCCTGATGCGTG  
AACGTGACGGACGTAACCACCGCGACATGTGTGTGCTGTTCCGCTGGGCATGCTCCC  
TATCAGTGATAGAGATTGACATCCCTATCAGTGATAGAGATACTGAGCACAGCTAGC

### Appendix B.1.3 Linear pTXTL-PLtetO1-deGFP Fragment Sequence



Appendix Figure 4. Linear PLtetO1-deGFP fragment.

CTGGCGAATCCTCTGACCAGCCAGAAAACGACCTTTCTGTGGTGAAACCGGATGCTG  
CAATTCAGAGCGCCAGCAAGTGGGGGACAGCAGAAGACCTGACCGCCGCAGAGTG  
GATGTTTGACATGGTGAAGACTATCGCACCATCAGCCAGAAAACCGAATTTTGCTGG  
GTGGGCTAACGATATCCGCCTGATGCGTGAACGTGACGGACGTAACCACCGCGACA  
TGTGTGTGCTGTTCCGCTGGGCATGCTCCCTATCAGTGATAGAGATTGACATCCCTAT  
CAGTGATAGAGATACTGAGCACAGCTAGCAATAATTTGTTTAACTTTAAGAAGGAG  
ATATAACCATGGAGCTTTTCACTGGCGTTGTTCCCATCCTGGTCGAGCTGGACGGCGA  
CGTAAACGGCCACAAGTTCAGCGTGTCCGGCGAGGGCGAGGGCGATGCCACCTACG

GCAAGCTGACCCTGAAGTTCATCTGCACCACCGGCAAGCTGCCCCGTGCCCTGGCCCA  
 CCCTCGTGACCACCCTGACCTACGGCGTGCAGTGCTTCAGCCGCTACCCCGACCACA  
 TGAAGCAGCACGACTTCTTCAAGTCCGCCATGCCCCGAAGGCTACGTCCAGGAGCGC  
 ACCATCTTCTTCAAGGACGACGGCAACTACAAGACCCGCGCCGAGGTGAAGTTCGA  
 GGGCGACACCCTGGTGAACCGCATCGAGCTGAAGGGCATCGACTTCAAGGAGGACG  
 GCAACATCCTGGGGCACAAGCTGGAGTACAACACTACAACAGCCACAACGTCTATATC  
 ATGGCCGACAAGCAGAAGAACGGCATCAAGGTGAACTTCAAGATCCGCCACAACAT  
 CGAGGACGGCAGCGTGCAGCTCGCCGACCACTACCAGCAGAACACCCCCATCGGCG  
 ACGGCCCCGTGCTGCTGCCCCGACAACCACTACCTGAGCACCCAGTCCGCCCTGAGCA  
 AAGACCCCAACGAGAAGCGCGATCACATGGTCCTGCTGGAGTTCGTGACCGCCGCC  
 GGGATCTAACTCGAGCAAAGCCCGCCGAAAGGGCGGGCTTTTCTGTGTCAACCGATG  
 CCCTTGAGAGCCTTCAACCCAGTCAGCTCCTTCCGGTGGGCGCGGGGCATGACTATC  
 GTCGCCGCACTTATGACTGTCTTCTTTATCAT

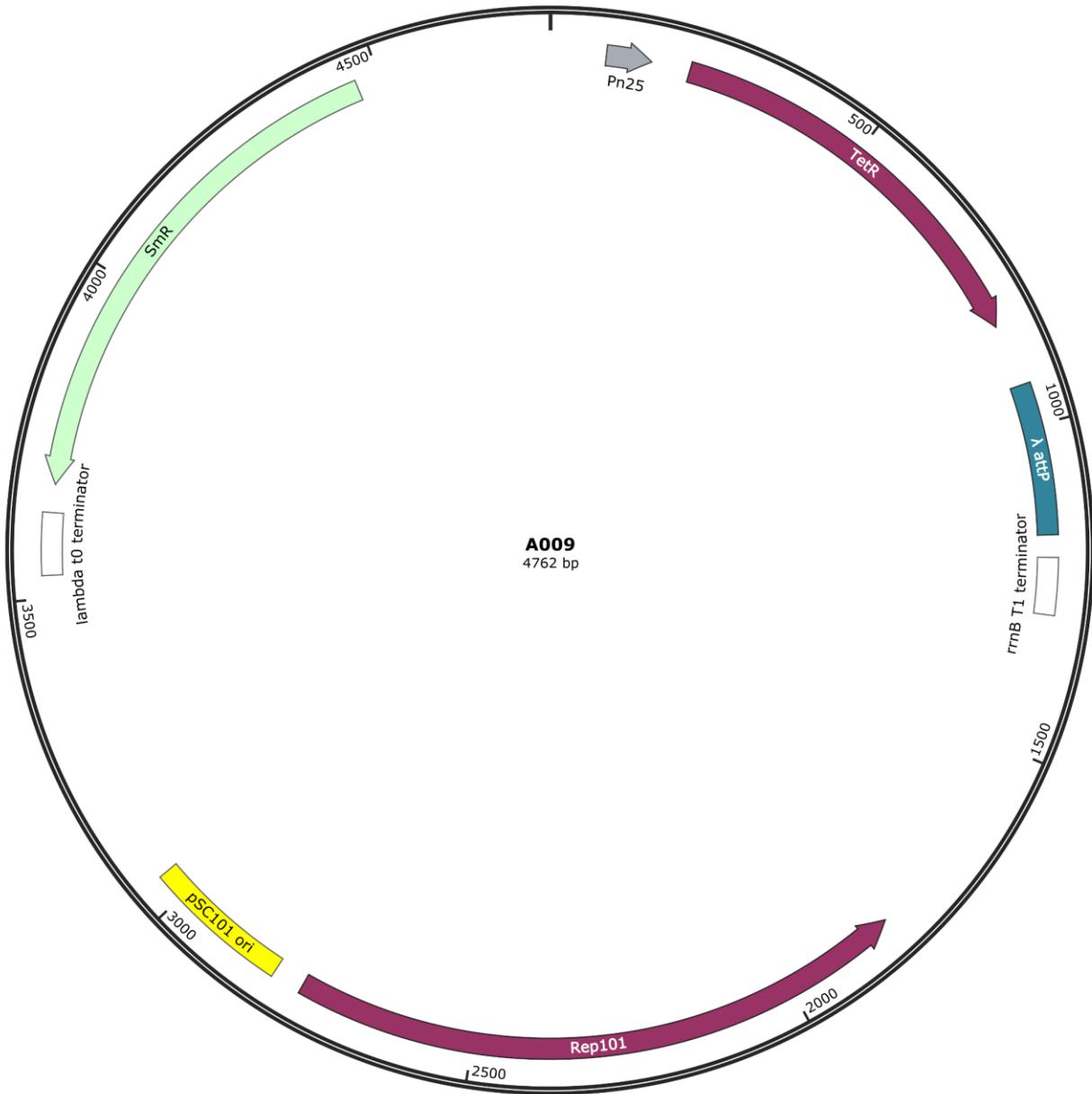
## Appendix B.2 pZS4Int-tetR

### Appendix B.2.1 Primers for pZS4Int-tetR

Appendix Table 2. Primer for pZS4Int-tetR.

Primer Name	Sequence (5' 3')
tetR Forward Primer	ATGTCATAACAAGAAGCCATGAAAACCG
tetR Reverse Primer	TGTAACAGAGCATTAGCGCAAGG

## Appendix B.2.2 pZS4Int-tetR Plasmid Map and Sequence



Appendix Figure 5. pZS4Int-tetR plasmid map.

GACGTCTAAGAAACCATTATTATCATGACATTAACCTATAAAAATAGGCGTATCACG  
 AGGCCCTTTCGTCTTCACCTCGAGGGAAATCATAAAAAATTTATttgcttTCAGGAAAAT

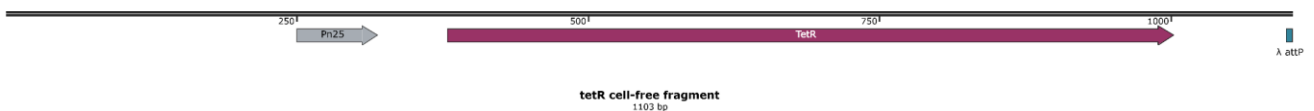
TTTTCTGtataatAGATTCaTAAATTTGAGAGAAGAGTTTAAATATGGCTGGTTCTCGCA  
GAAAGAAACATATCCATGAAATCCCGCCCCGAATTCATatgTCTAGATTAGATAAAAG  
TAAAGTGATTAACAGCGCATTAGAGCTGCTTAATGAGGTCGGAATCGAAGGTTTAA  
CAACCCGTAAACTCGCCCAGAAGCTAGGTGTAGAGCAGCCTACATTGTATTGGCATG  
TAAAAATAAGCGGGCTTTGCTCGACGCCTTAGCCATTGAGATGTTAGATAGGCACC  
ATACTCACTTTTGCCTTTAGAAGGGGAAAGCTGGCAAGATTTTTTACGTAATAAGG  
CTAAAAGTTTTAGATGTGCTTTACTAAGTCATCGCGATGGAGCAAAGTACATTTAG  
GTACACGGCCTACAGAAAAACAGTATGAAACTCTCGAAAATCAATTAGCCTTTTTAT  
GCCAACAAGGTTTTTCACTAGAGAATGCATTATATGCACTCAGCGCTGTGGGGCATT  
TTACTTTAGGTTGCGTATTGGAAGATCAAGAGCATCAAGTCGCTAAAGAAGAAAGG  
GAAACACCTACTACTGATAGTATGCCGCCATTATTACGACAAGCTATCGAATTATTT  
GATCACCAAGGTGCAGAGCCAGCCTTCTTATTCGGCCTTGAATTGATCATATGCGGA  
TTAGAAAAACAACCTTAAATGTGAAAGTGGGTCTtaaGCTTTCTAGATAGCTGAGTAGC  
CTAGAGTGCGCGACAGGTTTGATGACAAAAAATTAGCGCAAGAAGACAAAAATCAC  
CTTGCGCTAATGCTCTGTTACAGGTCCTAATACCATCTAAGTAGTTGATTCATAGTG  
ACTGCATATGTTGTGTTTTACAGTATTATGTAGTCTGTTTTTTATGCAAATCTAATT  
TAATATATTGATATTTATATCATTTTACGTTTCTCGTTCAgctttttatactaaGTTGGCATTAT  
AAAAAAGCATTGCTTATCAATTTGTTGCAACGAACAGGTCCTATCAGTCAAATAA  
AATCATTATTTGATTTCAATTTTGTCCCACTCCCCCTAGAGGCATCAAATAAAACGA  
AAGGCTCAGTCGAAAGACTGGGCCTTTCGTTTTATCTGTTGTTTGTCCGGTGAACGCTC  
TCCTGAGTAGGACAAATCCGCCGCCCTAGACCTAGGGTACGGGTTTTGCTGCCCGCA  
AACGGGCTGTTCTGGTGTGCTAGTTTGTATCAGAATCGCAGATCCGGCTTCAGGT  
TTGCCGGCTGAAAGCGCTATTTCTTCCAGAATTGCCATGATTTTTTCCCCACGGGAG

GCGTCACTGGCTCCCGTGTGTCGGCAGCTTTGATTGATAAGCAGCATCGCCTGTT  
CAGGCTGTCTATGTGTGACTGTTGAGCTGTAACAAGTTGTCTCAGGTGTTCAATTTCA  
TGTTCTAGTTGCTTTGTTTTACTGGTTTCACCTGTTCTATTAGGTGTTACATGCTGTTC  
ATCTGTTACATTGTCGATCTGTTTCATGGTGAACAGCTTTAAATGCACCAAAAACTCG  
TAAAAGCTCTGATGTATCTATCTTTTTTACACCGTTTTTCATCTGTGCATATGGACAGT  
TTCCCTTTGATATCTAACGGTGAACAGTTGTTCTACTTTTGTTTGTTAGTCTTGATGC  
TTCCTGATAGATAACAAGAGCCATAAGAACCTCAGATCCTTCCGTATTTAGCCAGTA  
TGTTCTCTAGTGTGGTTCGTTGTTTTTGCCTGAGCCATGAGAACGAACCATTGAGATC  
ATGCTTACTTTGCATGTCCTCAAAAATTTGCCTCAAACTGGTGAGCTGAATTTTT  
GCAGTTAAAGCATCGTGTAGTGTTTTTCTTAGTCCGTTACGTAGGTAGGAATCTGAT  
GTAATGGTTGTTGGTATTTTGTCCACCATTCATTTTTATCTGGTTGTTCTCAAGTTCGGT  
TACGAGATCCATTTGTCTATCTAGTTCAACTTGGAAAATCAACGTATCAGTCGGGCG  
GCCTCGCTTATCAACCACCAATTCATATTGCTGTAAGTGTTTAAATCTTTACTTATT  
GGTTTCAAACCCATTGGTTAAGCCTTTTAAACTCATGGTAGTTATTTTCAAGCATT  
ACATGAACTTAAATTCATCAAGGCTAATCTCTATATTTGCCTTGTGAGTTTTCTTTG  
TGTTAGTTCTTTTAAATAACCACTCATAAATCCTCATAGAGTATTTGTTTTCAAAGAC  
TTAACATGTTCCAGATTATATTTTATGAATTTTTTTAACTGGAAAAGATAAGGCAAT  
ATCTCTTCACTAAAACTAATTCATTTTTTTCGCTTGAAGAACTTGGCATAGTTTGTCC  
ACTGGAAAATCTCAAAGCCTTTAACCAAAGGATTCCTGATTTCCACAGTTCTCGTCA  
TCAGCTCTCTGGTTGCTTTAGCTAATACACCATAAGCATTTCCTACTGATGTTTCAT  
CATCTGAGCGTATTGGTTATAAGTGAACGATACCGTCCGTTCTTTCCTTGTAGGGTTT  
TCAATCGTGGGGTTGAGTAGTGCCACACAGCATAAAATTAGCTTGGTTTCATGCTCC  
GTTAAGTCATAGCGACTAATCGCTAGTTCATTTGCTTTGAAAACAATAATTCAGAC

ATACATCTCAATTGGTCTAGGTGATTTTAATCACTATAACCAATTGAGATGGGCTAGT  
CAATGATAAATACTAGTCCTTTTCCTTTGAGTTGTGGGTATCTGTAAATTCTGCTAGA  
CCTTTGCTGGAAAACCTTGTAATTCTGCTAGACCCTCTGTAAATTCCGCTAGACCTTT  
GTGTGTTTTTTTTGTTTATATTCAAGTGGTTATAATTTATAGAATAAAGAAAGAATAA  
AAAAAGATAAAAAGAATAGATCCCAGCCCTGTGTATAACTCACTACTTTAGTCAGTT  
CCGCAGTATTACAAAAGGATGTCGCAAACGCTGTTTGCTCCTCTACAAAACAGACCT  
TAAAACCCTAAAGGCTTAAGTAGCACCCCTCGCAAGCTCGGGCAAATCGCTGAATATT  
CCTTTTGTCTCCGACCATCAGGCACCTGAGTCGCTGTCTTTTTTCGTGACATTCAGTTC  
GCTGCGCTCACGGCTCTGGCAGTGAATGGGGGTAAATGGCACTACAGGCGCCTTTTA  
TGGATTCATGCAAGGAACTACCCATAATAACAAGAAAAGCCCGTCACGGGCTTCTC  
AGGGCGTTTTATGGCGGGTCTGCTATGTGGTGCTATCTGACTTTTTGCTGTTTCAGCAG  
TTCCTGCCCTCTGATTTTCCAGTCTGACCACTTCGGATTATCCCGTGACAGGTCATTC  
AGACTGGCTAATGCACCCAGTAAGGCAGCGGTATCATCAACAGGCTTACCCGTCTTA  
CTGTCCCTAGTGCTTGGATTCTCACCAATAAAAAACGCCCGGCGGCAACCGAGCGTT  
CTGAACAAATCCAGATGGAGTTCTGAGGTCATTAAGGATCTATCAACAGGAGTCCA  
AGCGAGCTCGATATCCGTCGGCTTGAACGAATTGTTAGACATTATTTGCCGACTACC  
TTGGTGATCTCGCCTTTCACGTAGTGGACAAATTCTTCCAAGTATGACGGGC  
GCCAAGCGATCTTCTTCTTGTCCAAGATAAGCCTGTCTAGCTTCAAGTATGACGGGC  
TGATACTGGGCCGGCAGGCGCTCCATTGCCAGTCGGCAGCGACATCCTTCGGCGCG  
ATTTTGCCGGTTACTGCGCTGTACCAATGCGGGACAACGTAAGCACTACATTTGCGC  
TCATCGCCAGCCCAGTCGGGCGGCGAGTTCATAGCGTTAAGGTTTCATTTAGCGCC  
TCAAATAGATCCTGTTTCAGGAACCGGATCAAAGAGTTCCTCCGCCGCTGGACCTACC  
AAGGCAACGCTATGTTCTTCTTGCTTTTGTGTCAGCAAGATAGCCAGATCAATGTCGTAC

GTGGCTGGCTCGAAGATACCTGCAAGAATGTCATTGCGCTGCCATTCTCCAAATTGC  
 AGTTCGCGCTTAGCTGGATAACGCCACGGAATGATGTCGTCGTGCACAACAATGGTG  
 ACTTCTACAGCGCGGAGAATCTCGCTCTCTCCAGGGGAAGCCGAAGTTTCCAAAAG  
 GTCGTTGATCAAAGCTCGCCGCGTTGTTTCATCAAGCCTTACGGTCACCGTAACCAG  
 CAAATCAATATCACTGTGTGGCTTCAGGCCGCCATCCACTGCGGAGCCGTACAAATG  
 TACGGCCAGCAACGTCGGTTCGAGATGGCGCTCGATGACGCCAACTACCTCTGATA  
 GTTGAGTCGATACTTCGGCGATCACCGCTTCCCTCATGATGTTTAACTTTGTTTTAGG  
 GCGACTGCCCTGCTGCGTAACATCGTTGCTGCTCCATAACATCAAACATCGACCCAC  
 GCGGTAACGCGCTTGCTGCTTGGATGCCCGAGGCATAGACTGTACCCCAAAAAAAC  
 ATGTCATAACAAGAAGCCATGAAAACCGCCACTGCGCCGTTACCACCGCTGCGTTC  
 GGTCAAGGTTGTGGACCAGTTGCGTGACGGCAGTTACGCTACTTGCATTACAGCTTA  
 CGAACCGAACGAGGCTTATGTCCACTGGGTTTCGTGCCTTCATCCGGATATC

### Appendix B.2.3 Linear pZS4Int-tetR Fragment



Appendix Figure 6. Linear pZS4Int-tetR fragment.

ATGTCATAACAAGAAGCCATGAAAACCGCCACTGCGCCGTTACCACCGCTGCGTTC  
 GGTCAAGGTTGTGGACCAGTTGCGTGACGGCAGTTACGCTACTTGCATTACAGCTTA  
 CGAACCGAACGAGGCTTATGTCCACTGGGTTTCGTGCCTTCATCCGGATATCGACGTC  
 TAAGAAACCATTATTATCATGACATTAACCTATAAAAATAGGCGTATCACGAGGCC

TTTCGTCTTCACCTCGAGGGAAATCATAAAAAATTTATtggcttTCAGGAAAATTTTTCT  
GtataatAGATTCaTAAATTTGAGAGAAGAGTTTAAATATGGCTGGTTCTCGCAGAAAGA  
AACATATCCATGAAATCCCGCCCCGAATTCATatgTCTAGATTAGATAAAAAGTAAAGT  
GATTAACAGCGCATTAGAGCTGCTTAATGAGGTTCGGAATCGAAGGTTTAACAACCC  
GTAAACTCGCCCAGAAGCTAGGTGTAGAGCAGCCTACATTGTATTGGCATGTAAAA  
AATAAGCGGGCTTTGCTCGACGCCTTAGCCATTGAGATGTTAGATAGGCACCATACT  
CACTTTTGCCCTTTAGAAGGGGAAAGCTGGCAAGATTTTTTACGTAATAAGGCTAAA  
AGTTTTAGATGTGCTTTACTAAGTCATCGCGATGGAGCAAAAGTACATTTAGGTACA  
CGGCCTACAGAAAAACAGTATGAAACTCTCGAAAATCAATTAGCCTTTTTATGCCAA  
CAAGGTTTTTCACTAGAGAATGCATTATATGCACTCAGCGCTGTGGGGCATTTTACT  
TTAGGTTGCGTATTGGAAGATCAAGAGCATCAAGTCGCTAAAGAAGAAAGGGAAAC  
ACCTACTACTGATAGTATGCCGCCATTATTACGACAAGCTATCGAATTATTTGATCA  
CCAAGGTGCAGAGCCAGCCTTCTTATTCGGCCTTGAATTGATCATATGCGGATTAGA  
AAAACA ACTTAAATGTGAAAGTGGGTCTtaaGCTTTCTAGATAGCTGAGTAGCCTAGA  
GTGCGCGACAGGTTTGATGACAAAAAATTAGCGCAAGAAGACAAAAATCACCTTGC  
GCTAATGCTCTGTTACA

## Bibliography

1. Li, J., et al., *Micro/nanorobots for biomedicine: Delivery, surgery, sensing, and detoxification*. *Sci. Robot*, 2017. **2**(4).
2. Nelson, B.J., I.K. Kaliakatsos, and J.J. Abbott, *Microrobots for minimally invasive medicine*. *Annual review of biomedical engineering*, 2010. **12**: p. 55-85.
3. Park, B.-W., et al., *Multifunctional Bacteria-Driven Microswimmers for Targeted Active Drug Delivery*. *ACS Nano*, 2017. **11**(9): p. 8910-8923.
4. Li, J., et al., *Development of a magnetic microrobot for carrying and delivering targeted cells*. *Sci. Robot*, 2018. **3**(19).
5. Yan, X., et al., *Multifunctional biohybrid magnetite microrobots for imaging-guided therapy*. *Science Robotics*, 2017. **2**(12): p. eaaq1155.
6. Xie, H., et al., *Reconfigurable magnetic microrobot swarm: Multimode transformation, locomotion, and manipulation*. *Sci. Robot*, 2019. **4**(28).
7. Valdastri, P., et al., *Micromanipulation, communication and swarm intelligence issues in a swarm microrobotic platform*. *Robotics and Autonomous Systems*, 2006. **54**(10): p. 789-804.
8. Khalil, A.S. and J.J. Collins, *Synthetic biology: applications come of age*. *Nature Reviews Genetics*, 2010. **11**(5): p. 367-379.
9. Wang, B., et al., *Engineering modular and orthogonal genetic logic gates for robust digital-like synthetic biology*. *Nature communications*, 2011. **2**(1): p. 1-9.
10. Siuti, P., J. Yazbek, and T.K. Lu, *Synthetic circuits integrating logic and memory in living cells*. *Nature biotechnology*, 2013. **31**(5): p. 448-452.
11. Gardner, T.S., C.R. Cantor, and J.J. Collins, *Construction of a genetic toggle switch in *Escherichia coli**. *Nature*, 2000. **403**(6767): p. 339-342.

12. Friedland, A.E., et al., *Synthetic gene networks that count*. science, 2009. **324**(5931): p. 1199-1202.
13. Kim, H., D. Bojar, and M. Fussenegger, *A CRISPR/Cas9-based central processing unit to program complex logic computation in human cells*. Proceedings of the National Academy of Sciences, 2019. **116**(15): p. 7214-7219.
14. Niederholtmeyer, H., C. Chaggan, and N.K. Devaraj, *Communication and quorum sensing in non-living mimics of eukaryotic cells*. Nature communications, 2018. **9**(1): p. 1-8.
15. Tamsir, A., J.J. Tabor, and C.A. Voigt, *Robust multicellular computing using genetically encoded NOR gates and chemical 'wires'*. Nature, 2011. **469**(7329): p. 212-215.
16. Joesaar, A., et al., *DNA-based communication in populations of synthetic protocells*. Nature nanotechnology, 2019. **14**(4): p. 369-378.
17. Steager, E.B., et al. *Sensors for micro bio robots via synthetic biology*. in *2014 IEEE International Conference on Robotics and Automation (ICRA)*. 2014. IEEE.
18. Heyde, K.C. and W.C. Ruder, *Exploring host-microbiome interactions using an in silico model of biomimetic robots and engineered living cells*. Scientific reports, 2015. **5**(1): p. 1-12.
19. Park, S.-J., et al., *Phototactic guidance of a tissue-engineered soft-robotic ray*. Science, 2016. **353**(6295): p. 158-162.
20. Raman, R., et al., *Optogenetic skeletal muscle-powered adaptive biological machines*. Proceedings of the National Academy of Sciences, 2016. **113**(13): p. 3497-3502.
21. Sakar, M.S., et al., *Formation and optogenetic control of engineered 3D skeletal muscle bioactuators*. Lab on a Chip, 2012. **12**(23): p. 4976-4985.
22. Vizsnyiczai, G., et al., *Light controlled 3D micromotors powered by bacteria*. Nature communications, 2017. **8**(1): p. 1-7.
23. Justus, K.B., et al., *A biosensing soft robot: Autonomous parsing of chemical signals through integrated organic and inorganic interfaces*. Sci. Robot, 2019. **4**.

24. Tinafar, A., K. Jaenes, and K. Pardee, *Synthetic Biology Goes Cell-Free*. BMC biology, 2019. **17**(1): p. 64.
25. Hodgman, C.E. and M.C. Jewett, *Cell-free synthetic biology: thinking outside the cell*. Metabolic engineering, 2012. **14**(3): p. 261-269.
26. Garamella, J., et al., *The all E. coli TX-TL toolbox 2.0: a platform for cell-free synthetic biology*. ACS synthetic biology, 2016. **5**(4): p. 344-355.
27. Sitti, M., *Voyage of the microrobots*. Nature, 2009. **458**(7242): p. 1121-1122.
28. Yang, G.-Z., et al., *The grand challenges of Science Robotics*. Science robotics, 2018. **3**(14): p. eaar7650.
29. Li, J., et al., *Biohybrid Micro-and Nanorobots for Intelligent Drug Delivery*. Cyborg and Bionic Systems, 2022. **2022**.
30. Palagi, S., et al., *Structured light enables biomimetic swimming and versatile locomotion of photoresponsive soft microrobots*. Nature materials, 2016. **15**(6): p. 647-653.
31. Hu, W., et al., *Small-scale soft-bodied robot with multimodal locomotion*. Nature, 2018. **554**(7690): p. 81-85.
32. Li, J., et al., *Development of a magnetic microrobot for carrying and delivering targeted cells*. Science Robotics, 2018. **3**(19).
33. Yan, X., et al., *Multifunctional biohybrid magnetite microrobots for imaging-guided therapy*. Science Robotics, 2017. **2**(12).
34. Behrens, M.R. and W.C. Ruder, *Smart Magnetic Microrobots Learn to Swim with Deep Reinforcement Learning*. arXiv preprint arXiv:2201.05599, 2022.
35. Ricotti, L., et al., *Biohybrid actuators for robotics: A review of devices actuated by living cells*. Science Robotics, 2017. **2**(12).
36. Kabir, A.M.R., D. Inoue, and A. Kakugo, *Molecular swarm robots: recent progress and future challenges*. Science and technology of advanced materials, 2020. **21**(1): p. 323-332.

37. Maier, A.M., et al., *Magnetic propulsion of microswimmers with DNA-based flagellar bundles*. Nano letters, 2016. **16**(2): p. 906-910.
38. Alapan, Y., et al., *Soft erythrocyte-based bacterial microswimmers for cargo delivery*. Science Robotics, 2018. **3**(17).
39. Akin, D., et al., *Bacteria-mediated delivery of nanoparticles and cargo into cells*. Nature nanotechnology, 2007. **2**(7): p. 441-449.
40. Xie, S., et al., *Doxorubicin-conjugated Escherichia coli Nissle 1917 swimmers to achieve tumor targeting and responsive drug release*. Journal of Controlled Release, 2017. **268**: p. 390-399.
41. Liu, Q., et al., *Escherichiacoli Nissle 1917 as a Novel Microrobot for Tumor-Targeted Imaging and Therapy*. Pharmaceutics, 2021. **13**(8): p. 1226.
42. Sauvage, J.-P., *Transition metal-containing rotaxanes and catenanes in motion: toward molecular machines and motors*. Accounts of chemical research, 1998. **31**(10): p. 611-619.
43. Wilson, M.R., et al., *An autonomous chemically fuelled small-molecule motor*. Nature, 2016. **534**(7606): p. 235-240.
44. Cheng, C., et al., *An artificial molecular pump*. Nature nanotechnology, 2015. **10**(6): p. 547-553.
45. Valero, J., et al., *A bio-hybrid DNA rotor–stator nanoengine that moves along predefined tracks*. Nature nanotechnology, 2018. **13**(6): p. 496-503.
46. García-López, V., et al., *Molecular machines open cell membranes*. Nature, 2017. **548**(7669): p. 567-572.
47. Li, B., A.D. Ellington, and X. Chen, *Rational, modular adaptation of enzyme-free DNA circuits to multiple detection methods*. Nucleic acids research, 2011. **39**(16): p. e110-e110.
48. Douglas, S.M., I. Bachelet, and G.M. Church, *A logic-gated nanorobot for targeted transport of molecular payloads*. Science, 2012. **335**(6070): p. 831-834.

49. Jones, M.R., N.C. Seeman, and C.A. Mirkin, *Programmable materials and the nature of the DNA bond*. Science, 2015. **347**(6224).
50. Zhan, P., et al., *DNA-assembled nanoarchitectures with multiple components in regulated and coordinated motion*. Science Advances, 2019. **5**(11): p. eaax6023.
51. Thubagere, A.J., et al., *A cargo-sorting DNA robot*. Science, 2017. **357**(6356).
52. Bazrafshan, A., et al., *Tunable DNA Origami Motors Translocate Ballistically Over  $\mu\text{m}$  Distances at nm/s Speeds*. Angewandte Chemie International Edition, 2020.
53. Kopperger, E., et al., *A self-assembled nanoscale robotic arm controlled by electric fields*. Science, 2018. **359**(6373): p. 296-301.
54. Rubenstein, M., A. Cornejo, and R. Nagpal, *Programmable self-assembly in a thousand-robot swarm*. Science, 2014. **345**(6198): p. 795-799.
55. Xie, H., et al., *Reconfigurable magnetic microrobot swarm: Multimode transformation, locomotion, and manipulation*. Science robotics, 2019. **4**(28).
56. Deng, Z., et al., *Swarming and collective migration of micromotors under near infrared light*. Applied Materials Today, 2018. **13**: p. 45-53.
57. Keya, J.J., et al., *DNA-assisted swarm control in a biomolecular motor system*. Nature communications, 2018. **9**(1): p. 1-8.
58. Schroeder, T.B., et al., *An electric-eel-inspired soft power source from stacked hydrogels*. Nature, 2017. **552**(7684): p. 214-218.
59. Contreras-Llano, L.E., et al., *Holistic engineering of cell-free systems through proteome-reprogramming synthetic circuits*. Nature communications, 2020. **11**(1): p. 1-10.
60. Chen, Z., et al., *De novo design of protein logic gates*. Science, 2020. **368**(6486): p. 78-84.
61. Franco, E., et al., *Timing molecular motion and production with a synthetic transcriptional clock*. Proceedings of the National Academy of Sciences, 2011. **108**(40): p. E784-E793.

62. Green, L.N., et al., *Autonomous dynamic control of DNA nanostructure self-assembly*. Nature chemistry, 2019. **11**(6): p. 510-520.
63. Hamada, S., et al., *Dynamic DNA material with emergent locomotion behavior powered by artificial metabolism*. Science Robotics, 2019. **4**(29).
64. Gines, G., et al., *Microscopic agents programmed by DNA circuits*. Nature nanotechnology, 2017. **12**(4): p. 351-359.
65. Ruder, W.C., T. Lu, and J.J. Collins, *Synthetic biology moving into the clinic*. Science, 2011. **333**(6047): p. 1248-1252.
66. Rice, M.K. and W.C. Ruder, *Creating biological nanomaterials using synthetic biology*. Science and technology of advanced materials, 2013.
67. Zhang, R., et al., *Programming surface chemistry with engineered cells*. ACS synthetic biology, 2016. **5**(9): p. 936-941.
68. Tan, X., et al., *Synthetic biology in the clinic: engineering vaccines, diagnostics, and therapeutics*. Cell, 2021.
69. Perez, J.G., J.C. Stark, and M.C. Jewett, *Cell-free synthetic biology: engineering beyond the cell*. Cold Spring Harbor perspectives in biology, 2016. **8**(12): p. a023853.
70. Meyer, C., et al., *Analysis of the Innovation Trend in Cell-Free Synthetic Biology*. Life, 2021. **11**(6): p. 551.
71. Stark, J.C., et al., *BioBits™ Bright: A fluorescent synthetic biology education kit*. Science advances, 2018. **4**(8): p. eaat5107.
72. Garenne, D., et al., *Cell-free gene expression*. Nature Reviews Methods Primers, 2021. **1**(1): p. 1-18.
73. Nguyen, P.Q., et al., *Wearable materials with embedded synthetic biology sensors for biomolecule detection*. Nature Biotechnology, 2021. **39**(11): p. 1366-1374.
74. Pardee, K., et al., *Rapid, low-cost detection of Zika virus using programmable biomolecular components*. Cell, 2016. **165**(5): p. 1255-1266.

75. Agrawal, D.K., et al., *In vitro implementation of robust gene regulation in a synthetic biomolecular integral controller*. Nature communications, 2019. **10**(1): p. 1-12.
76. Laohakunakorn, N., et al., *Bottom-up construction of complex biomolecular systems with cell-free synthetic biology*. Frontiers in bioengineering and biotechnology, 2020. **8**: p. 213.
77. Ugrinic, M., A. deMello, and T.-Y.D. Tang, *Microfluidic tools for bottom-up synthetic cellularity*. Chem, 2019. **5**(7): p. 1727-1742.
78. Tayar, A.M., et al., *Propagating gene expression fronts in a one-dimensional coupled system of artificial cells*. Nature Physics, 2015. **11**(12): p. 1037-1041.
79. Karzbrun, E., et al., *Programmable on-chip DNA compartments as artificial cells*. science, 2014. **345**(6198): p. 829-832.
80. Hori, Y., et al., *Cell-free extract based optimization of biomolecular circuits with droplet microfluidics*. Lab on a Chip, 2017. **17**(18): p. 3037-3042.
81. van der Linden, A.J., et al., *A multilayer microfluidic platform for the conduction of prolonged cell-free gene expression*. JoVE (Journal of Visualized Experiments), 2019(152): p. e59655.
82. Garenne, D., et al., *The all-E. coliTXTL toolbox 3.0: new capabilities of a cell-free synthetic biology platform*. Synthetic Biology, 2021. **6**(1): p. ysab017.
83. Sun, Z.Z., et al., *Protocols for implementing an Escherichia coli based TX-TL cell-free expression system for synthetic biology*. Journal of visualized experiments: JoVE, 2013(79).
84. Marshall, R., C.L. Beisel, and V. Noireaux, *Rapid testing of CRISPR nucleases and guide RNAs in an E. coli cell-free transcription-translation system*. STAR protocols, 2020. **1**(1): p. 100003.
85. Shin, J. and V. Noireaux, *Efficient cell-free expression with the endogenous E. Coli RNA polymerase and sigma factor 70*. Journal of biological engineering, 2010. **4**(1): p. 1-9.
86. Klocke, M.A., et al., *Engineering DNA nanotubes for resilience in an E. coli TXTL system*. Synthetic Biology, 2018. **3**(1): p. ysy001.

87. Agarwal, S., et al., *Dynamic self-assembly of compartmentalized DNA nanotubes*. Nature communications, 2021. **12**(1): p. 1-13.
88. Pardee, K., et al., *based synthetic gene networks*. Cell, 2014. **159**(4): p. 940-954.
89. Fozouni, P., et al., *Amplification-free detection of SARS-CoV-2 with CRISPR-Cas13a and mobile phone microscopy*. Cell, 2021. **184**(2): p. 323-333. e9.
90. Cho, E. and Y. Lu, *Compartmentalizing Cell-Free Systems: Toward Creating Life-Like Artificial Cells and Beyond*. ACS Synthetic Biology, 2020. **9**(11): p. 2881-2901.
91. Vogele, K., et al., *Towards synthetic cells using peptide-based reaction compartments*. Nature communications, 2018. **9**(1): p. 1-7.
92. Garenne, D., A. Libchaber, and V. Noireaux, *Membrane molecular crowding enhances MreB polymerization to shape synthetic cells from spheres to rods*. Proceedings of the National Academy of Sciences, 2020. **117**(4): p. 1902-1909.
93. Adamala, K.P., et al., *Engineering genetic circuit interactions within and between synthetic minimal cells*. Nature chemistry, 2017. **9**(5): p. 431-439.
94. Tang, T.D., et al., *Gene-mediated chemical communication in synthetic protocell communities*. ACS synthetic biology, 2018. **7**(2): p. 339-346.
95. Hwang, Y., O.H. Paydar, and R.N. Candler, *3D printed molds for non-planar PDMS microfluidic channels*. Sensors and Actuators A: Physical, 2015. **226**: p. 137-142.
96. Shrestha, J., et al., *A rapidly prototyped lung-on-a-chip model using 3D-printed molds*. Organs-on-a-Chip, 2019. **1**: p. 100001.
97. Comina, G., A. Suska, and D. Filippini, *PDMS lab-on-a-chip fabrication using 3D printed templates*. Lab on a Chip, 2014. **14**(2): p. 424-430.
98. Villegas, M., et al., *Fabricating smooth PDMS microfluidic channels from low-resolution 3D printed molds using an omniphobic lubricant-infused coating*. Analytica chimica acta, 2018. **1000**: p. 248-255.

99. Ferraz, M.d.A.M.M., et al., *3D printed mold leachates in PDMS microfluidic devices*. Scientific reports, 2020. **10**(1): p. 1-9.
100. Li, J., et al., *Micro/nanorobots for biomedicine: Delivery, surgery, sensing, and detoxification*. Science Robotics, 2017. **2**(4).
101. Fuller, H.C., et al., *The future application of organ-on-a-chip technologies as proving grounds for microbiorobots*. Micromachines, 2020. **11**(10): p. 947.
102. Palagi, S. and P. Fischer, *Bioinspired microrobots*. Nature Reviews Materials, 2018. **3**(6): p. 113-124.
103. Alapan, Y., et al., *Microrobotics and microorganisms: Biohybrid autonomous cellular robots*. Annual Review of Control, Robotics, and Autonomous Systems, 2019. **2**: p. 205-230.
104. Hu, Q., et al., *DNA nanotechnology-enabled drug delivery systems*. Chemical reviews, 2018. **119**(10): p. 6459-6506.
105. Thubagere, A.J., et al., *A cargo-sorting DNA robot*. Science, 2017. **357**(6356): p. eaan6558.
106. Zhou, J. and J. Rossi, *Aptamers as targeted therapeutics: current potential and challenges*. Nature reviews Drug discovery, 2017. **16**(3): p. 181.
107. Bunka, D.H. and P.G. Stockley, *Aptamers come of age—at last*. Nature Reviews Microbiology, 2006. **4**(8): p. 588-596.
108. Zhang, C., et al., *Cancer diagnosis with DNA molecular computation*. Nature nanotechnology, 2020. **15**(8): p. 709-715.
109. Li, S., et al., *A DNA nanorobot functions as a cancer therapeutic in response to a molecular trigger in vivo*. Nature biotechnology, 2018. **36**(3): p. 258-264.
110. Cangialosi, A., et al., *DNA sequence-directed shape change of photopatterned hydrogels via high-degree swelling*. Science, 2017. **357**(6356): p. 1126-1130.

111. Fan, D., et al., *Propelling DNA Computing with Materials' Power: Recent Advancements in Innovative DNA Logic Computing Systems and Smart Bio-Applications*. Advanced Science, 2020. **7**(24): p. 2001766.
112. Li, J., et al., *Engineering nucleic acid structures for programmable molecular circuitry and intracellular biocomputation*. Nature chemistry, 2017. **9**(11): p. 1056-1067.
113. English, M.A., et al., *Programmable CRISPR-responsive smart materials*. Science, 2019. **365**(6455): p. 780-785.
114. Oishi, M. and S. Juji, *Acceleration of DNA Hybridization Chain Reactions on 3D Nanointerfaces of Magnetic Particles and Their Direct Application in the Enzyme-Free Amplified Detection of microRNA*. ACS Applied Materials & Interfaces, 2021. **13**(30): p. 35533-35544.
115. Oishi, M. and K. Saito, *Simple Single-Legged DNA Walkers at Diffusion-Limited Nanointerfaces of Gold Nanoparticles Driven by a DNA Circuit Mechanism*. ACS nano, 2020. **14**(3): p. 3477-3489.
116. Li, J., et al., *Construction of bio-nano interfaces on nanozymes for bioanalysis*. ACS Applied Materials & Interfaces, 2021. **13**(18): p. 21040-21050.
117. Nielsen, J. and J.D. Keasling, *Engineering cellular metabolism*. Cell, 2016. **164**(6): p. 1185-1197.
118. Green, A.A., et al., *Complex cellular logic computation using ribocomputing devices*. Nature, 2017. **548**(7665): p. 117-121.
119. Siciliano, V., et al., *Engineering modular intracellular protein sensor-actuator devices*. Nature communications, 2018. **9**(1): p. 1-7.
120. Mao, N., et al., *Probiotic strains detect and suppress cholera in mice*. Science Translational Medicine, 2018. **10**(445).
121. Tang, T.-C., et al., *Materials design by synthetic biology*. Nature Reviews Materials, 2021. **6**(4): p. 332-350.

122. Badeau, B.A. and C.A. DeForest, *Programming stimuli-responsive behavior into biomaterials*. Annual review of biomedical engineering, 2019. **21**: p. 241-265.
123. Heyde, K.C., et al., *Modeling information exchange between living and artificial cells*. Quantitative Biology, 2017. **5**(1): p. 76-89.
124. Wei, T.-Y. and W.C. Ruder, *Engineering control circuits for molecular robots using synthetic biology*. APL materials, 2020. **8**(10): p. 101104.
125. Heyde, K.C., et al., *Using synthetic biology to engineer living cells that interface with programmable materials*. Journal of visualized experiments: JoVE, 2017(121).
126. Tinafar, A., K. Jaenes, and K. Pardee, *Synthetic biology goes cell-free*. BMC biology, 2019. **17**(1): p. 1-14.
127. Lutz, R. and H. Bujard, *Independent and tight regulation of transcriptional units in Escherichia coli via the LacR/O, the TetR/O and AraC/I1-I2 regulatory elements*. Nucleic acids research, 1997. **25**(6): p. 1203-1210.
128. Medeiros, S., et al., *Stimuli-responsive magnetic particles for biomedical applications*. International journal of pharmaceutics, 2011. **403**(1-2): p. 139-161.
129. Dobson, J., *Magnetic nanoparticles for drug delivery*. Drug development research, 2006. **67**(1): p. 55-60.
130. Yu, J., et al., *Active generation and magnetic actuation of microrobotic swarms in biofluids*. Nature communications, 2019. **10**(1): p. 1-12.
131. Dundas, C.M., D. Demonte, and S. Park, *Streptavidin–biotin technology: improvements and innovations in chemical and biological applications*. Applied microbiology and biotechnology, 2013. **97**(21): p. 9343-9353.
132. Litcofsky, K.D., et al., *Iterative plug-and-play methodology for constructing and modifying synthetic gene networks*. Nature methods, 2012. **9**(11): p. 1077-1080.
133. Ohta, S., D. Glancy, and W.C. Chan, *DNA-controlled dynamic colloidal nanoparticle systems for mediating cellular interaction*. Science, 2016. **351**(6275): p. 841-845.

134. Leunissen, M.E., et al., *Switchable self-protected attractions in DNA-functionalized colloids*. Nature materials, 2009. **8**(7): p. 590-595.
135. Rogers, W.B., W.M. Shih, and V.N. Manoharan, *Using DNA to program the self-assembly of colloidal nanoparticles and microparticles*. Nature Reviews Materials, 2016. **1**(3): p. 1-14.
136. Dubuc, E., et al., *Cell-free microcompartmentalised transcription–translation for the prototyping of synthetic communication networks*. Current opinion in biotechnology, 2019. **58**: p. 72-80.
137. Grozinger, L., et al., *Pathways to cellular supremacy in biocomputing*. Nature communications, 2019. **10**(1): p. 1-11.
138. McCarty, N.S. and R. Ledesma-Amaro, *Synthetic biology tools to engineer microbial communities for biotechnology*. Trends in biotechnology, 2019. **37**(2): p. 181-197.
139. Regot, S., et al., *Distributed biological computation with multicellular engineered networks*. Nature, 2011. **469**(7329): p. 207-211.
140. Du, P., et al., *De novo design of an intercellular signaling toolbox for multi-channel cell–cell communication and biological computation*. Nature communications, 2020. **11**(1): p. 1-11.
141. Pardee, K., et al., *Portable, on-demand biomolecular manufacturing*. Cell, 2016. **167**(1): p. 248-259. e12.
142. de Ávila, B.E.-F., et al., *Hybrid biomembrane–functionalized nanorobots for concurrent removal of pathogenic bacteria and toxins*. Science Robotics, 2018. **3**(18): p. eaat0485.
143. Hamada, S., et al., *Dynamic DNA material with emergent locomotion behavior powered by artificial metabolism*. Science Robotics, 2019. **4**(29): p. eaaw3512.
144. Dey, S., et al., *DNA origami*. Nature Reviews Methods Primers, 2021. **1**(1): p. 1-24.
145. Praetorius, F., et al., *Biotechnological mass production of DNA origami*. Nature, 2017. **552**(7683): p. 84-87.

146. Katz, E. and I. Willner, *Biomolecule-functionalized carbon nanotubes: applications in nanobioelectronics*. ChemPhysChem, 2004. **5**(8): p. 1084-1104.
147. Thomas, C.R., et al., *Noninvasive remote-controlled release of drug molecules in vitro using magnetic actuation of mechanized nanoparticles*. Journal of the American Chemical Society, 2010. **132**(31): p. 10623-10625.
148. Ferry, M.S., I.A. Razinkov, and J. Hasty, *Microfluidics for synthetic biology: from design to execution*, in *Methods in enzymology*. 2011, Elsevier. p. 295-372.
149. Chen, M.-C., et al., *Three-dimensional printing of thermoplastic materials to create automated syringe pumps with feedback control for microfluidic applications*. JoVE (Journal of Visualized Experiments), 2018(138): p. e57532.